NASA CR-135352
R77AEG588

QUIET CLEAN SHORT-HAUL EXPERIMENTAL ENGINE (QCSEE) UNDER-THE-WING (UTW) COMPOSITE NACELLE FINAL DESIGN REPORT

AUGUST 1978

by

ADVANCED ENGINEERING & TECHNOLOGY PROGRAMS DEPARTMENT

GENERAL ELECTRIC COMPANY

National Aeronautics and Space Administration

NASA-Lewis Research Center

Contract NAS3-18021

FOREWORD

The Quiet Clean Short-Haul Experimental Engine (QCSEE) Program is currently being conducted by the General Electric Company, Aircraft Engine Group, in accordance with NASA Contract NAS3-18021, under the direction of Mr. C.C. Ciepluch, NASA Project Manager. The program includes the design, manufacture, and testing of under-the-wing (UTW) and over-the-wing (OTW) experimental engines. Both engines are intended to develop the technology needed for externally blown flaps, short takeoffs and landings, commercial short-haul aircraft.

Although earlier studies indicated a need to operate from a 609.6-m (2000-ft) runway, it was concluded by all contributors that the flight studies of a commerical short-haul transport should be based on a 914.4-m (3000-ft) runway which is typical of existing close-in airports.

The experimental system retained the 609.6-m (2000-ft) runway requirement to assure technology margin for the aircraft ready to enter airline service in the mid-1980's. This resulted in a slightly longer (19.1-cm; 7.5-in.) nacelle in order for the experimental system to house the fan exhaust acoustic splitter.

TABLE OF CONTENTS

LIST OF ILLUSTRATIONS

LIST OF ILLUSTRATIONS (Continued)

LIST OF ILLUSTRATIONS (Concluded)

LIST OF TABLES

1.0 INTRODUCTION

The Quiet Clean Short-Haul Experimental Engine (QCSEE) Program provides for the design, fabrication, and testing of experimental, high-bypass, geared turbofan engines and propulsion systems for short-haul passenger aircraft. The overall objective of the program is to develop the propulsion technology required for future externally blown flap types of aircraft with engines located both under-the-wing and over-the-wing.

The overall engine design process included the preliminary design of optimized flight engine installations during the initial phase of the program. But only the experimental installations were carried through the detail design and fabrication stages; only the under-the-wing system included the flight-type, lightweight, composite nacelle components. Design of these experimental components duplicated the flight-type in all areas except those where considerable cost savings could be accomplished through simplification without compromising the basic program objectives.

This report presents the results of the final detail design activity of the UTW experimental composite nacelle. Any discussions relating to the UTW flight system are included for the purpose of defining specific differences which exist between experimental and flight configurations.

2.0 SUMMARY

This document summarizes the detail design of the under-the-wing (UTW) experimental composite nacelle components. Results of the detail design, component, and subcomponent testing provide a high degree of confidence that the experimental composite nacelle will meet all stated program objectives. Design simplification in certain areas of the experimental nacelle design to minimize program expenditures has not resulted in any compromise of the program's technical objectives.

2.1 PROGRAM OBJECTIVES

The major purpose of the QCSEE Program is to develop and demonstrate the technology required for propulsion systems for quiet, clean, economically viable, commercial short-haul aircraft. In the area of the composite nacelle, this program includes the following objectives:

- Develop propulsion system technology which will permit a short-haul aircraft to achieve the system noise goal of 95 EPNdB along a 152-m (500-ft) sideline when the engines are scaled to a total installed thrust of 400,340 N (90,000 lb). The design will also minimize the ground area (foot print) exposed to objectionable noise levels.

- Develop the required technology to meet propulsion system performance, weight, and operational characteristics.

- Develop the material, design, and fabrication technology for quiet propulsion systems which will yield installed thrust-to-weight ratios greater than 3.5 to 1.

- Provide the technology which will permit the design of quiet, efficient, lightweight thrust reversing systems for powered-lift aircraft.

- Provide the technology to permit the design of integrated engine and nacelle installations which will be tolerant to aerodynamic distortion expected with operating flight conditions such as high crosswinds, large angles of attack, and sideslip, and still provide good cruise performance.

2.2 SPECIFIC TECHNICAL OBJECTIVES

The following specific design objectives have been established for the flight and experimental UTW nacelle:

2.2.1 Noise

The UTW experimental engine shall be designed to meet the following noise objectives when scaled to fit a four-engine 400,340-N (90,000-lb) thrust aircraft:

Takeoff and Approach	95 EPNdB at 152-m (500-ft) S.L.
Max. Reverse Thrust (35% Max. Forward Thrust)	100 EPNdB at 152-m (500-ft) S.L.

2.2.2 Weight

The full-scale, UTW experimental composite nacelle shall be designed to meet the following weight objectives for a flight-weight system:

- Inlet 156.5 kg (345 lb)
- Outer Fan Duct 73.9 kg (163 lb)
- Flare Nozzle 25.9 kg (57 lb)
- Core Cowl 44.5 kg (98 lb)

These weights shall include those items not included in the experimental design (but which are required for a flight design) and the analytically predicted flight weight of all nonflight design components.

2.2.3 Thrust Reversal

The UTW propulsion system shall provide the following thrust reversal capacity.

- Operation down to 5.1 m/sec (10 kn)
- Max. forward to max. reverse thrust transient in less than 1.5 seconds
- At least 35% static takeoff thrust in reverse
- Noise levels as specified in Section 2.2.1.

2.2.4 General Design Criteria

In addition to the specific objectives listed above, the experimental engine composite nacelle shall be designed with the following features:

- An accurate representation of external and internal aerodynamic contours of the flight nacelle
- Accurate acoustic representation of the flight-type design
- All electrical, fuel, oil, cooling, fire-detection and prevention, control, and instrumentation systems required to test the propulsion system
- Convenient access for maintenance
- The engine shall be easily removable from the nacelle without requiring removal of the fan exhaust duct.

The propulsion system shall be designed to perform within the flight maneuver forces envelope per MIL-E-5007C data December 30, 1965, paragraph 3.14, with the exception of conditions of catapult flight maneuver and precession rates.

2.3 OPERATING REQUIREMENTS

The foregoing objectives and general criteria are further amplified by the following propulsion system operating requirements.

2.3.1 Life and Duty Cycle

The nacelle shall be designed for a useful life of 36,000 hours over a 15-year period, based on the typical 403-km (250-mi) mission cycle shown in Table I.

Cyclic life shall be based on 48,000 mission cycles plus 1,000 ground checkout cycles to full power.

The nacelle shall be capable of operating throughout the flight envelope shown in Figure 1.

The nacelle and its supports shall withstand without permanent deformation the conditions specified in Figure 2.

2.4 UTW EXPERIMENTAL NACELLE

The UTW experimental composite nacelle, shown in Figure 3, includes:

- A lightweight, composite hybrid inlet providing acoustic suppression by means of a high throat Mach number (0.79) and integral acoustic treatment

Table I. Flight Duty Cycle.

Segment	Altitude km	Altitude ft	Mach No.	% Power	Time, Min.	% Time
Start	0	0	0	--	0.50	1.11
Idle/Taxi	0	0	0	4-20%	3.10	6.89
Takeoff	0	0	0.12	100%	1.22	2.71
Climb (1st seg)	0-3.05	0-10K	128.6 m/sec (250 kn) IAS*	Max. Continuous	5.00	11.11
(2nd seg)	3.05-7.63	10-25K	154.3 m/sec (299 kn)	Max. Continuous	5.00	11.11
Cruise	6.41-7.63	21-25K	0.70	Max. Cruise	14.00	31.11
Descent	6.1-0.06	20K-200 ft	0.60	Flight Idle	10.00	22.22
Approach	0.06	200 ft	0.12	65%	3.00	6.67
Reverse Thrust	0	0	0.12	Max. Reverse	0.08	0.18
Idle/Taxi	0	0	0	4-20%	3.10	6.89
					45.00	100.00

* Indicated Airspeed

- The composite fan duct with integral acoustic treatment (hinged from the pylon to provide access for engine maintenance) and a removable boilerplate-type acoustic splitter

- The composite core cowl with integral treatment and hinged from the pylon to provide access to the engine the same as the fan duct

- The fan exhaust nozzle composed of a variable-area four-flap configuration capable of area change takeoff to cruise, as well as opening to a flared position to form an inlet in the reverse thrust mode. The nozzle flaps are hydraulically actuated.

All experimental nacelle components have been designed to meet the propulsion system life and operating requirements defined in Section 2.3.

2.5 UTW FLIGHT PROPULSION SYSTEM

The UTW flight propulsion system cross section is shown in Figure 4. Comparing Figure 4 with Figure 3, it can be seen that the major configuration

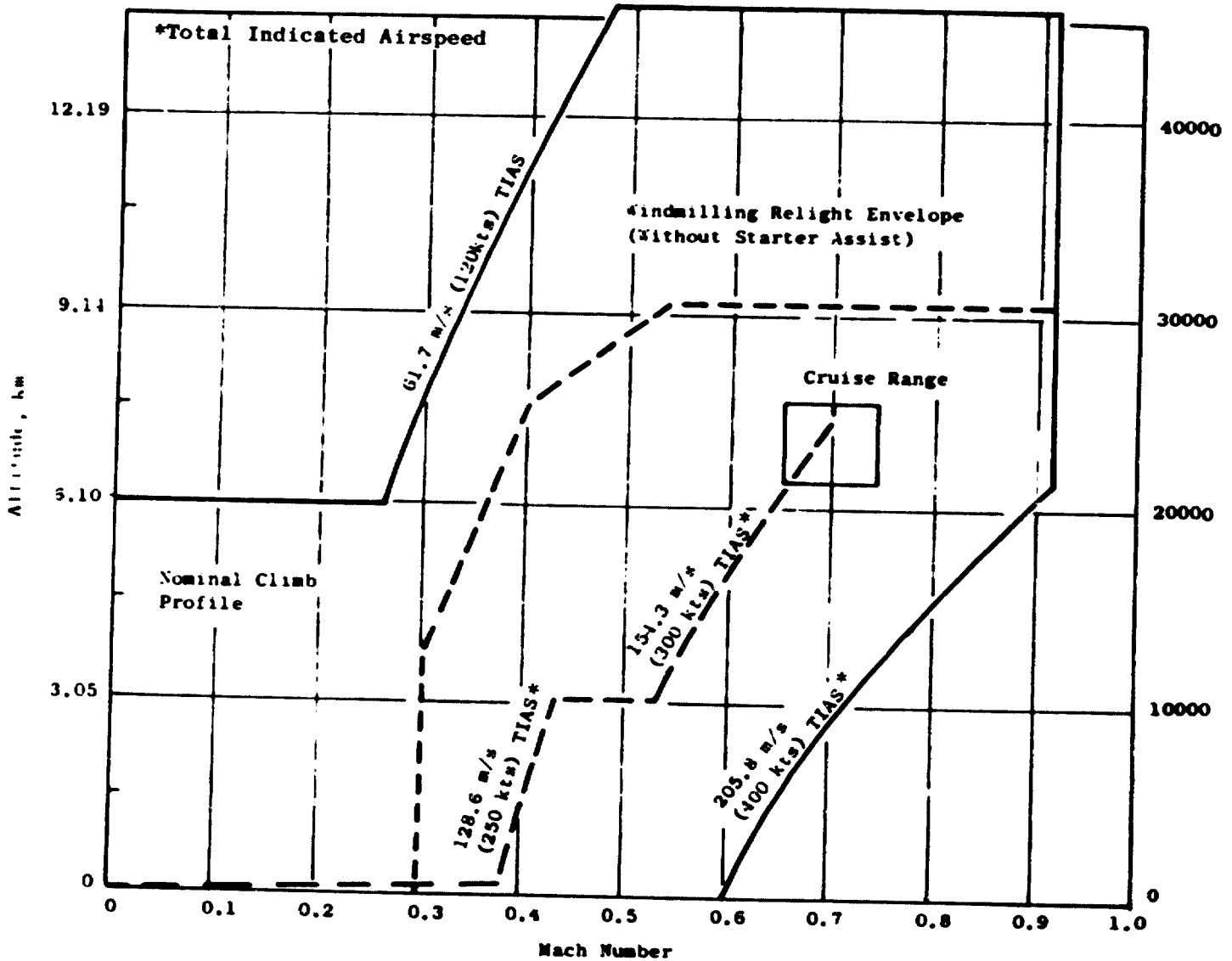

Figure 1. Operating Envelope.

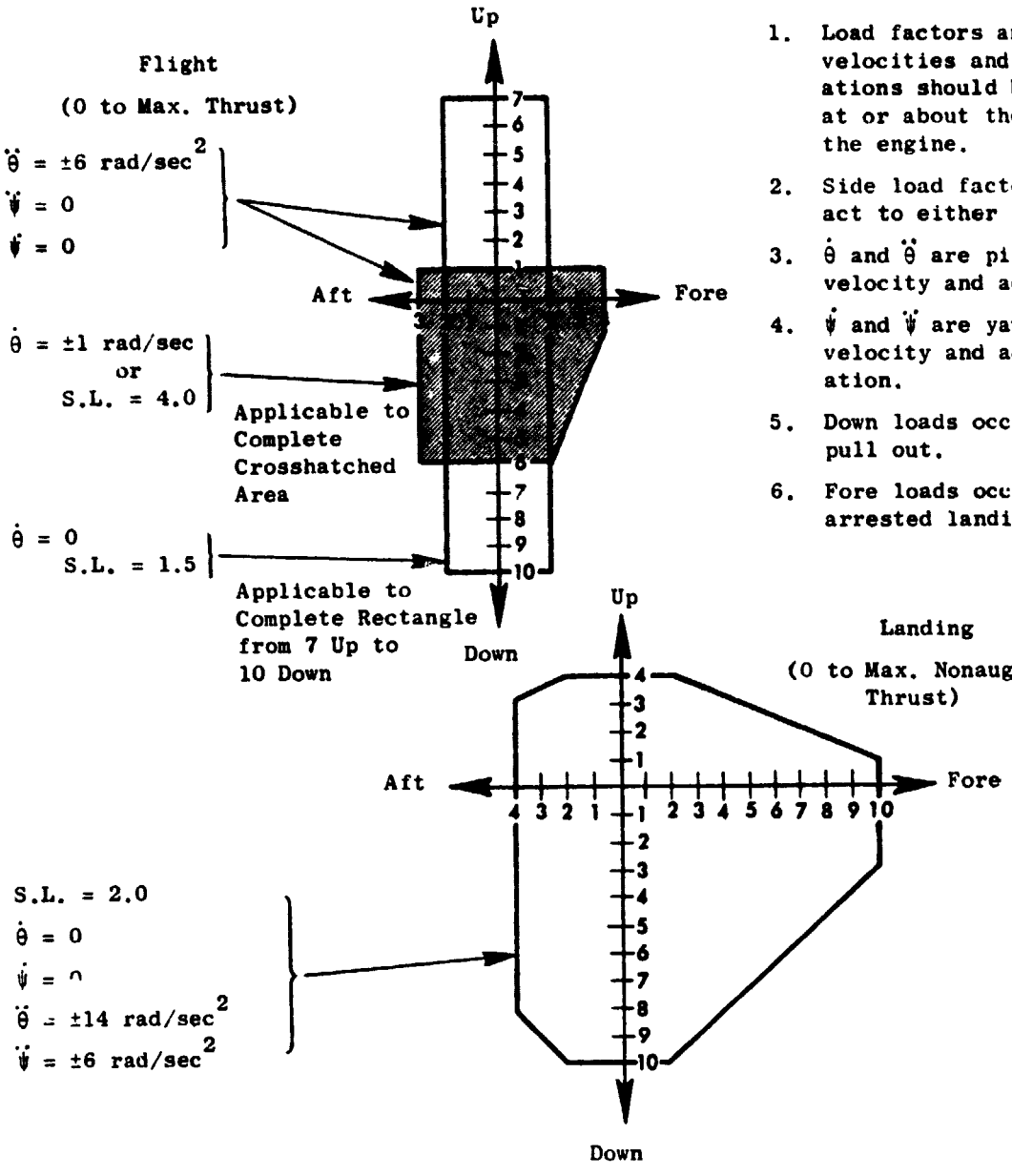

1. Load factors and angular velocities and accelerations should be taken at or about the C.G. of the engine.
2. Side load factors (S.L.) act to either side.
3. $\dot{\theta}$ and $\ddot{\theta}$ are pitching velocity and acceleration.
4. $\dot{\psi}$ and $\ddot{\psi}$ are yawing velocity and acceleration.
5. Down loads occur during pull out.
6. Fore loads occur during arrested landing.

Figure 2. Maneuver Loads, Design.

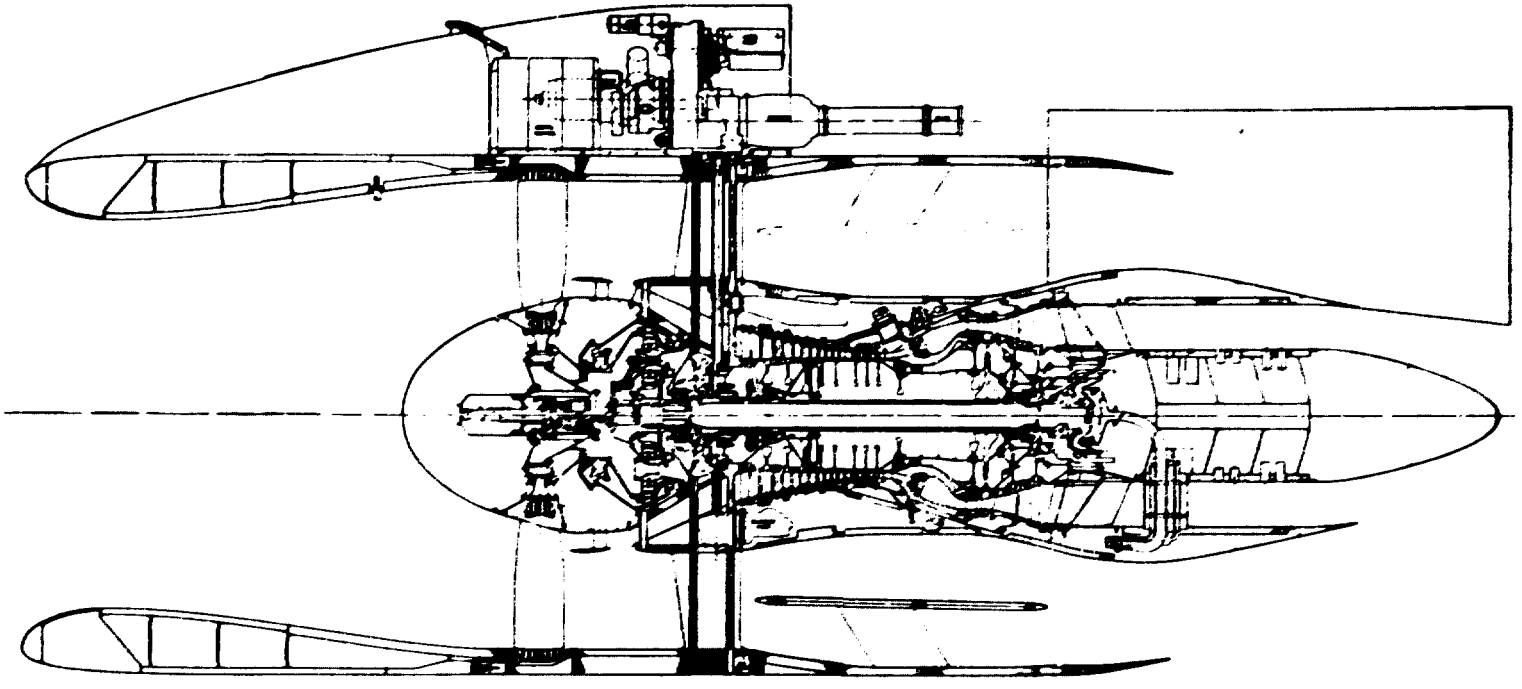

Figure 3. UTW Experimental Propulsion System.

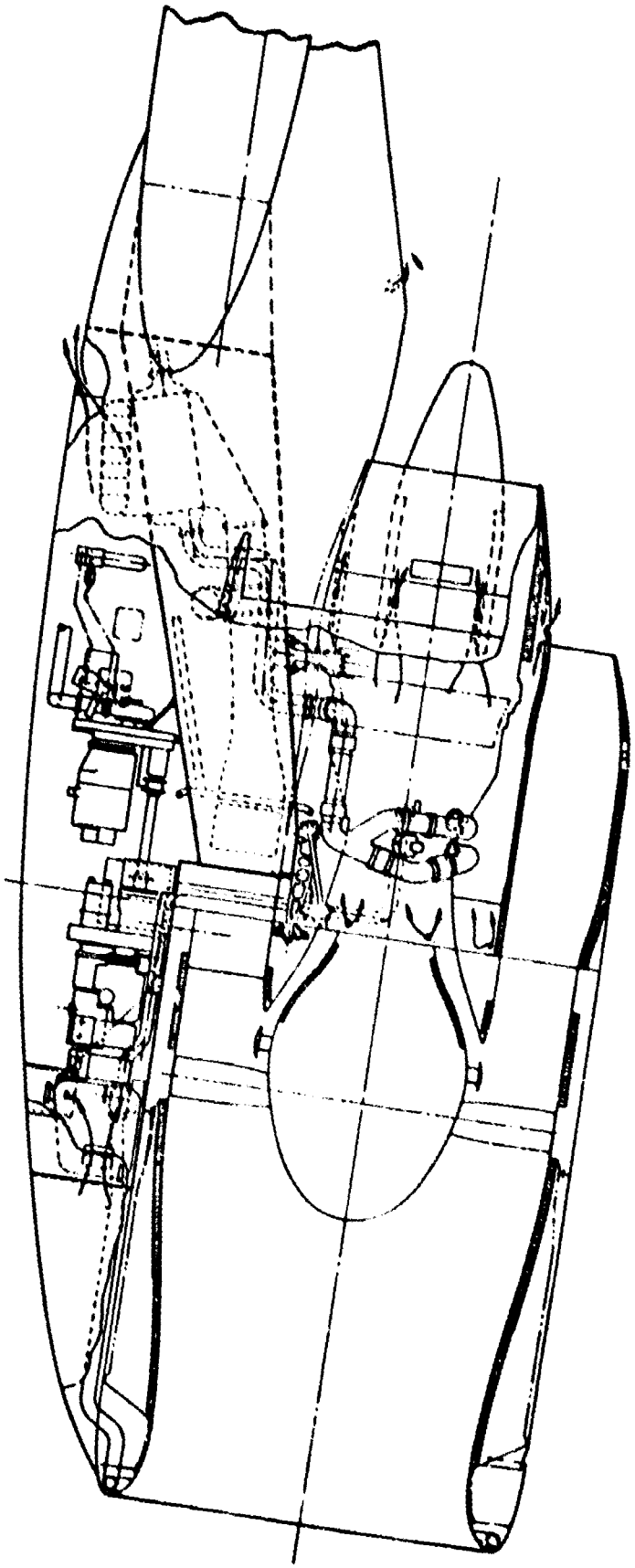

Figure 4. UTW Flight Propulsion System.

difference between the flight and experimental nacelles is the shortened fan duct and elimination of the acoustic splitter ring required to satisfy the experimental engine noise goal. The noise goal for the experimental engine is based on a 609.6-m (2000-ft) takeoff while acoustic design of the flight propulsion system is based on a noise goal set for a 914.5-m (3000-ft) takeoff.

Other differences between the two configurations are (1) the flight inlet anti-icing provision which is not included in the experimental system inlet, (2) the utilization of simplified components in the experimental nacelle to minimize program cost, and (3) the incorporation of test instrumentation in the experimental system which would not be required in the flight nacelle.

Both the experimental and flight UTW engines are top-mounted from a pylon. By opening the bypass duct and the core cowl, the engine and the inlet can be removed from the pylon in the downward direction.

Actual weights of the completed experimental composite nacelle components and analytical prediction of the weights of the flight nacelle components indicate that the design will be within 4% of meeting the total nacelle weight objective of 301 kg (663 lb).

Figure 5 shows the UTW experimental propulsion system installed on the test stand.

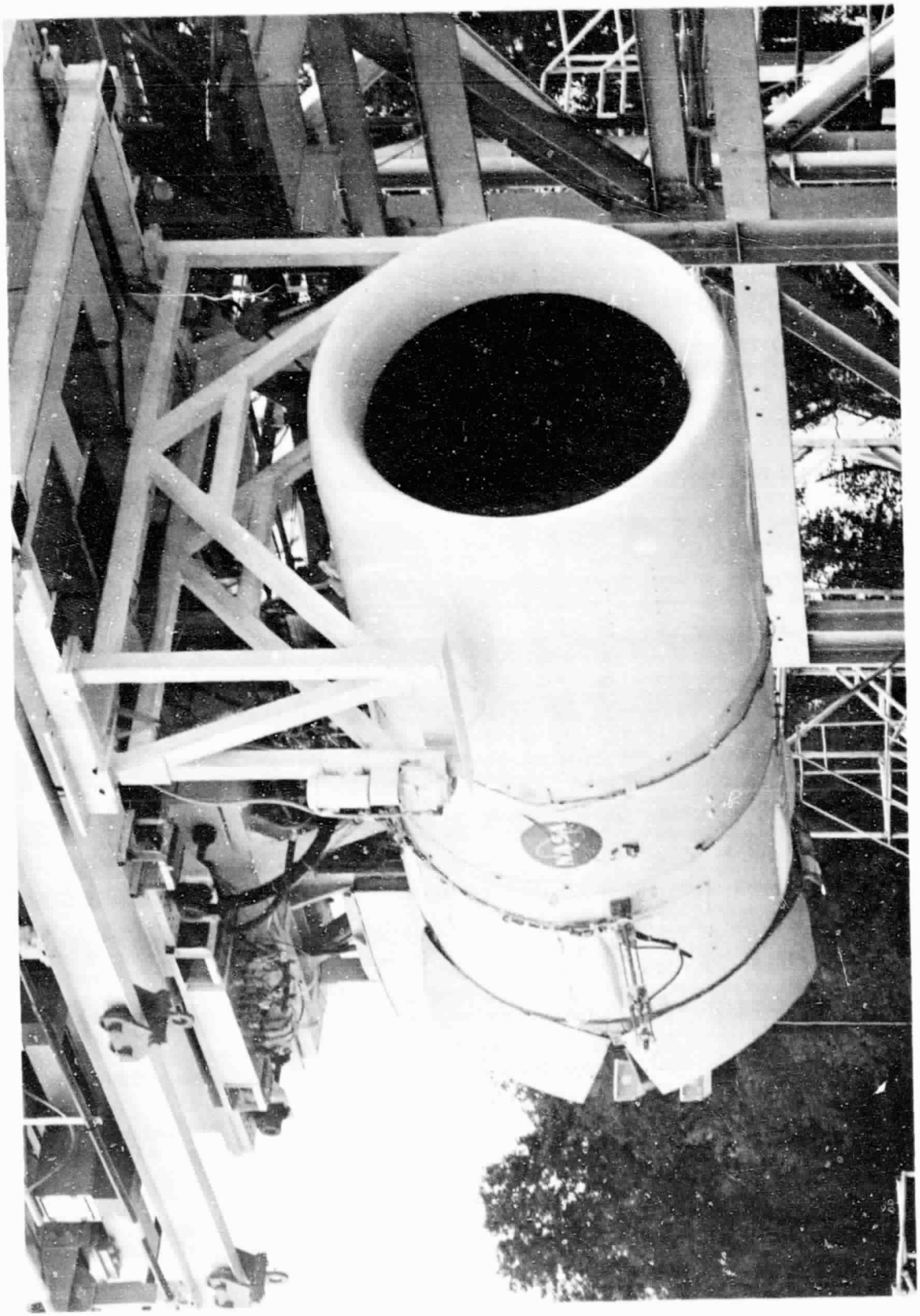

Figure 5. Composite Nacelle Test Installation.

3.0 NACELLE MECHANICAL DESIGN

3.1 SUMMARY

3.1.1 Flight Propulsion System

The under-the-wing flight propulsion system installation is shown in Figure 6. This propulsion system is designed for application to a high-wing short-haul aircraft utilizing externally blown flaps to provide powered lift. Major installation features of this propulsion system include a high-bypass engine configuration; variable-pitch fan to provide reverse thrust; variable-geometry fan exhaust nozzle; and top-mounted engine accessories enclosed within the aircraft engine pylon.

The top-mounted accessory configuration, in combination with the integrated-nacelle concept, yields the following significant advantages when compared with current, conventional aircraft propulsion system installations:

- Reduced Frontal Area - The top-mounted gearbox fits in the silhouette of the aircraft pylon and eliminates the bulge at the bottom of the nacelle which results when the accessories are mounted under the engine.

- Shorter Pipes and Wires - Location of the accessories on top results in the shortest "run" from the engine to the accessories and then on to the aircraft wing, reducing system weight and improving maintainability. On current conventional aircraft installation, with accessories located beneath the engine, pipes have to be routed around the fan casing.

- Eliminates Bottom Pylon - In the absence of bottom-mounted accessories, the need for a bottom pylon is eliminated, thereby reducing internal aerodynamic losses.

- Integrated Engine Nacelle Structure - The high Mach inlet reduces the required throat area (i.e., smaller diameter throat). The throat-to-highlight-diameter ratio required for good crosswind capability (and the highlight-to-maximum-diameter ratio consistent with aircraft Mach number requirements) permits nacelle thickness and maximum diameter to be kept to a minimum. At this minimum thickness, the fan cowl (nacelle component) can be combined with the fan frame structure to complete the integration of nacelle and engine structure.

The integrated engine/nacelle design approach results in thin nacelle walls [9.9 cm (3.9 in.)] uniformly around the nacelle. The walls of this configuration are in the range of 20% to 40% of the wall thickness of current aircraft nacelle configurations. The resulting nacelle maximum diameter is 200 cm (78.8 in.); the overall length is 414 cm (163.0 in.) to the fan exhaust plane and 536 cm (211.0 in.) to the tip of the core exhaust nozzle plug.

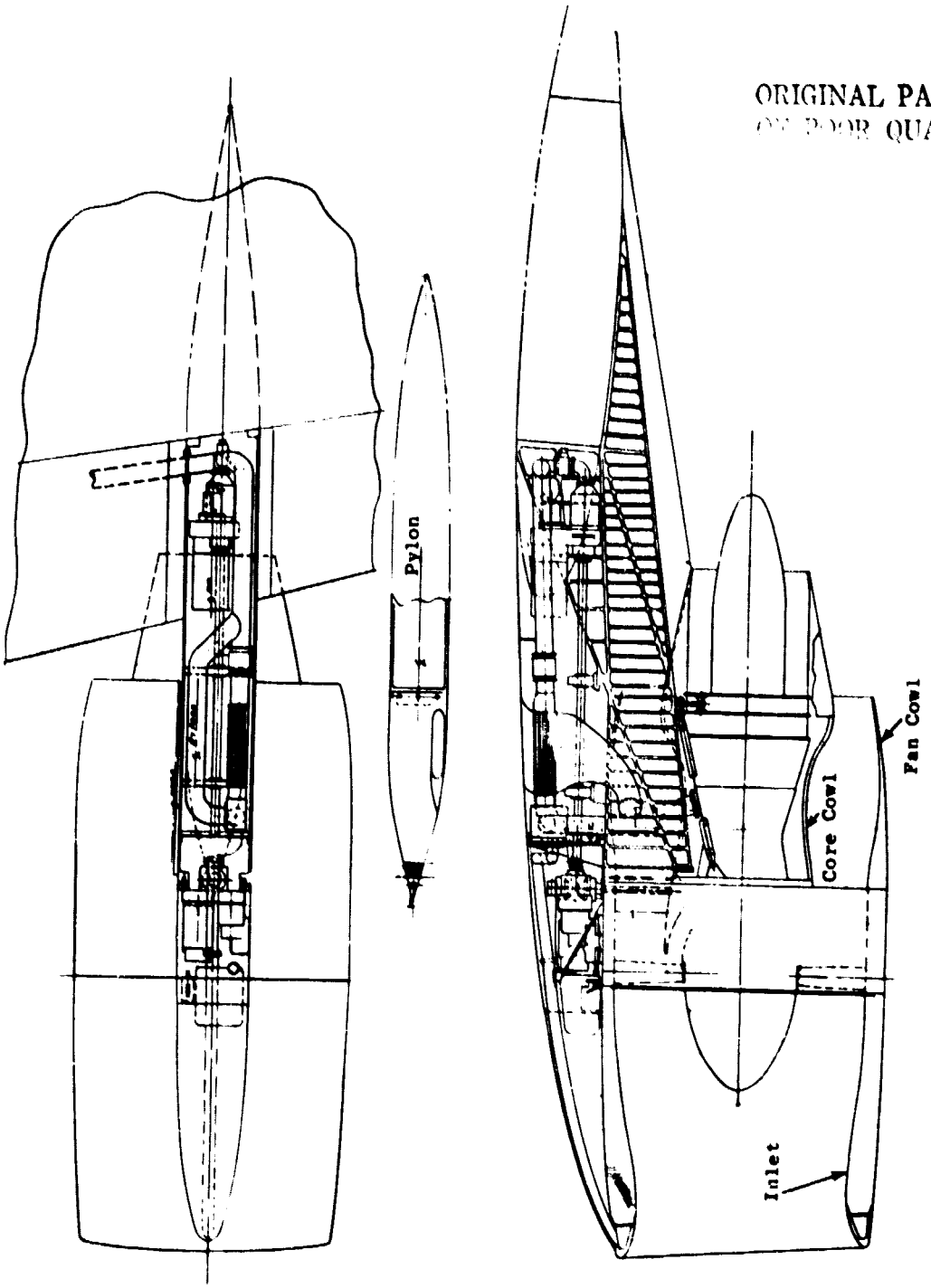

Figure 6. Baseline QCSEE UTW Propulsion Unit.

The aircraft installation results in a height, from top-to-bottom of the nacelle, of approximately 3.05 m (10 ft). A maintenance stand is therefore required to reach the engine accessories. The accessory cover for the top gearbox rotates in halves aft to expose the engine accessories and then slides aft, as shown in Figure 7, to expose the aircraft accessories. This permits direct access to install or remove any component and allows visual inspection of accessories and piping joints while the engine is operating.

3.1.2 Experimental Propulsion System

The UTW experimental propulsion system is shown in Figure 3. The overall configuration is basically the same as the flight configuration, except that a fan exhaust duct splitter has been added to meet the experimental engine acoustic objectives. The nacelle maximum diameter is the same as in the flight installation, but the overall length is 19.1 cm (7.5 in.) greater in order to house the 101.6-cm-long (40-in.-long) fan exhaust splitter. The overall length is 433 cm (170.5 in.) to the fan exhaust plane and 556 cm (218.8 in.) to the core nozzle tip. The noise goal for the experimental engine is based on meeting the acoustic requirements of a 609.6-m (2000-ft) takeoff, while acoustic design of the flight propulsion system is based on a noise goal set for a 914.4-m (3000-ft) takeoff.

3.2 DESIGN CRITERIA

All components have been designed consistent with the requirements specified in Section 2.0. In addition to the normal range and combination of steady-state pressure, thermal, maneuver, and buffet loads, the nacelle has been designed to withstand the loads defined in Table II. Other specific nacelle component design criteria are as follows:

Inlet

- Design of the experimental engine composite inlet is compatible with anti-icing system requirements; however, neither anti-icing system components or inlet metal leading edge are included in the design.
- Design is a one-piece 6.28-radian (360°) structure with quick-connect/-disconnect-type fasteners. The experimental engine composite design does not include forward extension of the external pylon/accessory cover.
- Composite hardware will be supported from the engine.

Fan Cowl and Exhaust Nozzle

- Fan nozzle actuation system is submerged within the nacelle wall with the required bulges flared externally on the composite nacelle.

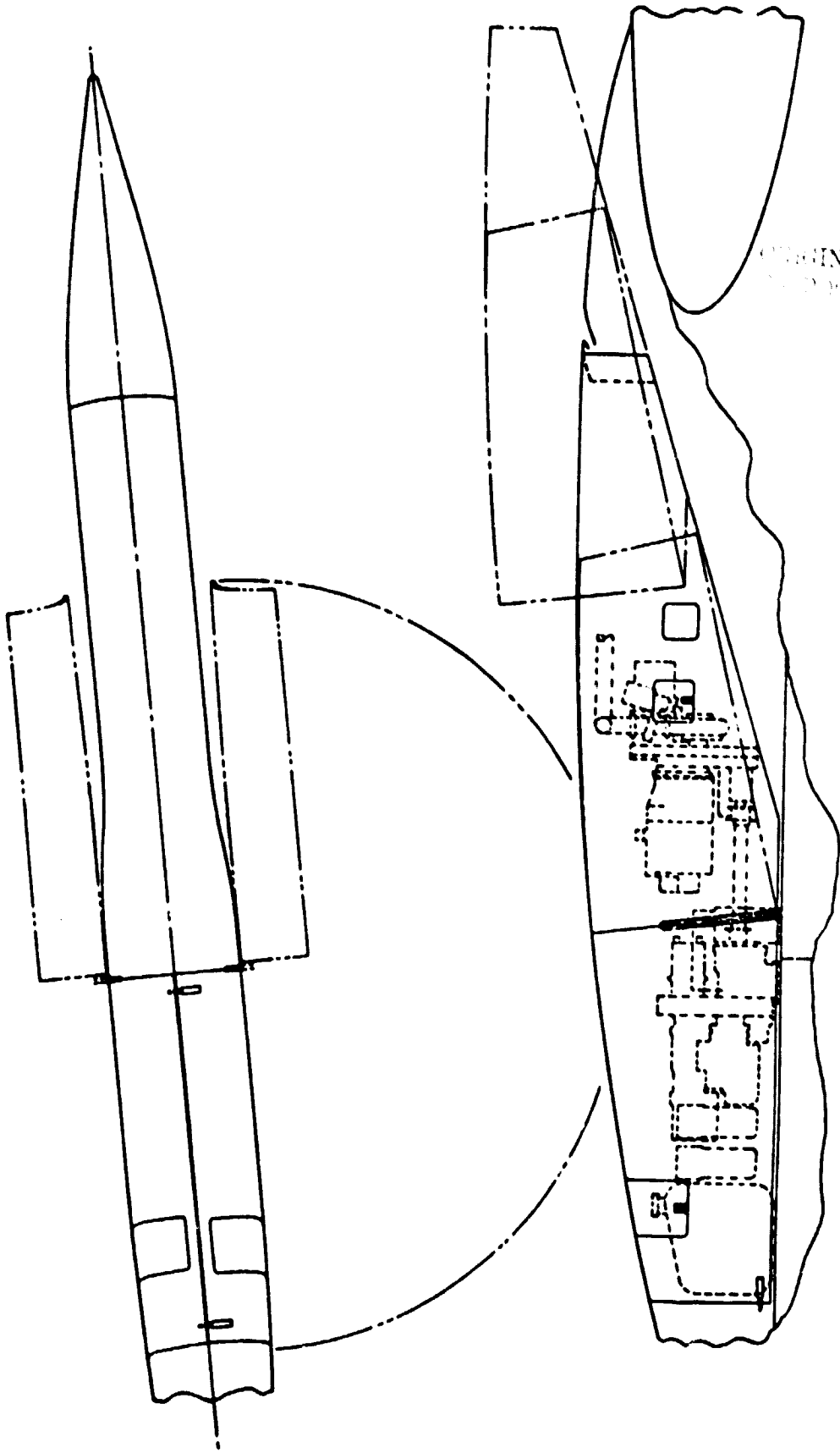

Figure 7. Accessory Access Provisions.

Table II. QCSEE Nacelle Loads.

Limit Loads

For any one of the following load conditions, all stresses shall remain within the material elastic limits.

Condition I: Flight and Landing - see load diagram, Figure 2.

Condition II: Gust Load - an equivalent load from a 51.44-m/sec (100-kn) crosswind acting at any angle within a plane 1.5708 radians (90°) to the axis of the engine, zero-to-minimum thrust.

Condition III: Side Load - a 4-g side load combined with 1/3 of the equivalent load as defined in Condition II, zero-to-maximum thrust.

Ultimate Loads

The nacelle shall not separate from the aircraft when subjected to Condition IV and for static loads equivalent to 1.5 times the loads specified as limit loads in metal parts, and 3.0 times the loads specified as limit loads in composite parts.

Condition IV: Crash Load - the crash load is defined as 10-g forward, 2.25-g side, and 4.5-g down at maximum thrust or up to zero thrust.

- No cowl power-operating devices are included for either flight or experimental propulsion system hardware.

- Aft cowl to fan frame attachment is a tongue-and-groove type similar to DC-10/CF6 design.

- The variable-fan nozzle is designed to be sealed against leakage in all forward thrust conditions, i.e., fan exhaust area from 11,871 to 16,774 cm^2 (1840 to 2600 $in.^2$).

- The variable-fan nozzle is capable of withstanding inadvertent deployment in the reverse thrust position under the following operating conditions:

  - At speeds up to 154 m/sec (300 kn) from 0 to 3048-m (10,000-ft) altitude at cruise power without damage.

  - At speeds up to 193 m/sec (375 kn) above 3048-m (10,000-ft) altitude at maximum power without separation from the aircraft.

- All composite hardware will be supported from the engine.

Core Cowl

- No cowl power-operating devices are included for either the flight or experimental propulsion system hardware.

- The cowl to fan frame attachment is a tongue-and groove type similar to the DC-10/CF6 design.

- All composite hardware will be supported from the engine.

Maintainability

- The engine is capable of removal from an aircraft wing and/or facility:

  - Vertically downward (after uncoupling facility-mounted component on the experimental engine)

  - Without disassembly of fan exhaust cowl doors and variable-geometry fan nozzle.

3.3 COMPOSITE NACELLE DESIGN

The UTW experimental propulsion system includes an acoustically treated nacelle which is integrated with the fan frame and casing to achieve a low-noise, minimum drag, lightweight design. To accomplish this integration function efficiently at minimum cost and weight, conventional metal construction is replaced with advanced composite materials.

3.3.1 Materials

The major portion of the nacelle, with the exception of the core cowl, operates at very modest temperatures - less than 355 K (180° F) - permitting use of a wide variety of composite materials. The primary composite material selected consists of a woven Kevlar 49 fabric, style 181, impregnated with NARMCO 8517 epoxy resin. This material exhibits light weight, good tensile strength, moderate stiffness, and excellent impact strength. Its major drawback is its poor compressive strength. Type AS graphite fiber in a Hercule's 3501 epoxy matrix is used for those components requiring a greater degree of stiffness or compressive strength than is available with Kevlar 49. The graphite/epoxy system is used also for those perforated inner flowpath skins with high degrees of porosity which obviated the use of Kevlar 49 due to manufacturing difficulties; laser drilling is used in these cases to manufacture the perforations rather than molding them in place. In areas where only a moderate strength, moderately stiff material is required, E293/7581 fiberglass fabric is used for a cost reduction.

For the core cowl, which must operate at elevated temperatures, woven graphite fabric HMF182HC/66 impregnated with PMR15 polyimide resin is used allowing long-term operation at 561 K (550° F).

The honeycomb core material in the low-temperature areas is flexible honeycomb made from 5052 aluminum foil coated for corrosion protection. For the higher temperature in the core cowl, HRH327 glass/polyimide honeycomb core is used. The honeycomb core in the acoustically treated panels is slotted to provide drainage.

The metal fittings in the lower temperature areas are machined from 2024-T351 aluminum bar or plate and for corrosion protection are chemical conversion treated per MIL-C-5541 and coated with epoxy primer. All hinge and clevis pin holes have AMS 5616 corrosion-resistant steel bushings. In the higher temperature regions, the fittings are AMS 5604 corrosion-resistant steel weldments.

The basic materials properties are taken from a variety of sources. The sources are as follows:

Material	Source
Kevlar 49/epoxy	E.I. du Pont de Nemours & Co.
Graphite/epoxy	Advanced Composites Design Guide
Graphite/polyimide	General Electric Co.
Fiberglass/epoxy	MIL-HDBK-17A
5052 aluminum honeycomb	Hexcel
2024 aluminum	MIL-HDBK-5
AMS 5616 steel	General Electric Co.
AMS 5604 steel	General Electric Co.

The specific nacelle components which utilize composite materials are the inlet, fan bypass duct, variable-fan exhaust nozzle flaps, and the core cowl. These are discussed individually in the following sections.

3.3.2 Inlet

The acoustically treated inlet is the largest single component of the overall UTW nacelle structure, being 184.07-cm (72.74-in.) long and 200.15 cm (78.8 in.) in diameter as shown in Figure 8. To reduce the weight of this large structure as much as possible, it was constructed mainly of lightweight Kevlar/epoxy material and the acoustic treatment was incorporated as part of the permanent structure.

The basic structural elements of the inlet are shown in Figures 8 and 9. It consists primarily of inner and outer honeycomb-sandwich walls separated and supported by circumferential stiffeners. The face sheets of these sandwiches are made from Kevlar/epoxy. The inner skin of the inner wall is perforated with hole configurations that satisfy the acoustic requirements of the inlet. The inner wall thickness (honeycomb depth) was established early during design to encompass all probable acoustic requirements. This allowed the majority of the inlet pieces to be fabricated prior to the final determination of the acoustic requirements. After final determination of the required honeycomb depths, fiberglass/epoxy septum skins were incorporated into the inner wall design to establish the required depths, with the overall inner wall thickness being maintained as previously designed. This is shown in Figure 10. In the flight design, the inner wall thickness would be stepped to be consistent with the acoustic requirements, thereby eliminating the septum skin. At the aft end, where the inner and outer walls are in close proximity, they are separated by a low, wide bulkhead of fiberglass/epoxy laminations designed to transmit axial shear loads between the two walls. The remaining space between the walls is filled with dry, woven Kevlar fabric layered to fill the void so as to provide containment capability in case of a fan blade failure. Fiberglass end caps complete the wall ties and close out the wall honeycomb cores. The honeycomb core is Hexcel aluminum flexcase, coated for corrosion protection.

Provisions for engine ground-testing instrumentation, as well as control sensor requirements, are included in the experimental design. Figure 9 shows some of the instrumentation support installations. When instrumentation is not required, combination wall plugs and covers are provided. These are shown in Figure 11.

Provision for inlet leading edge anti-icing is not included in the experimental engine inlet design. As a result the leading edge is fabricated from fiberglass/epoxy materials. In a flight-engine design the leading edge would be titanium to provide anti-icing capability and to increase resistance to foreign object damage and erosion. A sketch of this concept is shown in Figure 12. A corrugated backup sheet would provide passages for the anti-icing airflow. This arrangement offers the advantages of isolating the anti-icing air from the composite material and containing the flow for effective transfer and minimum air usage.

Aerodynamic loading of the inlet is far more significant than inertia loading. The primary reason for this is the large transverse load reacting on the inlet as it turns the entering engine airflow at flight conditions where

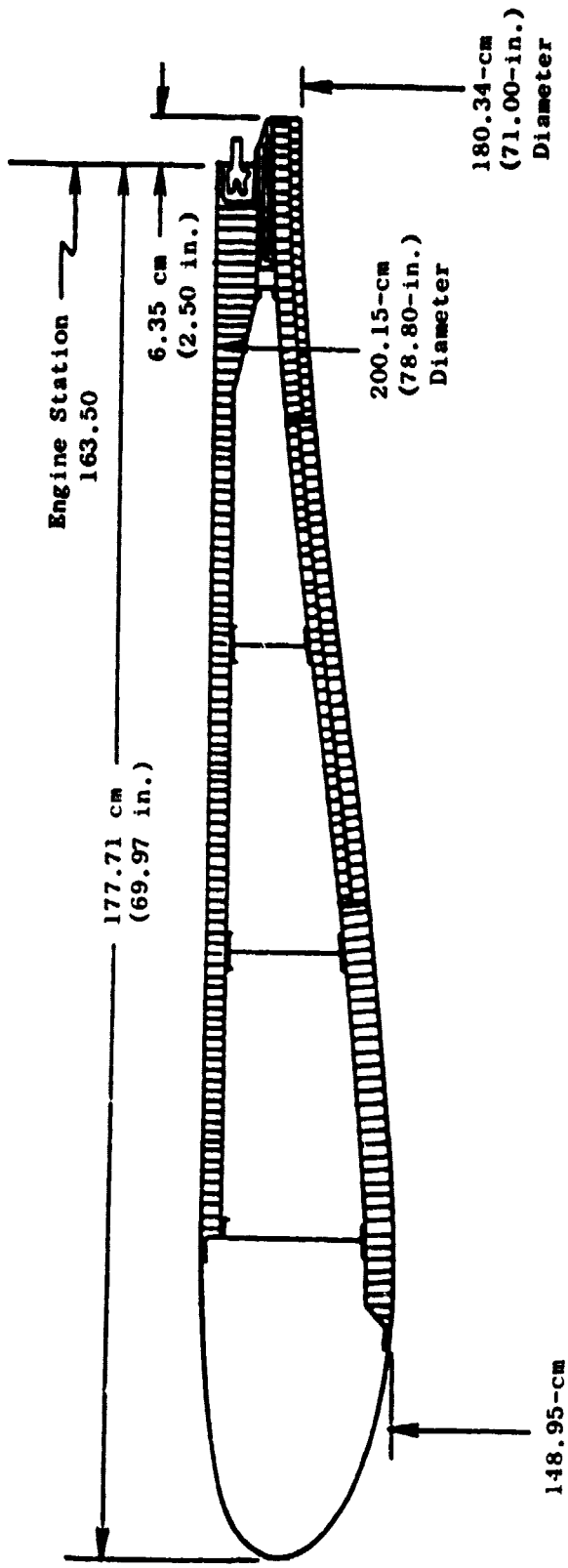

Figure 8. QCSEE Inlet Axial Cross Section.

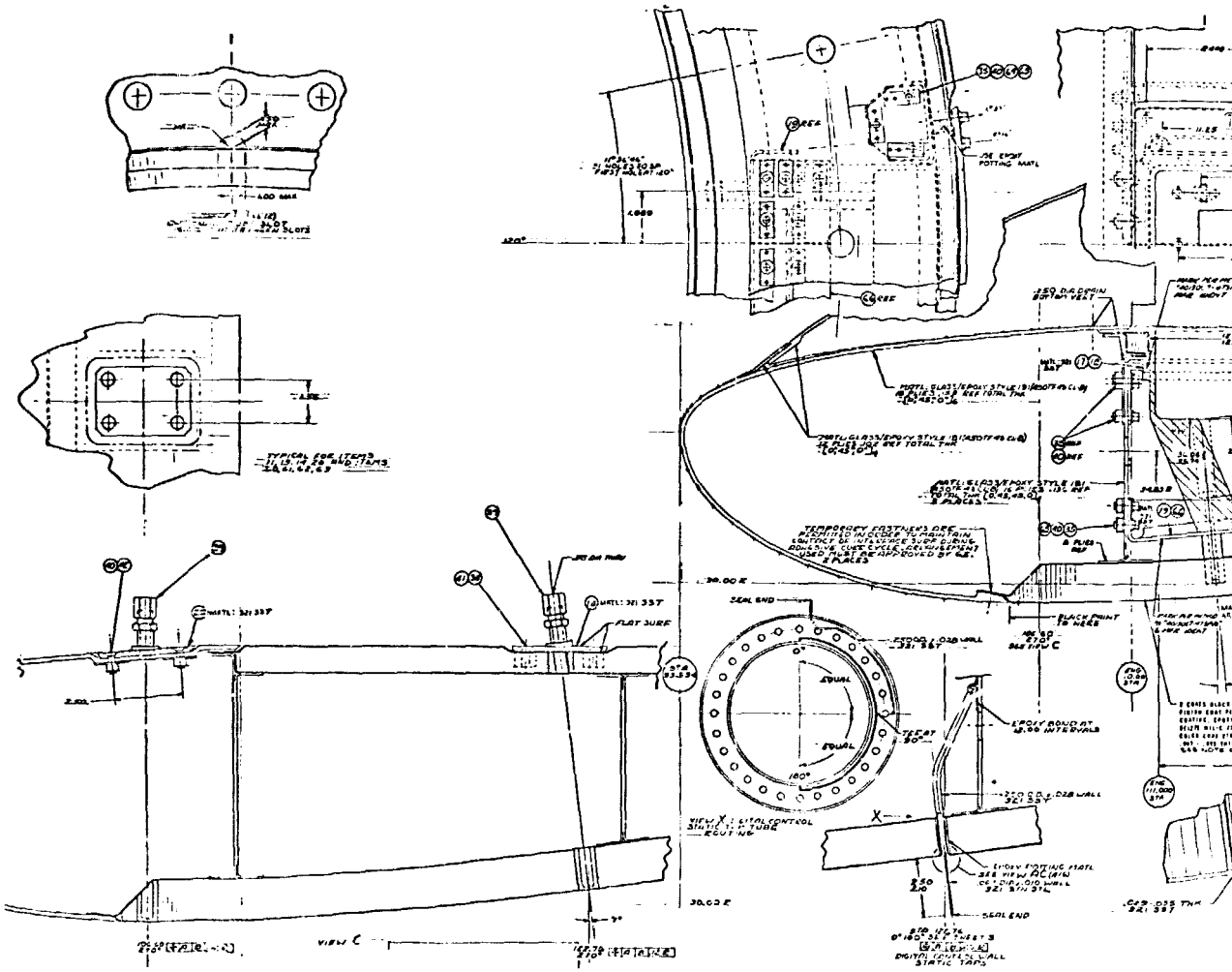

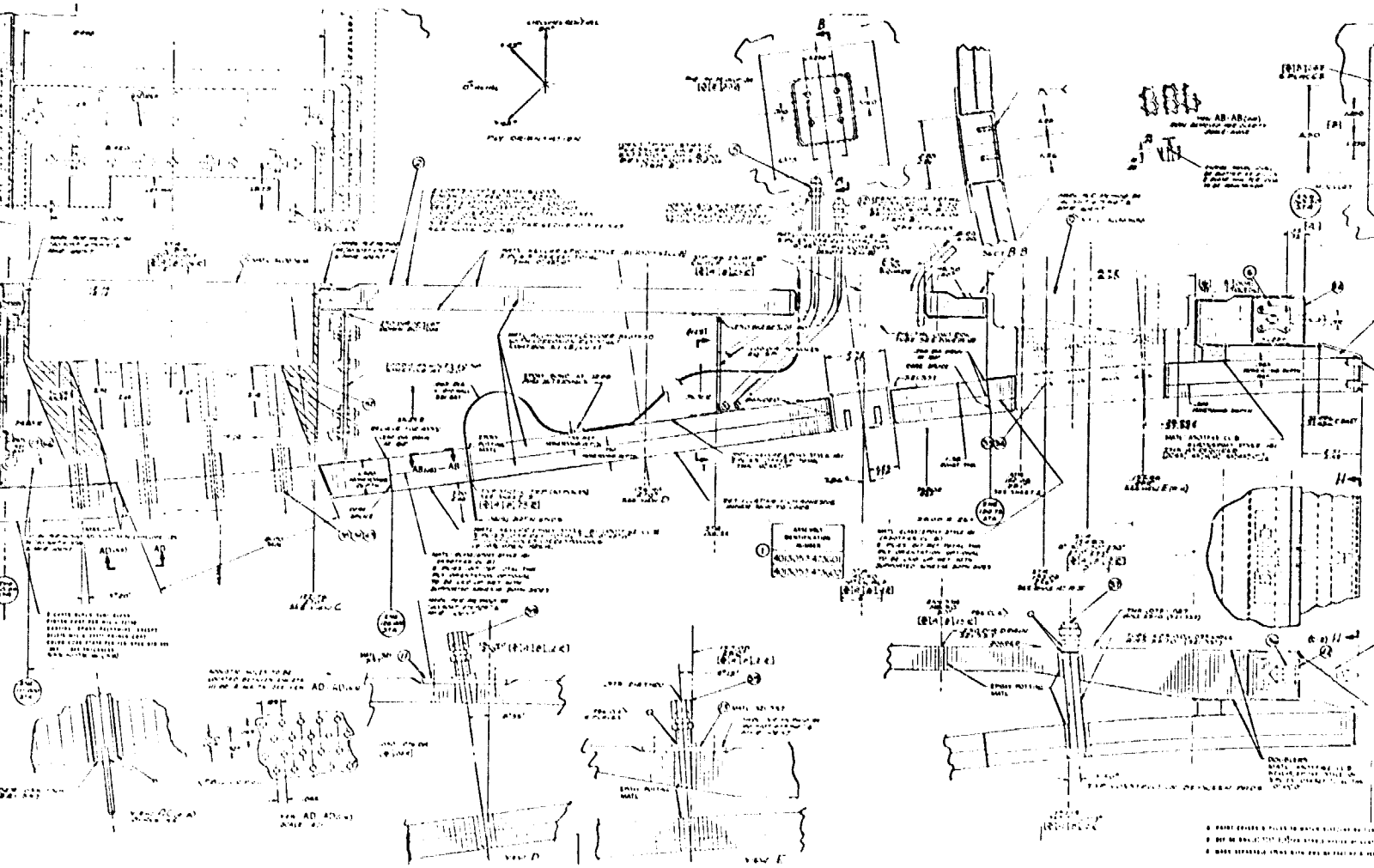

Figure 9. QCSEE Inlet.

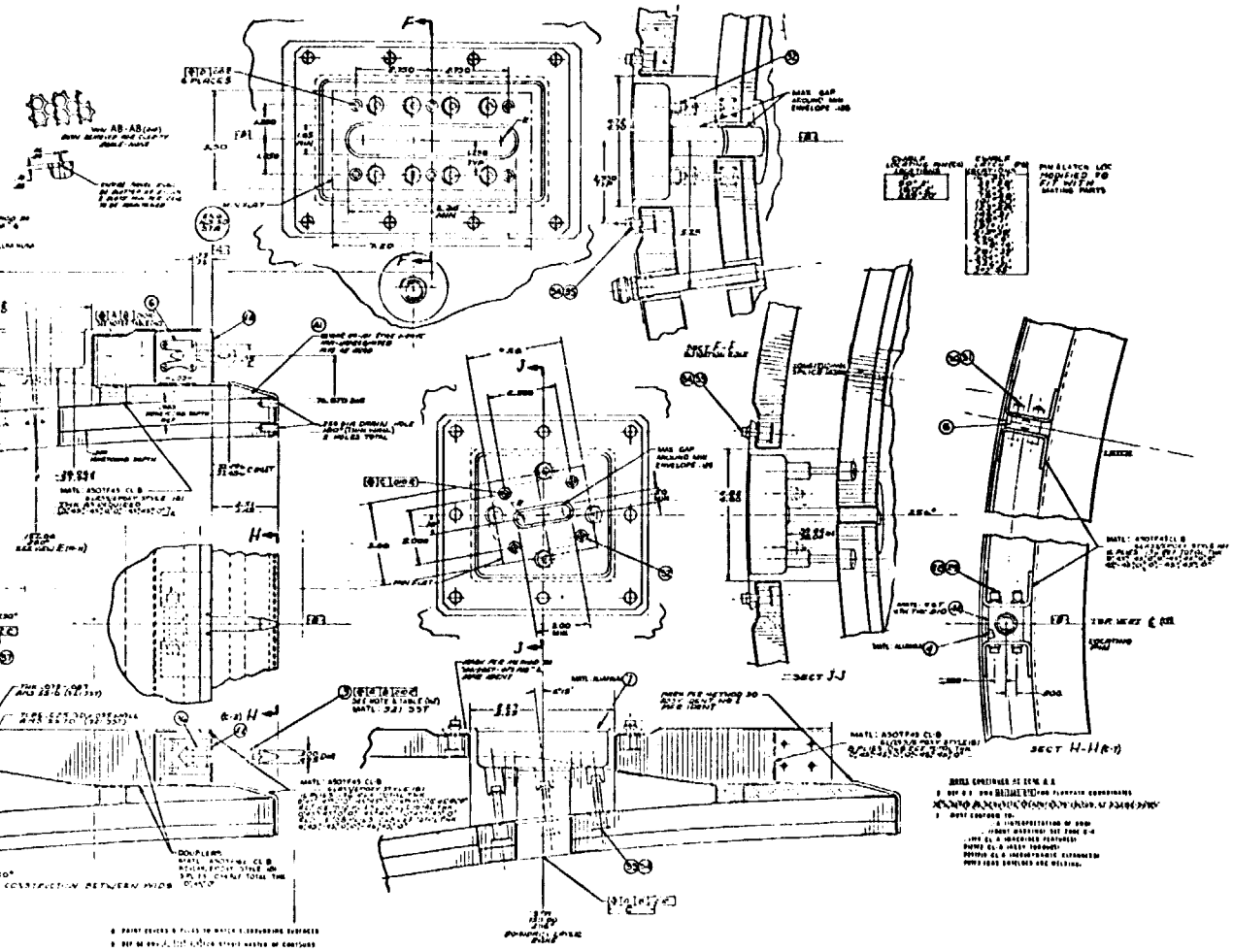

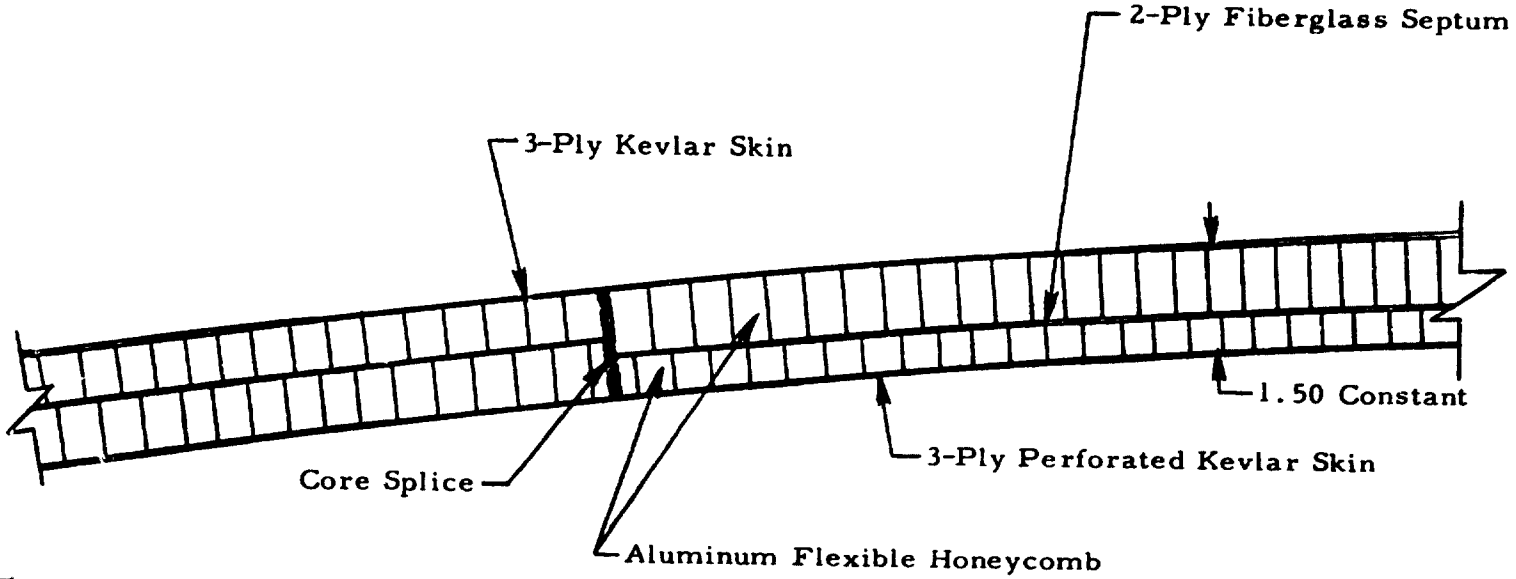

Figure 10. Inlet Inner Wall Configuration.

FOLDOUT FRAME

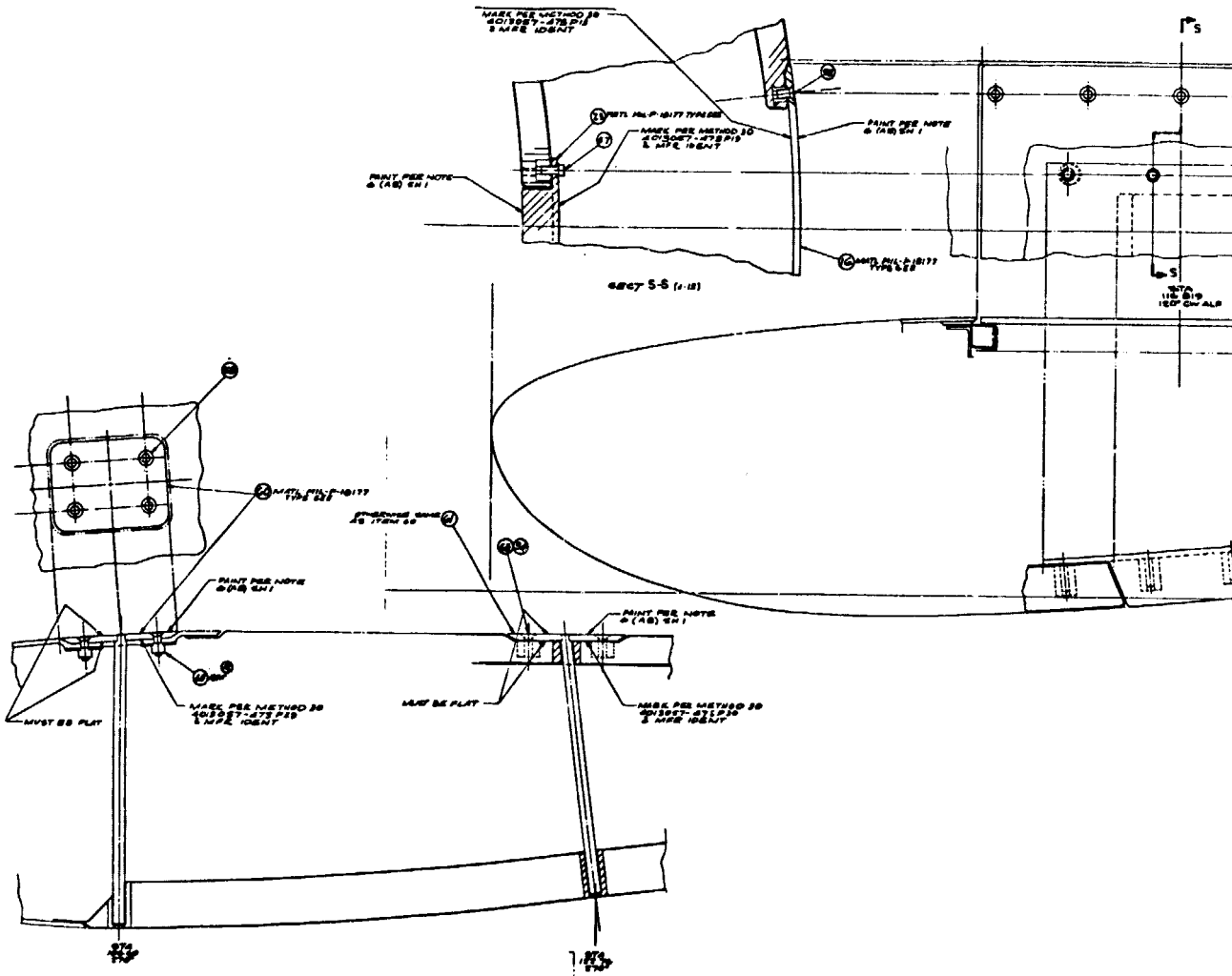

Figure 11.

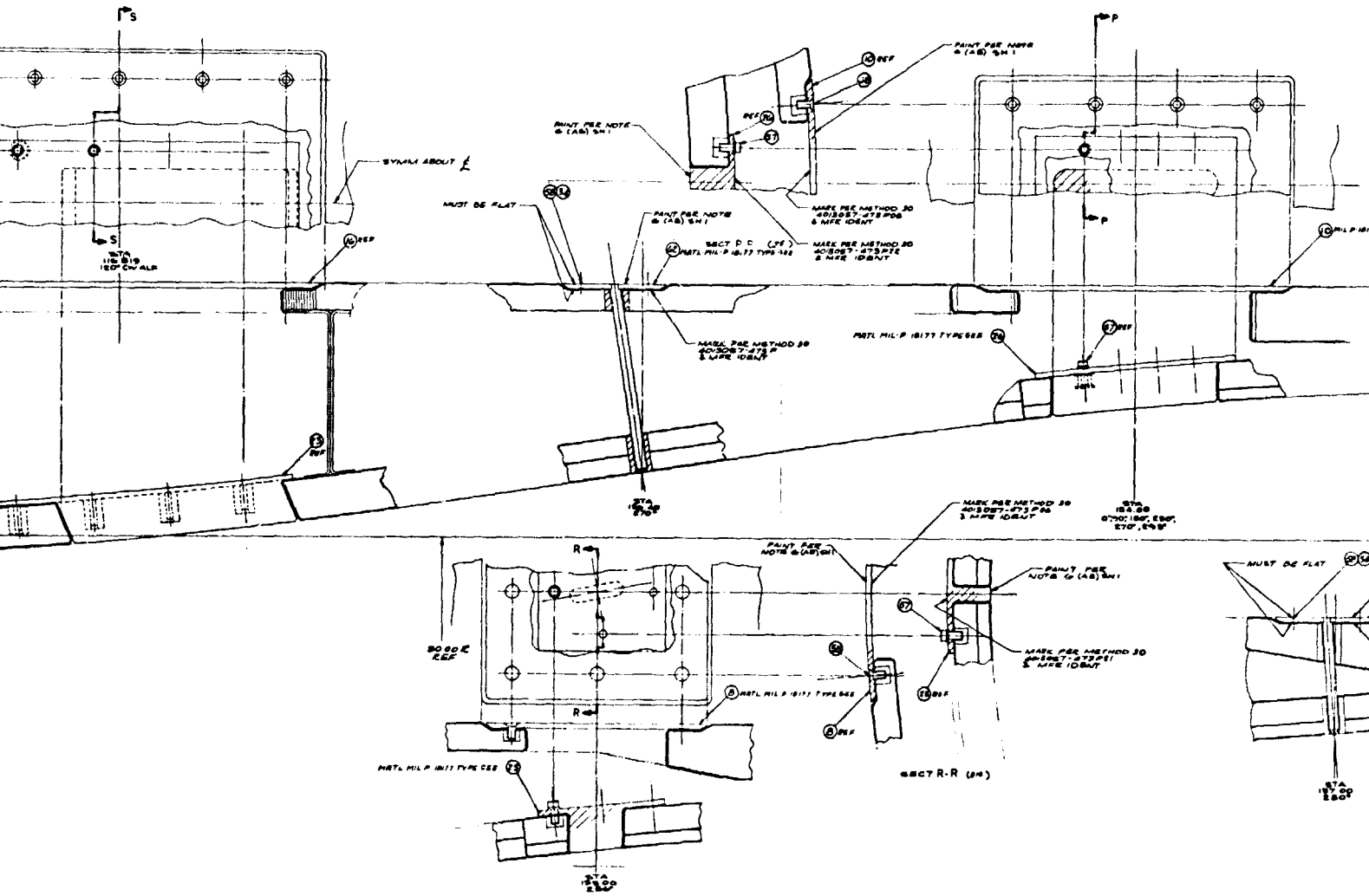

Figure 11. Inlet Instrumentation Plugs.

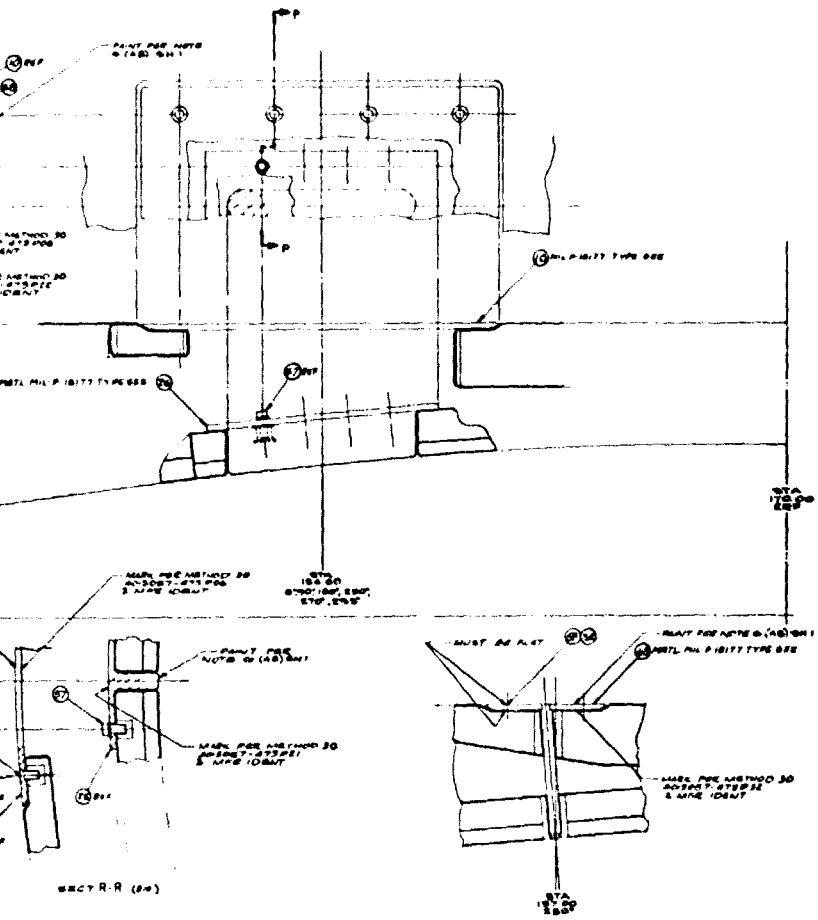

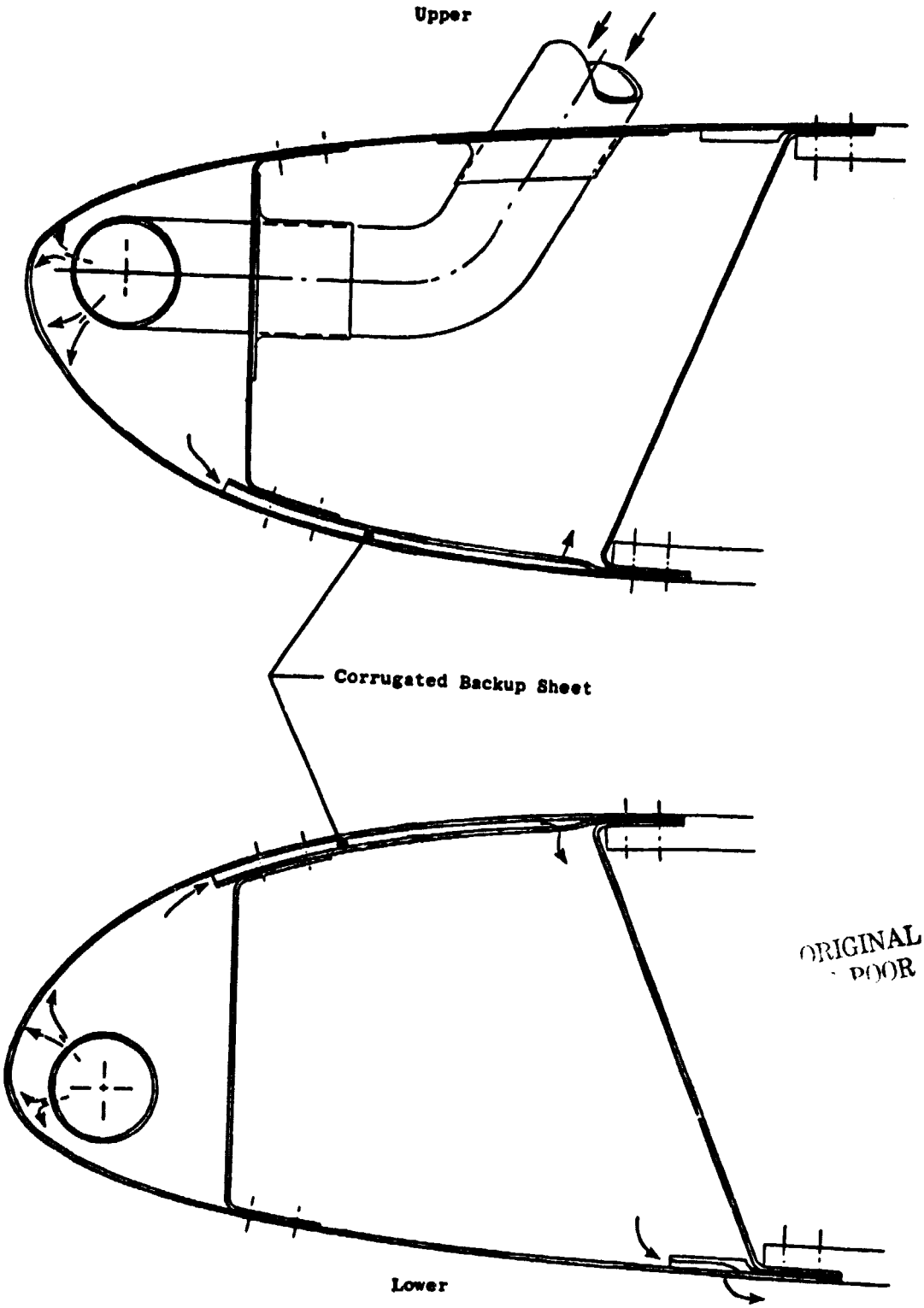

Figure 12. Inlet Anti-Icing Schematic.

the direction of the free-stream air is not parallel to the inlet axis. In contrast, the lightweight structure of the inlet produces relatively low inertia loads. The most severe aerodynamic loads occur during a 3-g aircraft stall at Mach 0.4 (sea level) and with the engine operating at maximum continuous power, as shown in Table III. For design analysis, the loads resulting from this condition were combined with the most severe additive inertia loads caused by dynamic loading. In addition, compressive hoop loads were considered for the sea level static takeoff power operating condition. The stress levels of these loads and this construction are shown in Table III. These are based on each facing consisting of three plies of woven Kevlar/epoxy material giving a total face sheet thickness of 0.084 cm (0.033 in.). Buckling allowables for this construction are shown in Table IV. The sensitivity of this configuration to local loads is shown in Figure 13. The fiberglass inner wall stiffeners are made from two 0.173-cm (0.068-in.) thick continuous channel rings bonded back-to-back to form an "I" cross section. These are pierced with a number of small-diameter holes, principally for the passage of instrumentation leads and to aid in the manufacturing assembly process. The stiffeners' flanges were designed to prevent the bearing load between the stiffener flange and sandwich wall from exceeding 2482 kPa (360 psi). This resulted in a minimum flange width of 1.55 cm (0.61 in.). In a flight design, these stiffeners would be made lighter in weight with integral stiffening beads and large lightening holes.

The inlet attaches to the fan frame by means of 16 rotary latches. Each of these latches is operated by turning a flush receptical. Analysis has established that the minimum latch factor of safety is greater than one, even with six latches left open. The latch loads for this installation are shown in Table V. A pressure and acoustic seal is achieved at this joint by means of a chevron elastomer gasket, the gasket being mounted in the fan frame and seating against the inlet aft closeout. A rabbeting diameter centers the inlet on the fan frame and four tapered pins align the inlet circumferentially. Figure 14 shows this joint design.

As can be seen from the analysis, the inlet is not highly stressed. The skin thicknesses selected were estimated minimum gages required for load-impact resistance during handling and engine maintenance.

The composite inlet described above weighs 150 kg (330 lb) in a flight configuration (minus experimental instrumentation) compared to 217 kg (479 lb) for a typical current technology metal inlet scaled to the same size.

Table III. Inlet Stresses and Deflections at Maximum Combined Load Conditions.*

Load			Stress				
Type	Magnitude	Direction	Type	Calculated MPa (psi)	Allowable MPa (psi)	Safety Factor	Deflection cm (in.)
Bending	69,317 N.m (613,423 in.-lb)	---	Compression	14.0 (2,034)	123.8 (17,950)	7.8	0.058 (0.023)
Axial	8,358 (1,879 lb)	Forward	Tension	15.8 (2,296)	271.0 (39,300)	16.1	
Transverse	37,120 N (8,345 lb)	---	Shear	4.0 (584)	60.3 (8,750)	14.1	0.414 (0.163)
Hoop	0.03 MPa (4.0 psi)	Burst	Tension	18.1 (2,620)	271.1 (39,300)	14.0	
(Max. Range Expected)	0.06 MPa (8.5 psi)	Crush	Compression	40.0 (5,672)	123.8 (17,950)	2.2	

*Derived from DAC "Design-to" Criteria. Aerodynamic loads from 3-g stall (M_o = 0.4 at SL) combined with inertia loads from dynamic landing.

Table IV. Critical Buckling Loads.

A. Buckling from Bending	Critical Moment		Actual Max. Moment		Safety
Load Conditions	N.m	(in.-lb)	N.m	(in.-lb)	Factor
Moment on Outer Skins	4,556,680	(40,329,928)	69,308	(613,423)	65.7
B. Buckling from Compressive Hoop Load					
Load Conditions	Critical Pressure		Actual Pressure		Safety
	kPa	psi	kPa	psi	Factor
Pressure supported by a single sandwich wall (2 skins) between 33.94 cm (13 in.) apart	1,538	(223)	58.6	(8.5)	26.2
Pressure supported by overall wall structure	2,751	(399)	58.6	(8.5)	46.9
Pressure supported by single fiberglass nose wall 0.39-cm (0.153-in.) thick	121	17.6	48.3	(7.0)	2.5

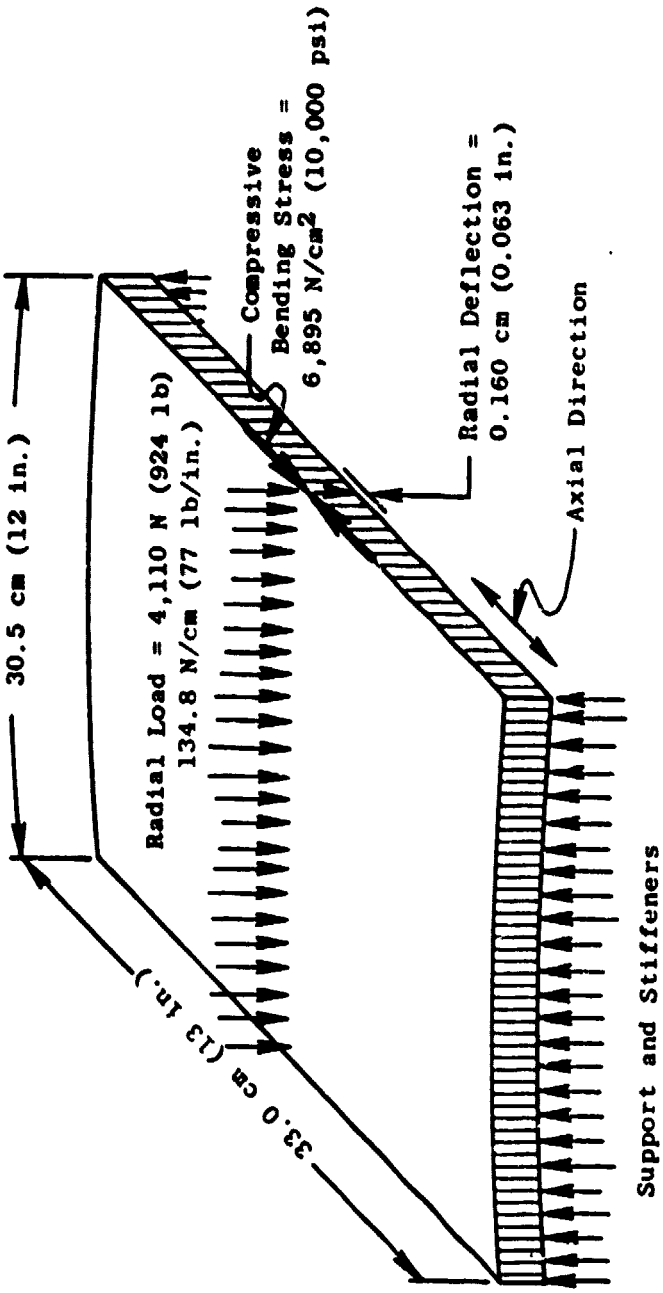

Figure 13. Inlet Wall Local Load Resistance.

Table V. Inlet Latch Loads.

(at Maximum Combined Load Conditions)

Latch Configuration	Maximum Latch Load		Ultimate Latch Strength		Latch Safety Factor
	N	(lb)	N	(lb)	
All 16 Latched	9,617	(2,162)	28,800	(6,475)	3.00
One Latch Open	10,737	(2,414)	28,800	(6,475)	2.68
Two Latches Open	13,135	(2,953)	28,800	(6,475)	2.19
Six Latches Open	25,073	(5,637)	28,800	(6,475)	1.15

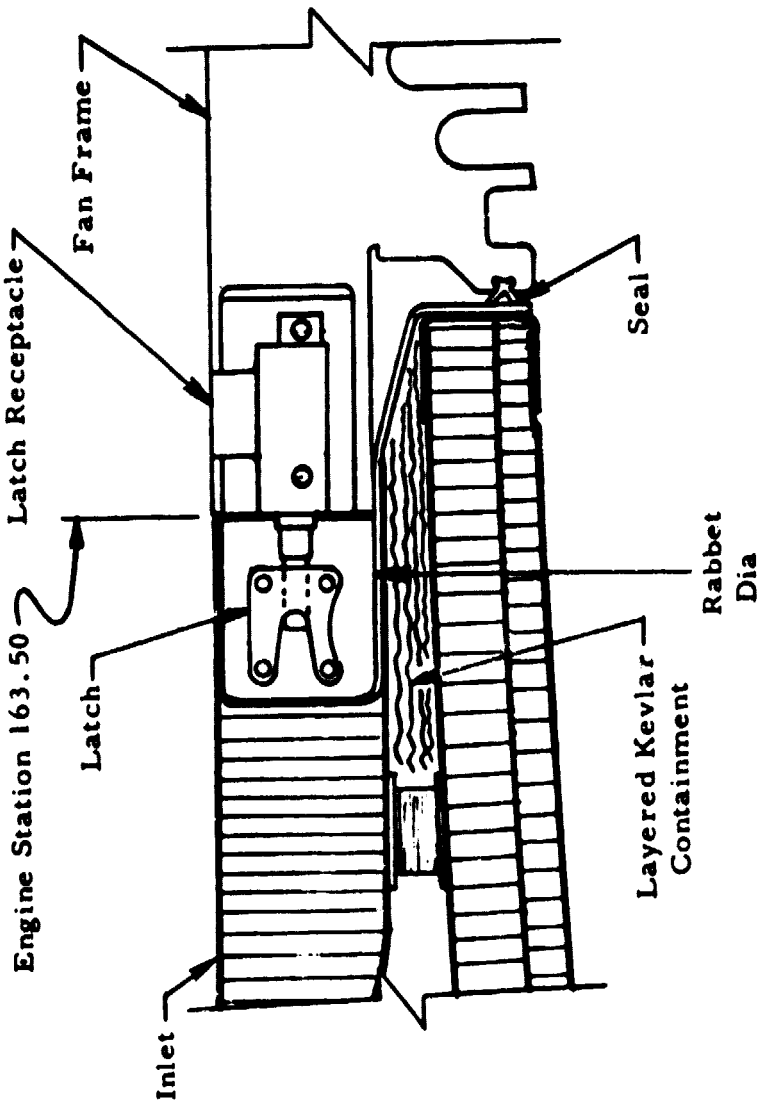

Figure 14. Inlet/Fan Frame Joint.

3.3.3 Fan Bypass Duct

The fan bypass duct and fan nozzle constitute the outer nacelle section aft of the fan frame. Figure 15 shows a cross section through the outer nacelle. The fan bypass duct is designed to take full advantage of advanced-type composite materials in order to provide a lightweight, thin profile nacelle suitable for advanced air transports.

The fan bypass duct is composed of two semicircular door sections, one each side of the vertical centerline. Figure 16 shows a rollout view of the outer surface of the two duct doors; Figures 17 and 18 show the completed product. Each door is fastened along its intersection with the aircraft outer pylon to the pylon by means of a segmented piano hinge and is sealed to the pylon as shown in Figure 19. The two cowl doors are fastened together along the bottom split line by seven toggle-type latches; the joint is sealed against acoustic and pressure loss by means of a chevron cross section elastomer gasket. Figure 20 shows a cross section through this joint. The piano hinges and latches allow the cowl doors to be opened for accessibility to the core engine and for engine installation and removal. The outer duct hoop loads are transmitted through the piano hinges to the pylon. A series of inward-facing radial lug segments are attached to the bypass duct door forward "closeout" rings. The lugs are tapered on the forward-facing surface and have a vertical aft face. These lugs engage a matching groove in the fan frame when the doors are closed, the tapered surfaces serving to aid in the engagement when closing the duct doors. The door piano hinges are made with a suitable amount of axial free play so as not to interfere with the engagement of the lugs with the fan frame groove. Once the bypass duct bottom latches are engaged, all axial duct loads are transmitted through the lugs into the fan frame and, hence, to the engine mounts. A chevron-type elastomer gasket also seals this joint against acoustic and pressure transmission. Figure 21 shows a cross section through this joint. The duct doors aft "closeout" ring is a channel section open in the aft direction. Located within this channel are a series of aluminum clevises which are attached to the door by radially oriented flush fasteners. These clevises are the door side of the fan nozzle flap hinges. Fastened to the aft end of the inner leg of the door closeout channel is a formed urethane molding which serves as a sealing surface for the nozzle flap circumferential gasket during the forward thrust mode. A cross section through this interface is shown in Figure 22.

Located in the outer surface of each bypass duct door are three cavities which house the fan nozzle actuators. Installation of the actuator cavity pans prior to assembly of the outer skin are shown in Figure 23. Located at the forward end of each cavity is a clevis-type mount which engages a spherical ball connection in the end of each actuator. The cavities are enclosed by flared covers which protrude above the outer nacelle flowpath and which are designed for minimum aerodynamic drag. At the forward end, the covers engage pins in the actuator mounts for transmitting the mount overturning moment loads back to the bypass duct in an efficient manner. Actuator slider guides are located at the aft end of the cavity and cover, with passageways through the duct aft closeout for the actuator to fan nozzle flap links. Figure 24 shows the mount and slider design in cross section. Tunnels internal to the

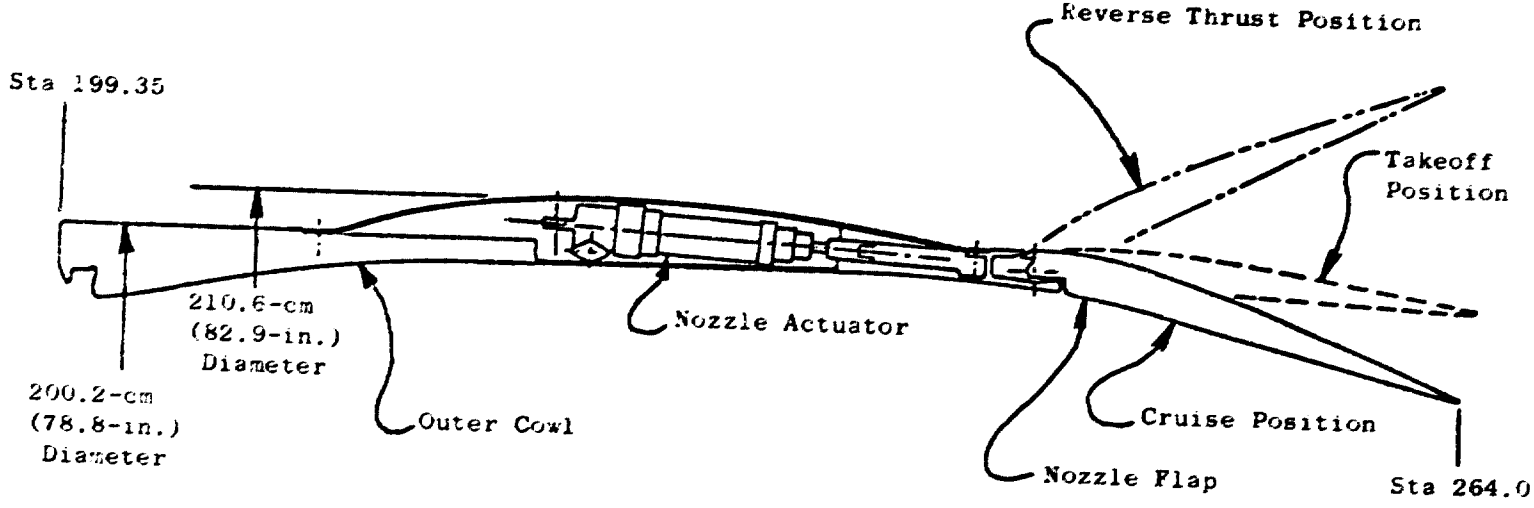

Figure 15. Outer Cowl Cross Section.

FOLDOUT FRAME

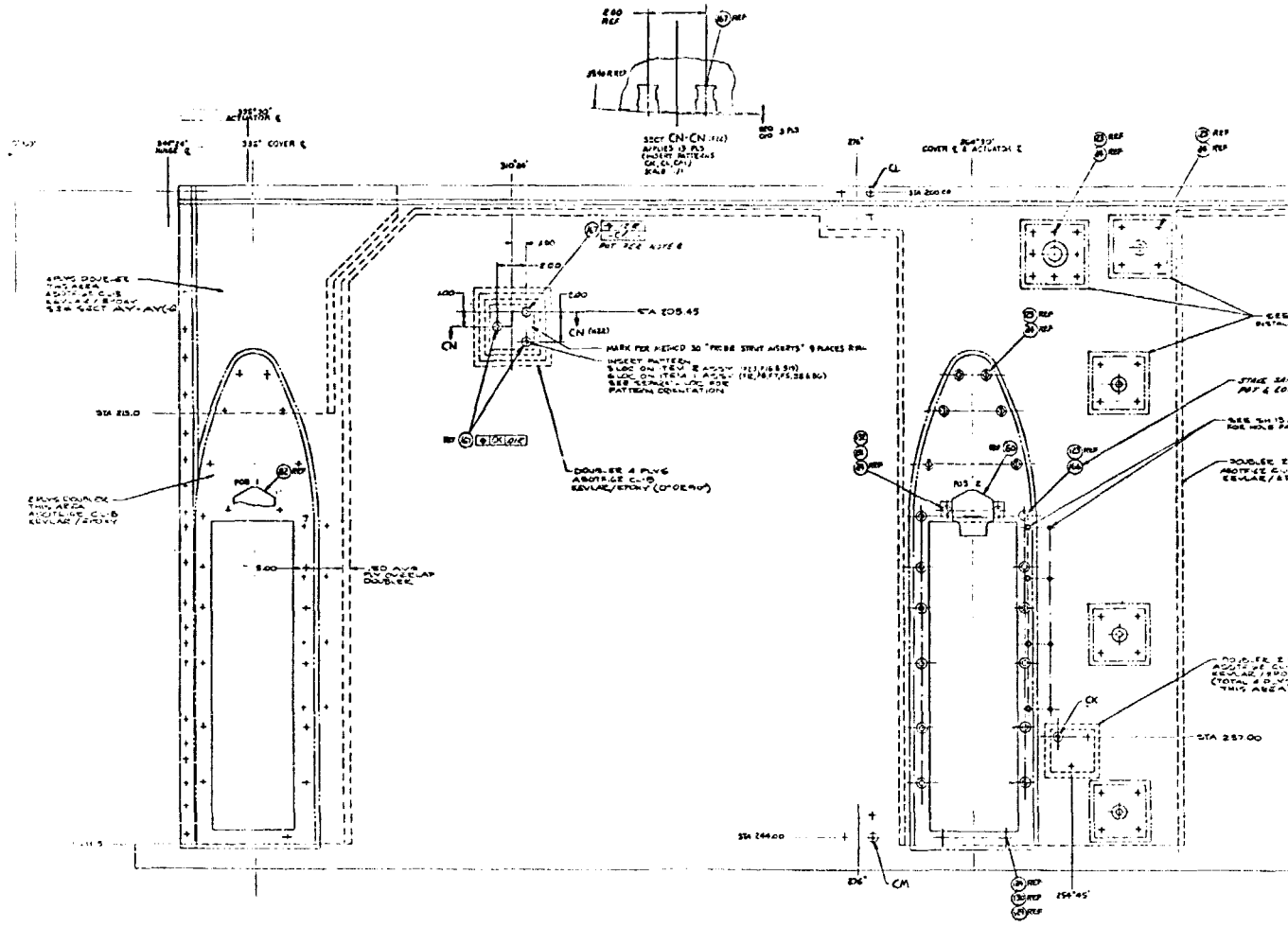

FOLDOUT FRAME 2

ORIGINAL PAGE IS
OF POOR QUALITY

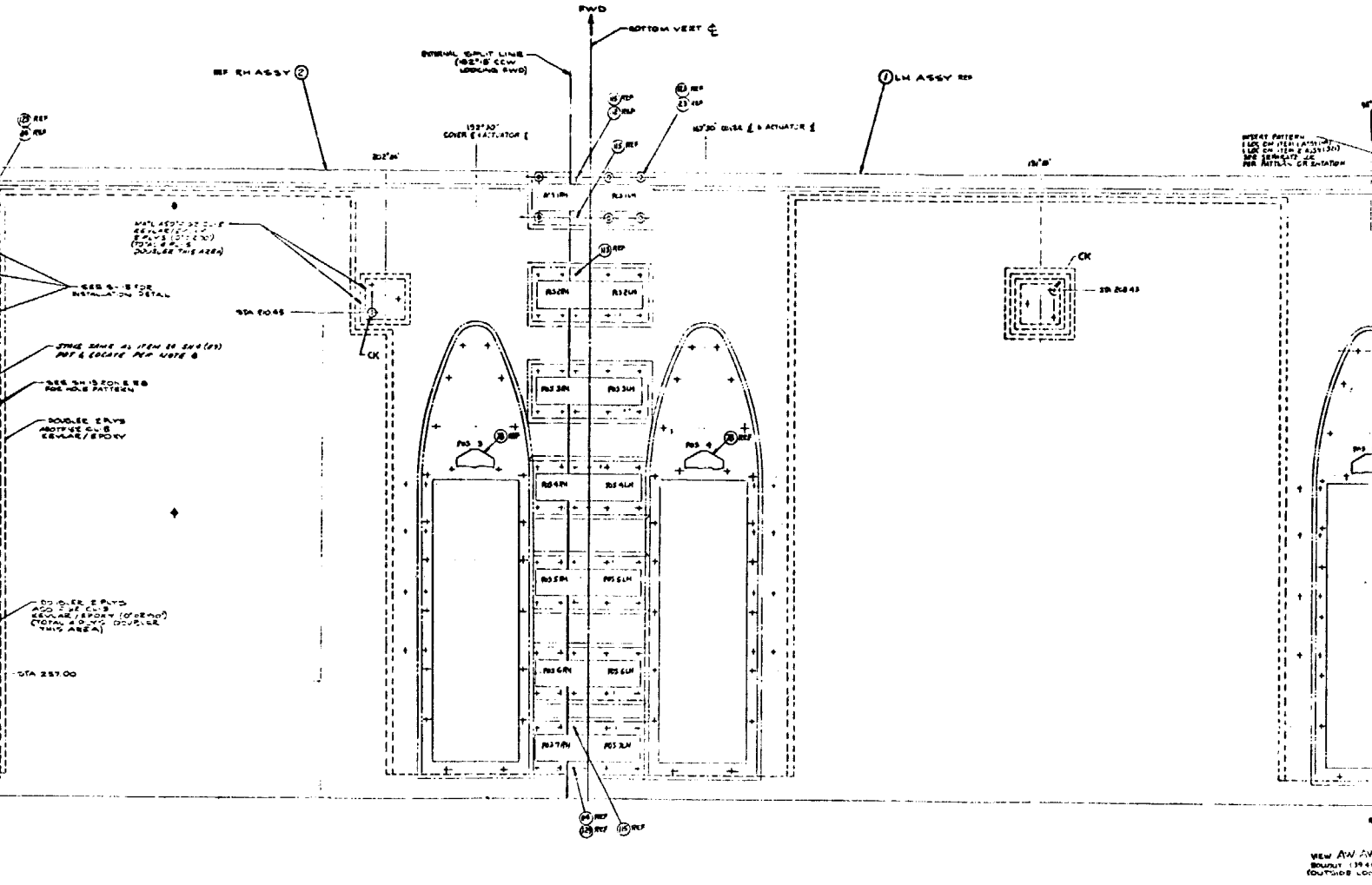

Figure 16. Bypass Duct Outer Surface Rollout.

...OUT FRAME 3

ORIGINAL PAGE IS
OF POOR QUALITY

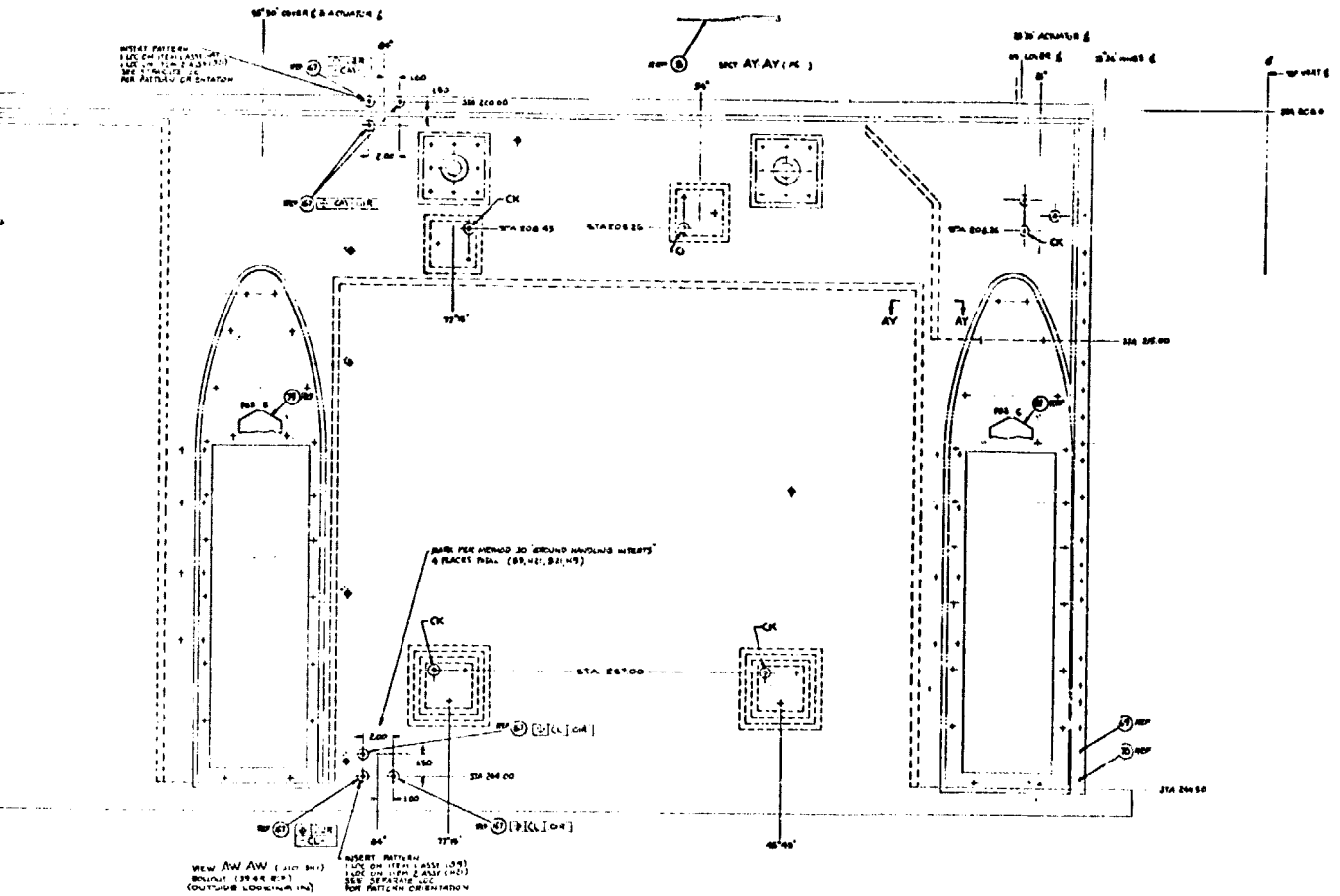

PRECEDING PAGE BLANK NOT F...

Figure 17. Bypass Duct, Piano Hinge View.

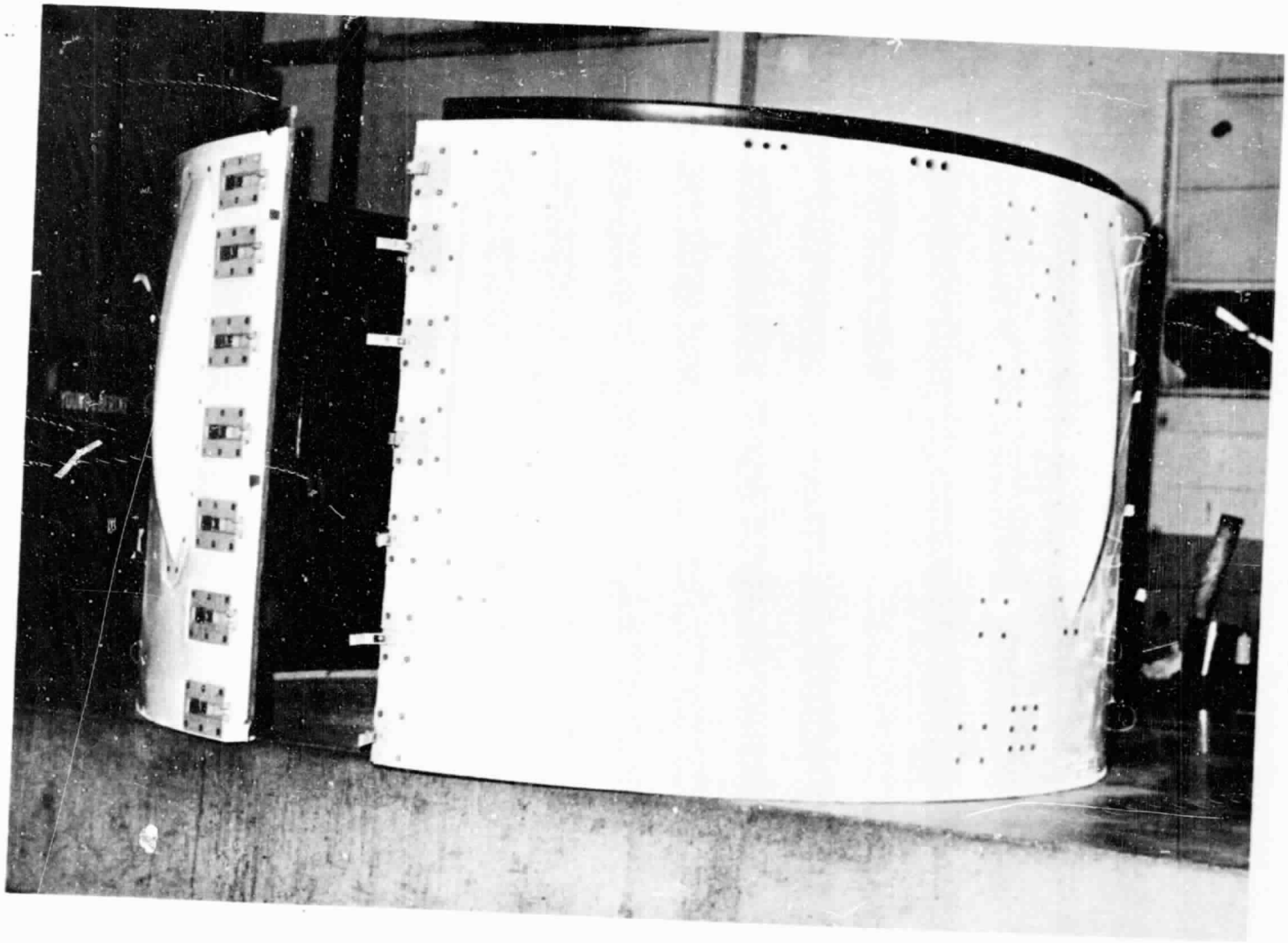

Figure 18. Bypass Duct, Bottom Latch View.

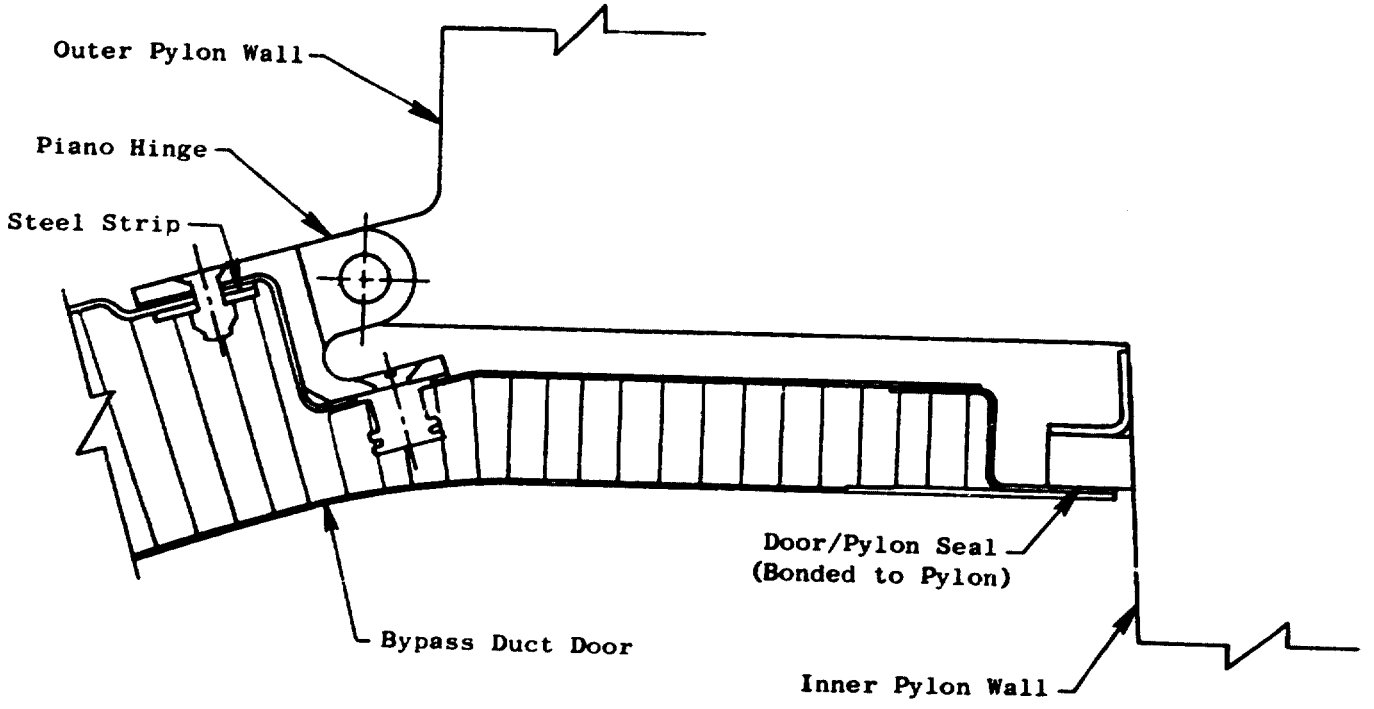

Figure 19. Bypass Duct/Pylon Installation.

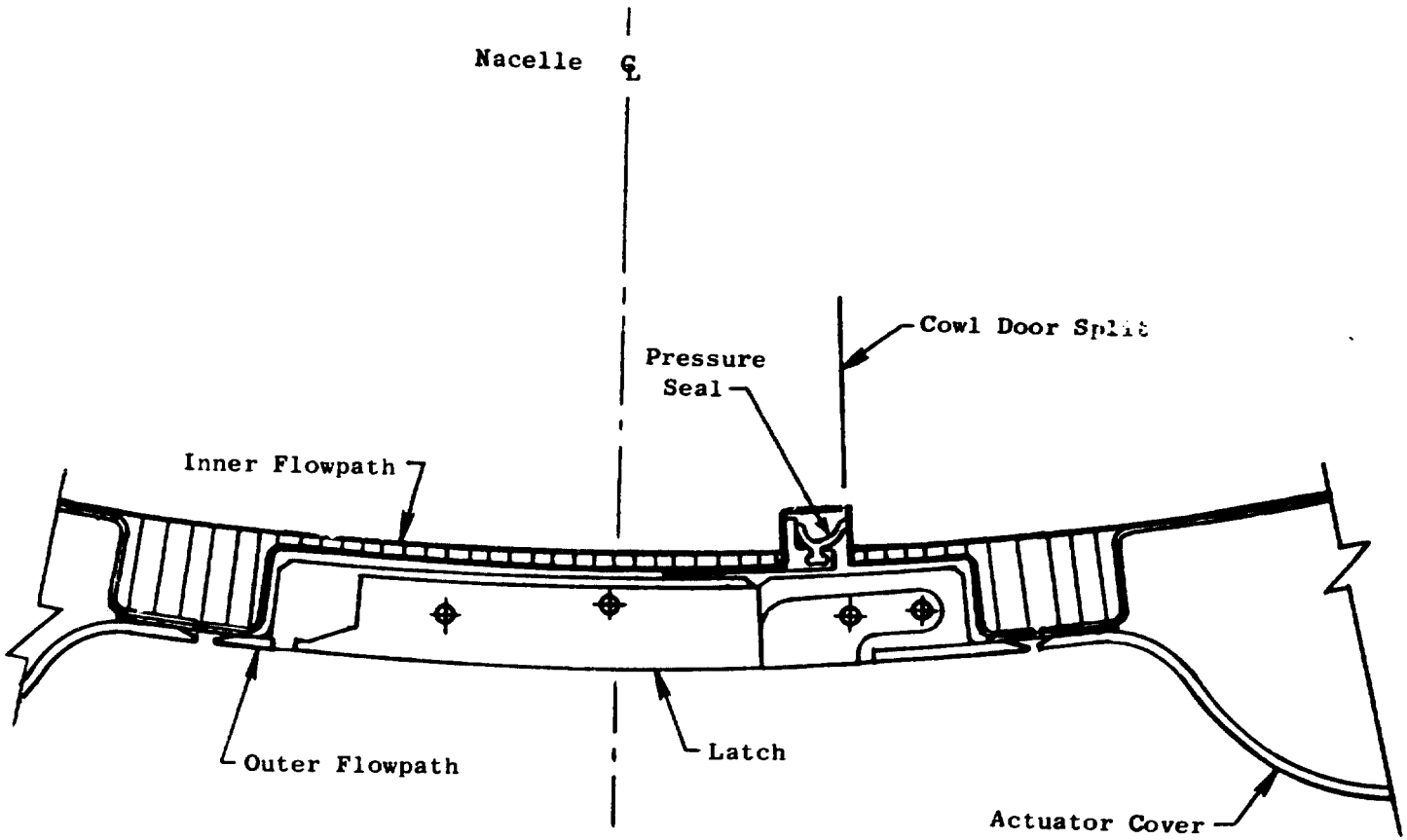

Figure 20. Bypass Duct/Latch Installation.

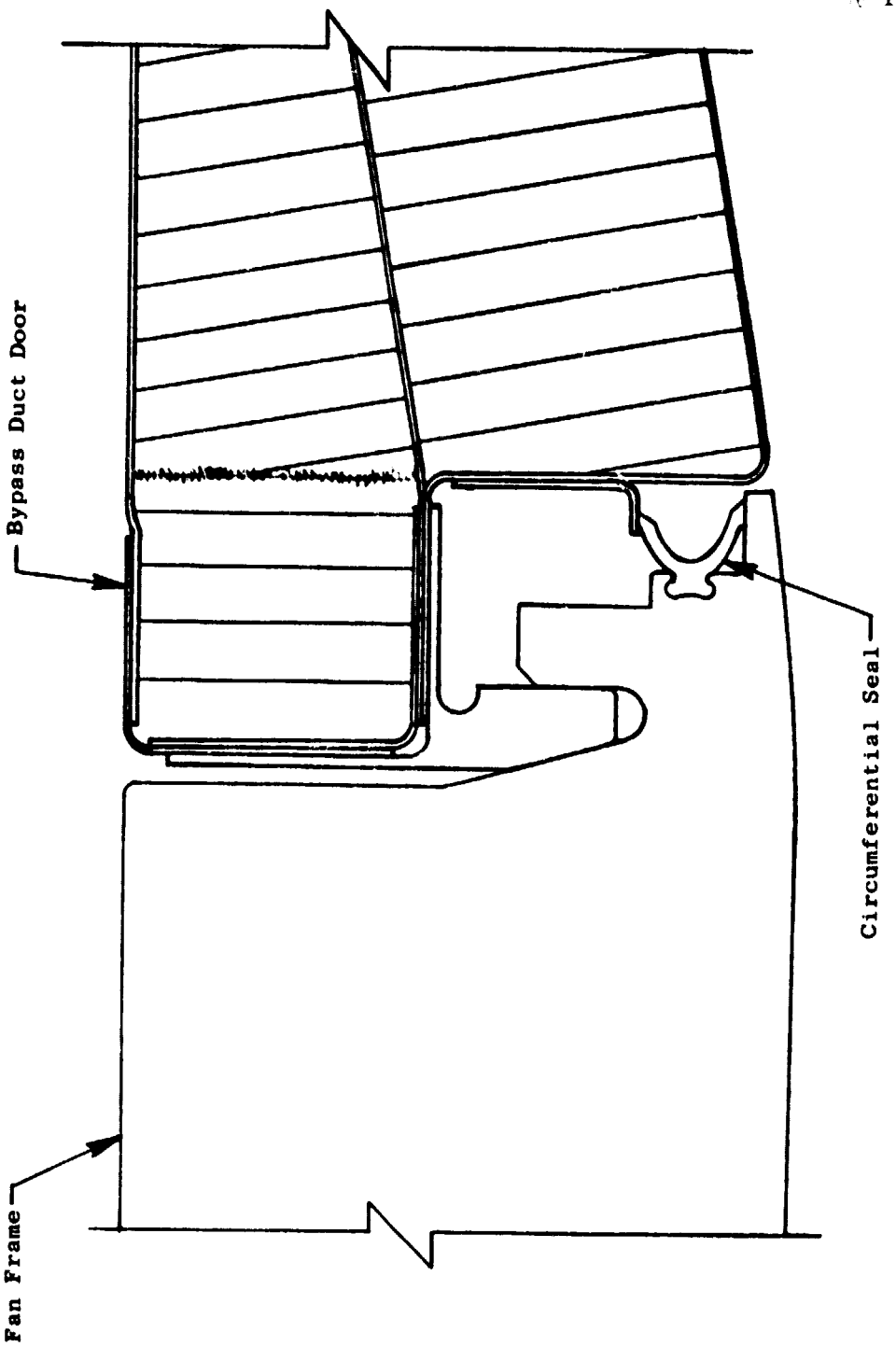

Figure 21. Bypass Duct/Fan Frame Attachment.

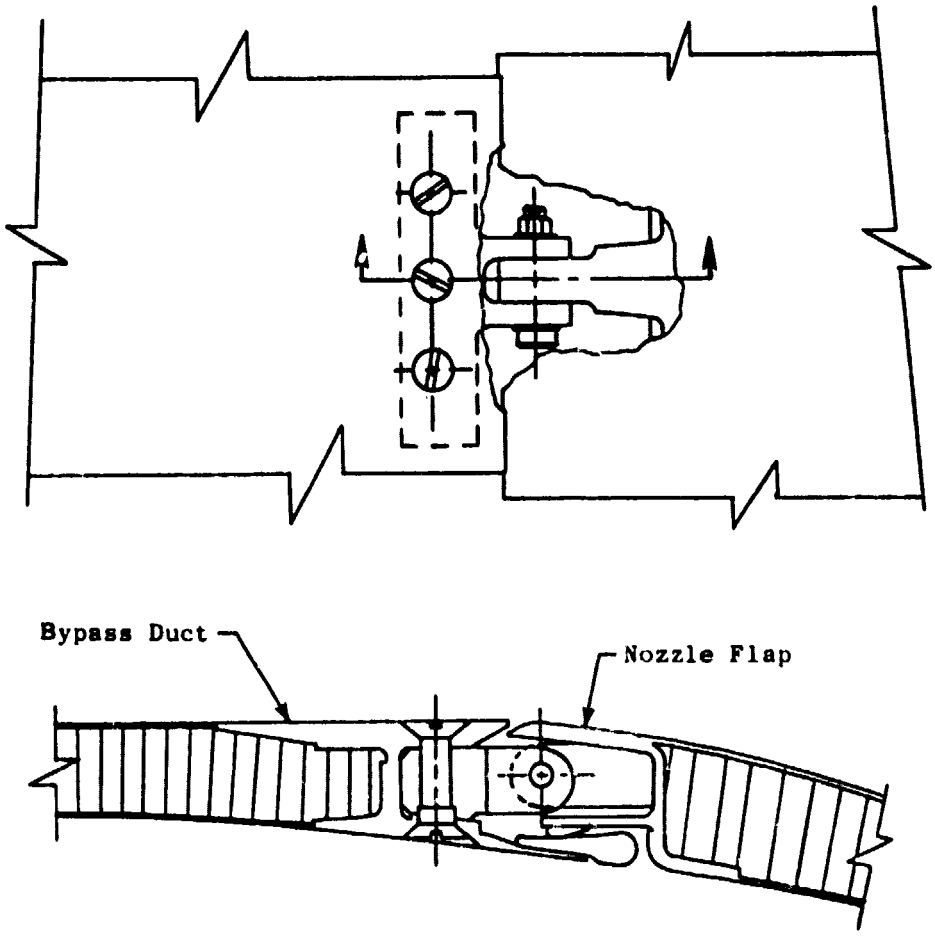

Figure 22. Bypass Duct/Fan Nozzle Attachment.

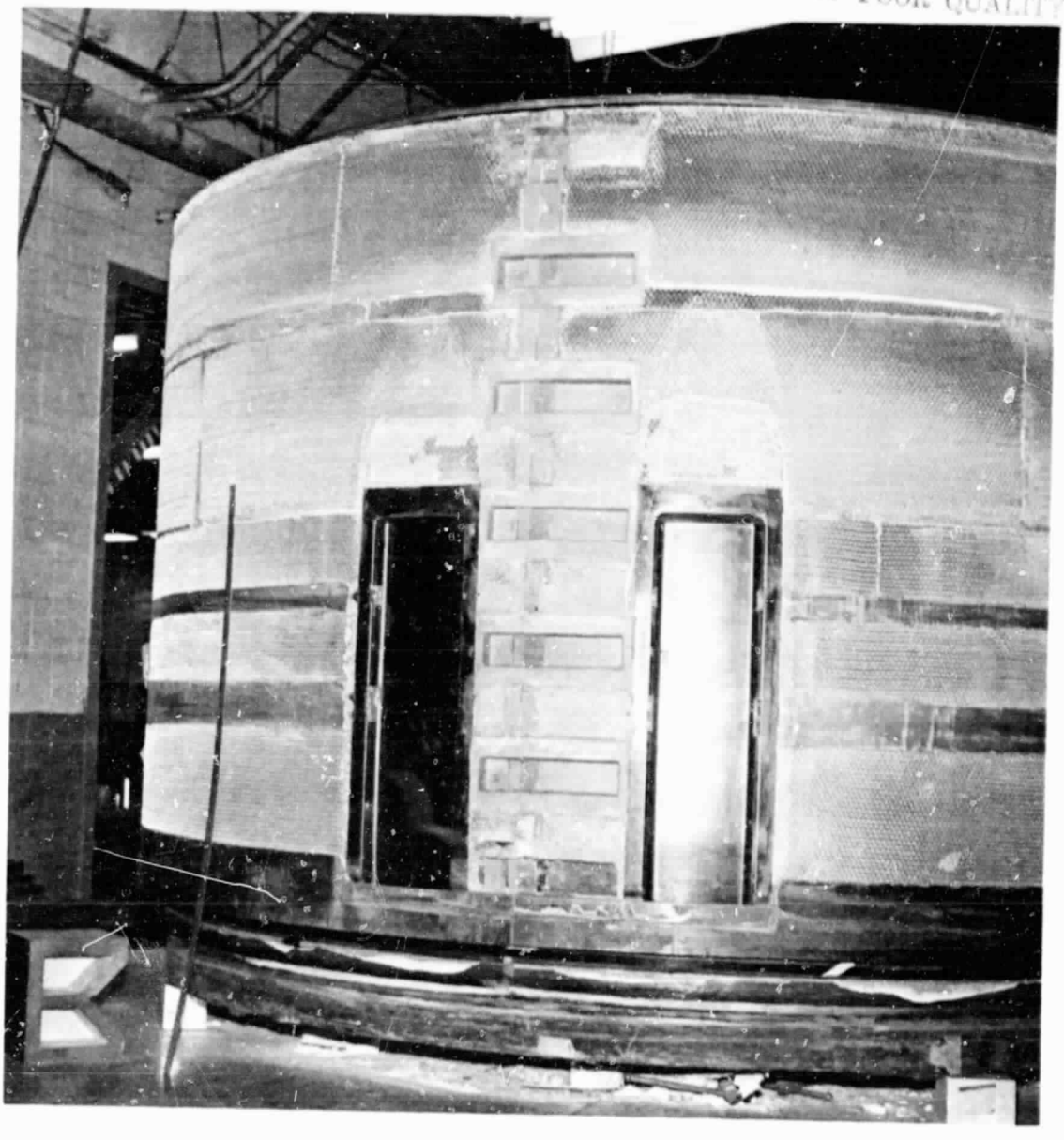

Figure 23. Bypass Duct In-Process Fabrication.

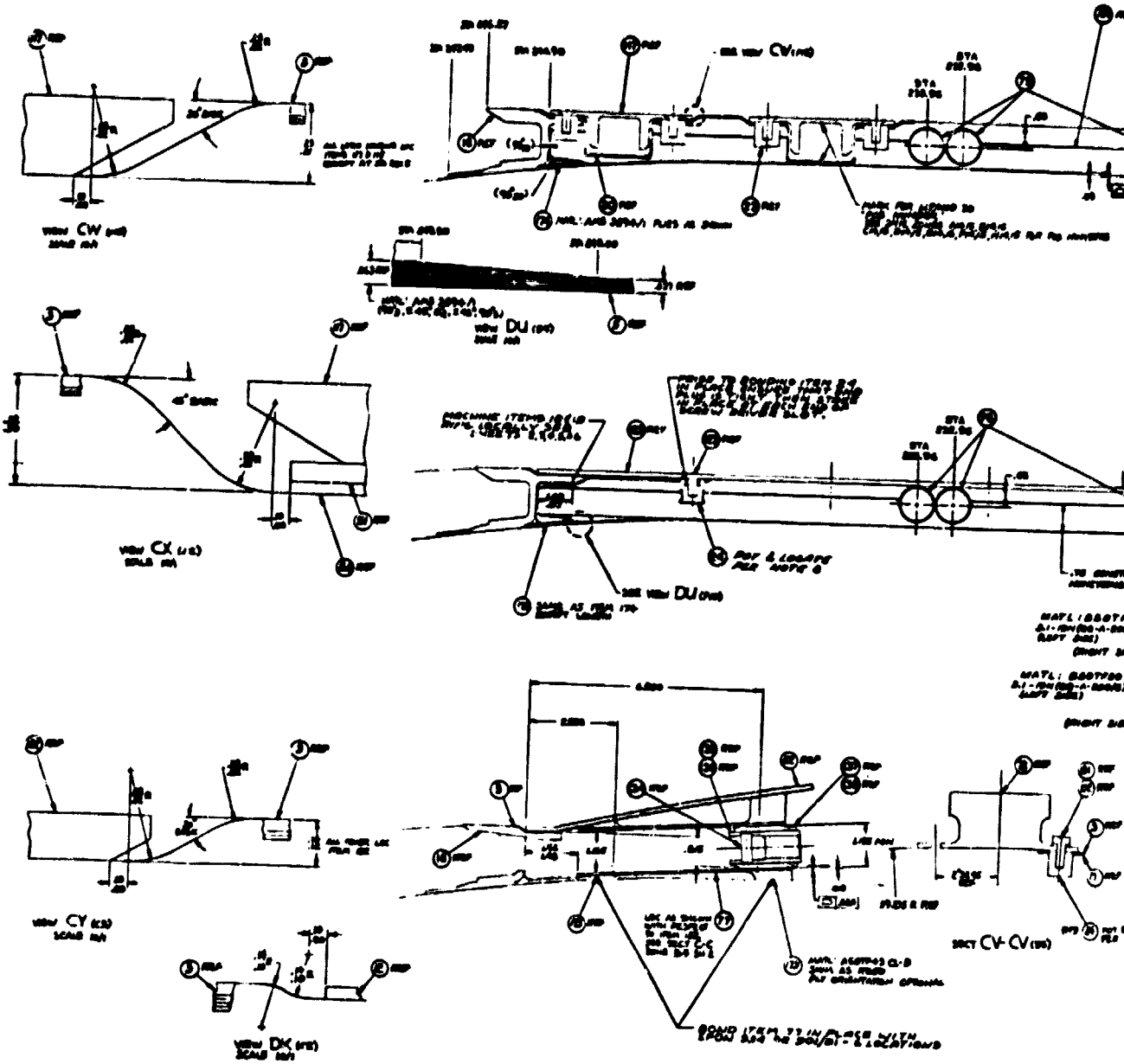

Figure 24. Bypass

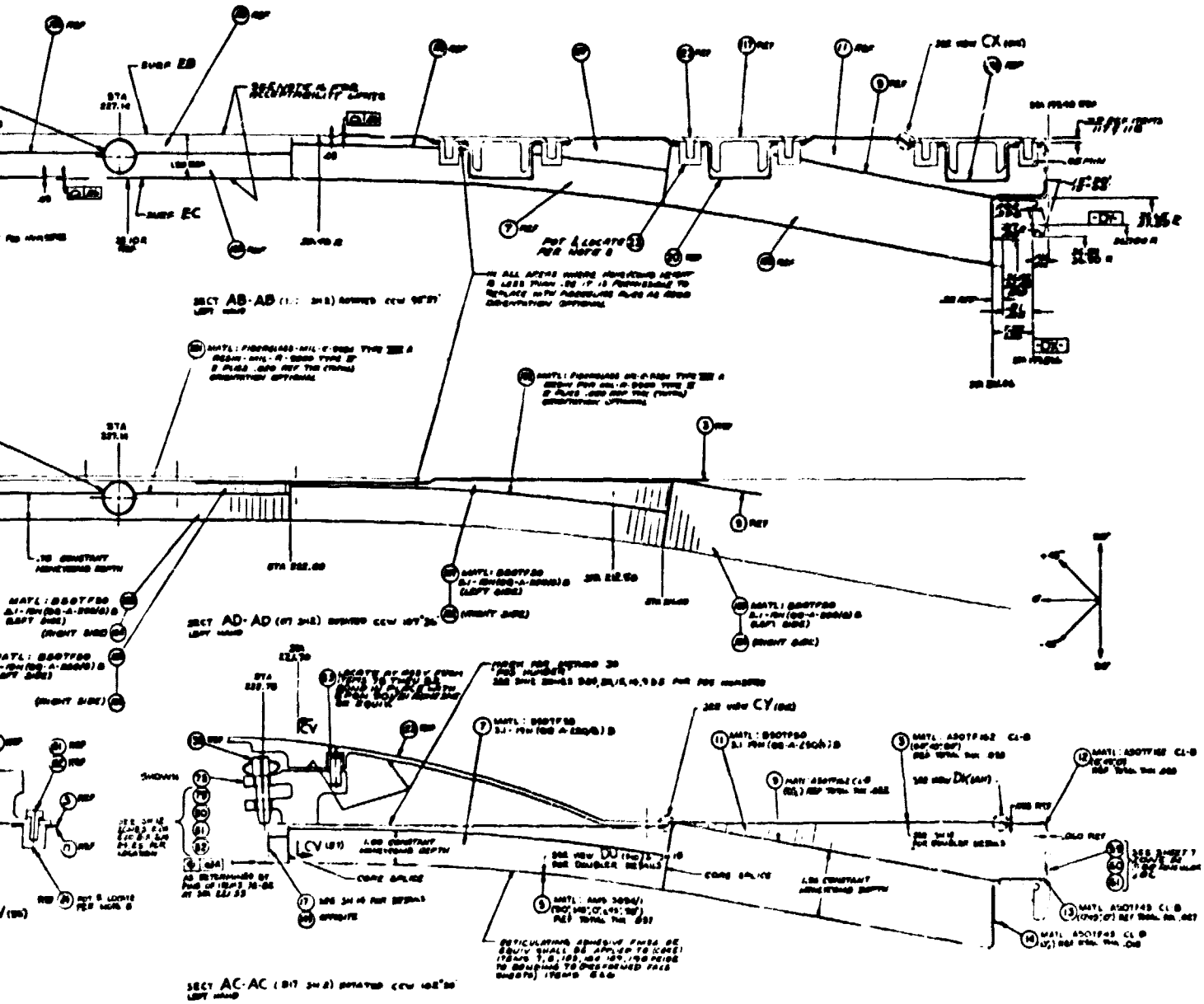

Bypass Duct Cross Sections.

duct wall, for passage of the actuator hydraulic pressure and drain tubes and the system synchronizing cable, are located between the cavities and between the upper and lower cavities and the axial duct closeouts. Figure 25 shows the tunnels in place prior to installation of the outer skin.

Provisions have been included in the doors for mounting the instrumentation and acoustic splitter required for the on-engine ground testing. The bypass duct doors are mirror images of each other, with the exception of the instrumentation mounting provisions and the bottom split line, which was offset from the bottom vertical centerline to accommodate the different length latch components.

The duct doors are of a full-depth honeycomb-sandwich-type construction with the outer surface forming the nacelle surface and the inner surface constituting the fan exhaust duct outer flowpath. Figure 24 shows a series of cross sections through the duct taken at various circumferential locations. The inner skin is perforated so that along with the sized honeycomb core it constitutes the sound-suppression treatment in the duct. This treatment, being integral with the duct, also is part of the load-carrying structure. Figure 26 is a rollout showing the extent of the perforated area in the inner skin, and Figure 27 shows the final product prior to application of the finish coating. The minimum thickness (core height) of the duct was set by the preliminary acoustic design requirements and, also, by the depths required for complete installation of the latches and actuator plumbing lines within the boundaries of the inner and outer flowpaths. As the time element did not allow for delay in the program until the final acoustic requirements were determined by boilerplate nacelle tests, design and fabrication of the duct were started prior to these data being available. At the determination of the composite nacelle final acoustic requirements, the design was modified to include septum sheets in the core area which established the proper honeycomb depths. Figure 24 shows these septums in place. These septums are considered nonstructural with the exception of the forward septum which aids in transmitting the axial loading to the forward ring radial lugs. The septum thickness is based on acoustic transmission requirements.

The bypass duct was designed as a body of revolution on both outer and inner flow surfaces with the exception that in the area of the duct-to-pylon piano hinge, the cross section was deepened to allow passage of the actuator system synchronization cable through the duct upper closeouts inboard of the hinge and outboard of the duct to pylon seal. This proturberance from the inner flowpath flares back to the flowpath on the lower circumferential side and at both the forward and aft ends so as to keep the changes in the fan exhaust duct area at a minimum. Figure 19 shows a cross section through this deviation from the inner flowpath.

The bypass duct is basically fabricated from two advanced composite materials. The outer skin, axial closeouts, latch pans, and forward closeout rings are of Kevlar 49/epoxy. This skin is reinforced in the areas of highest loading with from two to four double plies of the same material. The perforated inner skin, actuator pans, and aft closeout ring are made of graphite/epoxy.

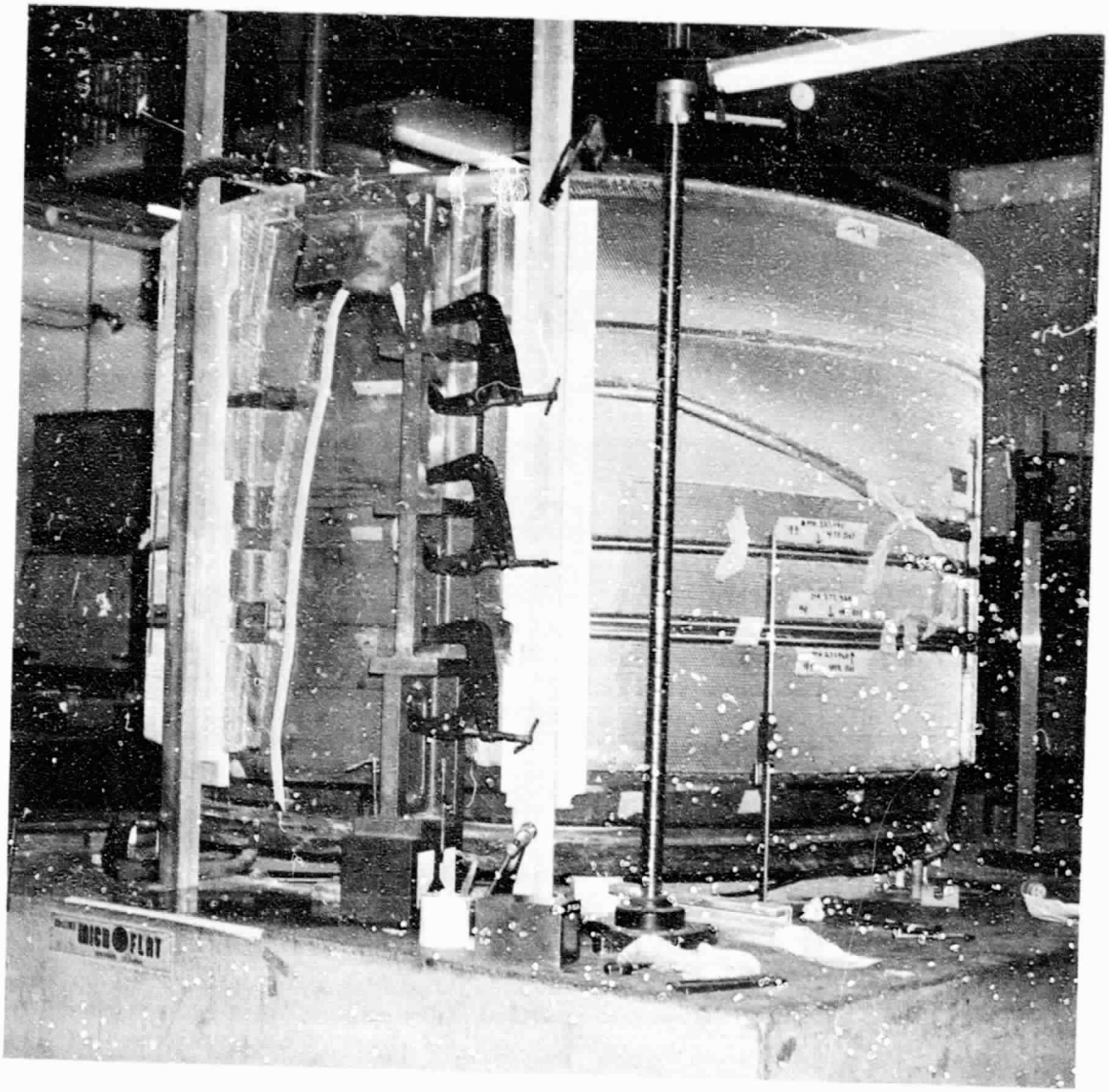

Figure 25. Bypass Duct Tunnel Installation.

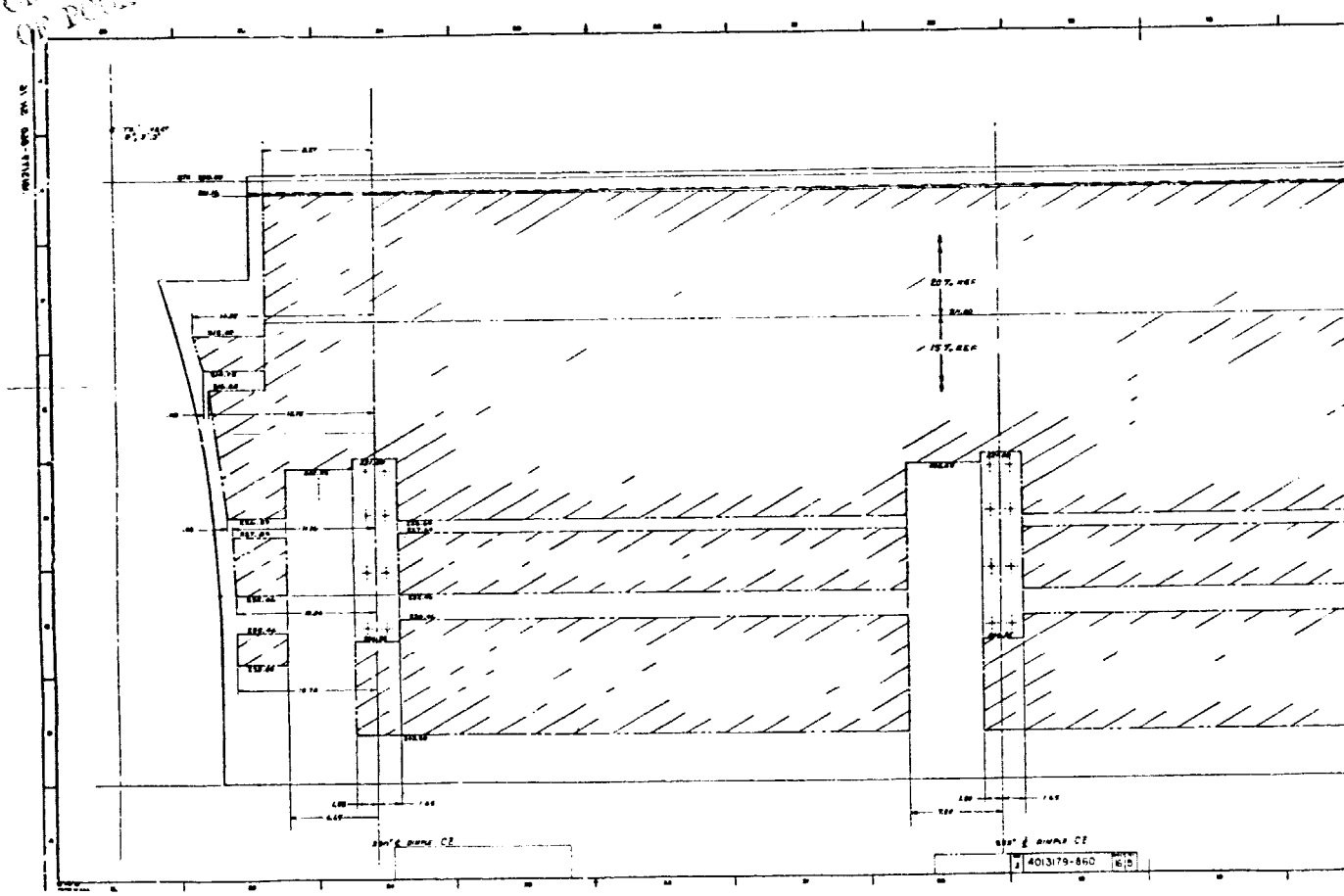

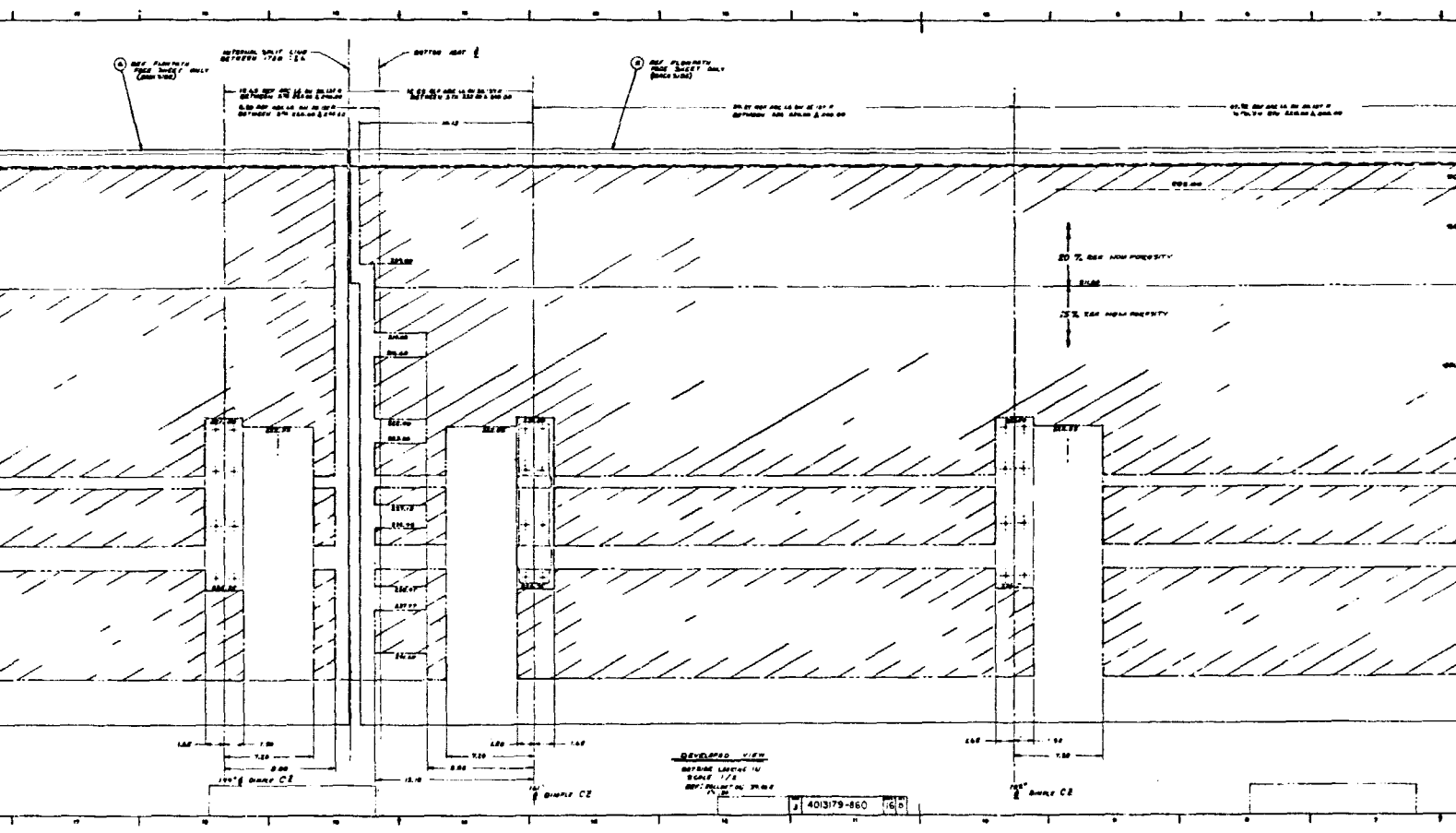

Figure 26. Bypass Duct Inner Skin Rollout.

ORIGINAL PAGE IS
OF POOR QUALITY

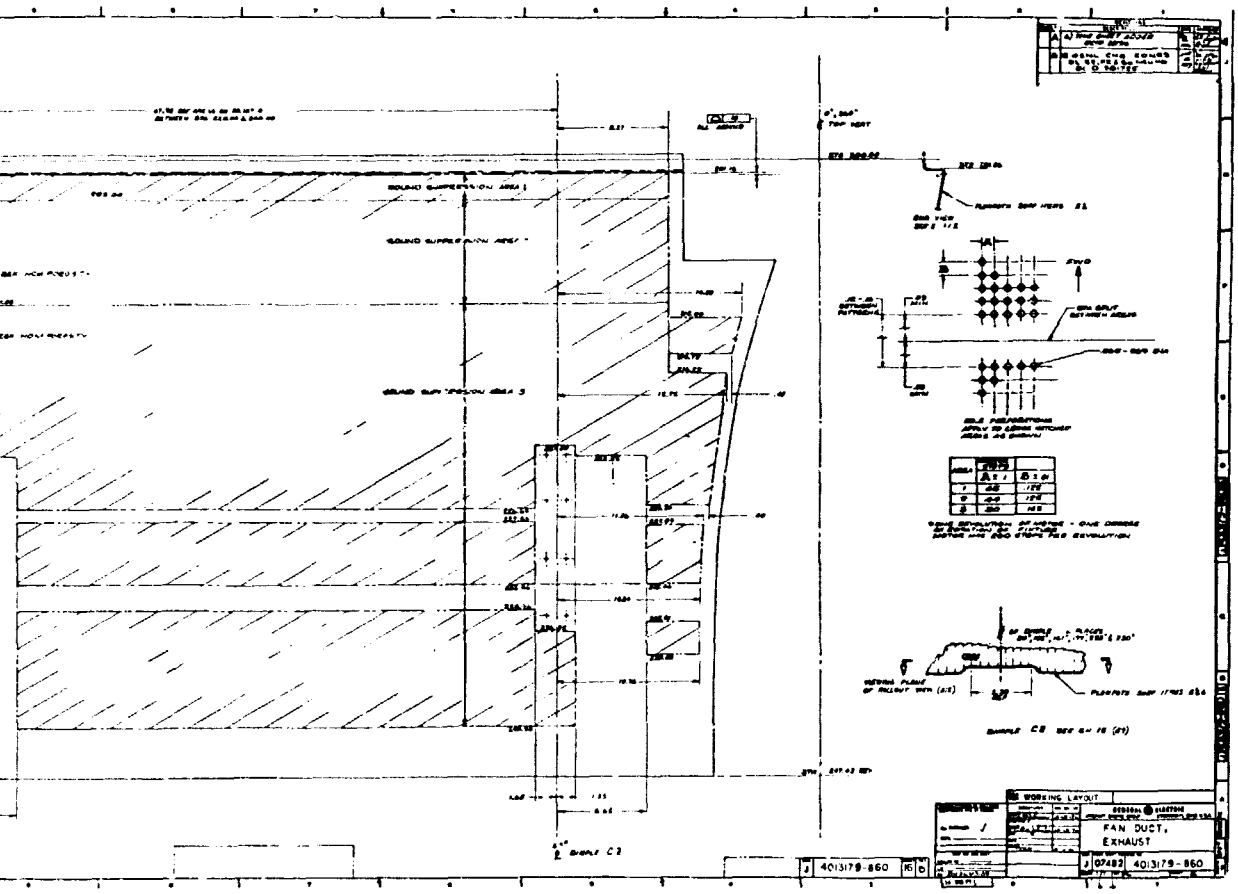

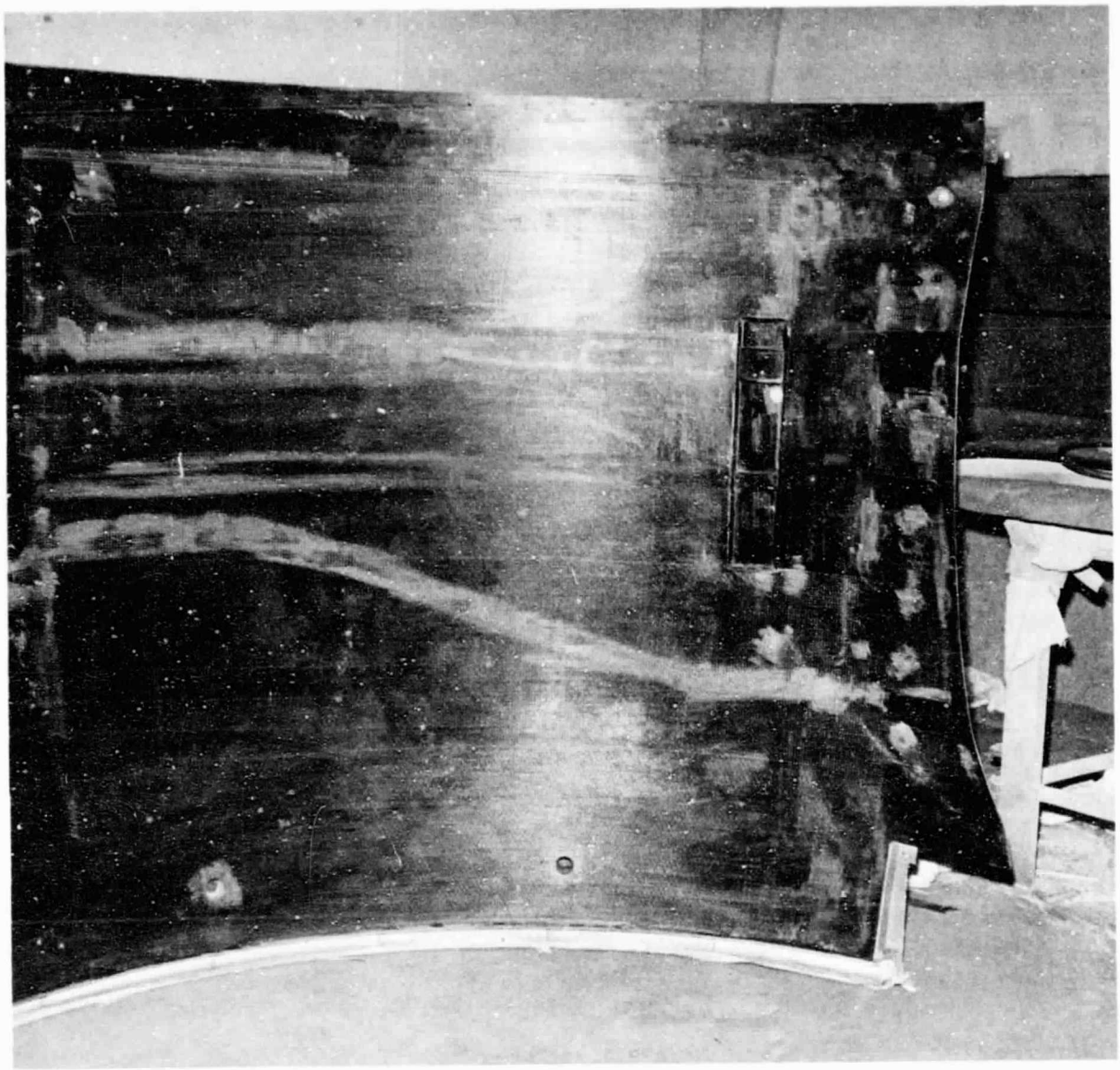

Figure 27. Bypass Duct Inner Skin Porosity.

The perforated inner skin was first projected to be made of Kevlar 49/epoxy laminations, but the required relatively high-porosity percentage generated manufacturing problems which could not be overcome within the dictates of the program. The desire to remain with advanced composite material for this item led to the decision to fabricate the inner skin of graphite/epoxy with the acoustic holes being laser-drilled.

The septum sheets are fiberglass/epoxy and the metallic fittings, forward radial lugs, and actuator guides are machined from 2024-T351 aluminum, while the sandwich core is a flexible honeycomb made from 5052 aluminum foil. All the aluminum machinings are chemically treated per MIL-C-5541 and coated with epoxy primer with the exception of the actuator-rod-end clevis guides which are hard-anodized with a teflon impregnation for greater lubricity.

Examination of the operating conditions determined that the critical forward thrust limit load case occurred at (1) Mach 0.92, 6041 m (21,000 ft), (2) maximum cruise power setting and (3) with the maximum maneuver loads of 10-g's down, ± 2-g's axial, and 1.5-g's side imposed on those components which input loads to the bypass duct (such as the fan nozzle flaps). The critical reverse thrust limit load case was established at Mach 0.227 at sea level with a power setting of maximum reverse thrust (takeoff power). No maneuver loads were imposed but, again, the 20-g buffet loading on the inputting load components was added. For the fan nozzle actuator mounts and flap hinges, the critical ultimate load case was determined to be the critical forward thrust limit load with a jammed fan nozzle actuator. Figure 28 shows the bypass duct differential pressures for these cases; Figures 29 and 30 show the imposed flap loads on the duct aft ring.

The various laminate stresses and allowables were calculated by the methods defined in MIL-HDBK-17 for anisotropic fiber-reinforced composites and the Point Stress Analysis computer program as described in the Advanced Composites Design Guide. The duct aft ring was analyzed as a separate body using a finite-element program which represented the ring as a series of connected curved beams having orthotropic material properties. The various component stresses are shown in Table VI.

3.3.4 Fan Nozzle

The fan exhaust nozzle is a fully modulating, variable-flap-type configuration capable of providing infinite variation of the nozzle exit area for forward thrust, and is also capable of flaring outwards to provide increased area for the inlet airflow to the variable-pitch fan in the reverse mode (see Figures 31 and 32).

The nozzle consists of four hinged flaps, each 44.96 cm (17.7 in.) from hinge centerline to trailing edge. The upper flaps are 1.461-radians (83.7°) wide and the lower flaps are 1.475-radians (84.5°) wide. A hinge/actuator link clevis arrangement (see Figure 32) is used to position the flaps. Each flap is attached to the bypass-duct aft ring by means of a pair of hinges 30.48-cm (12-in.) apart at the flap centerline along the flap forward edge

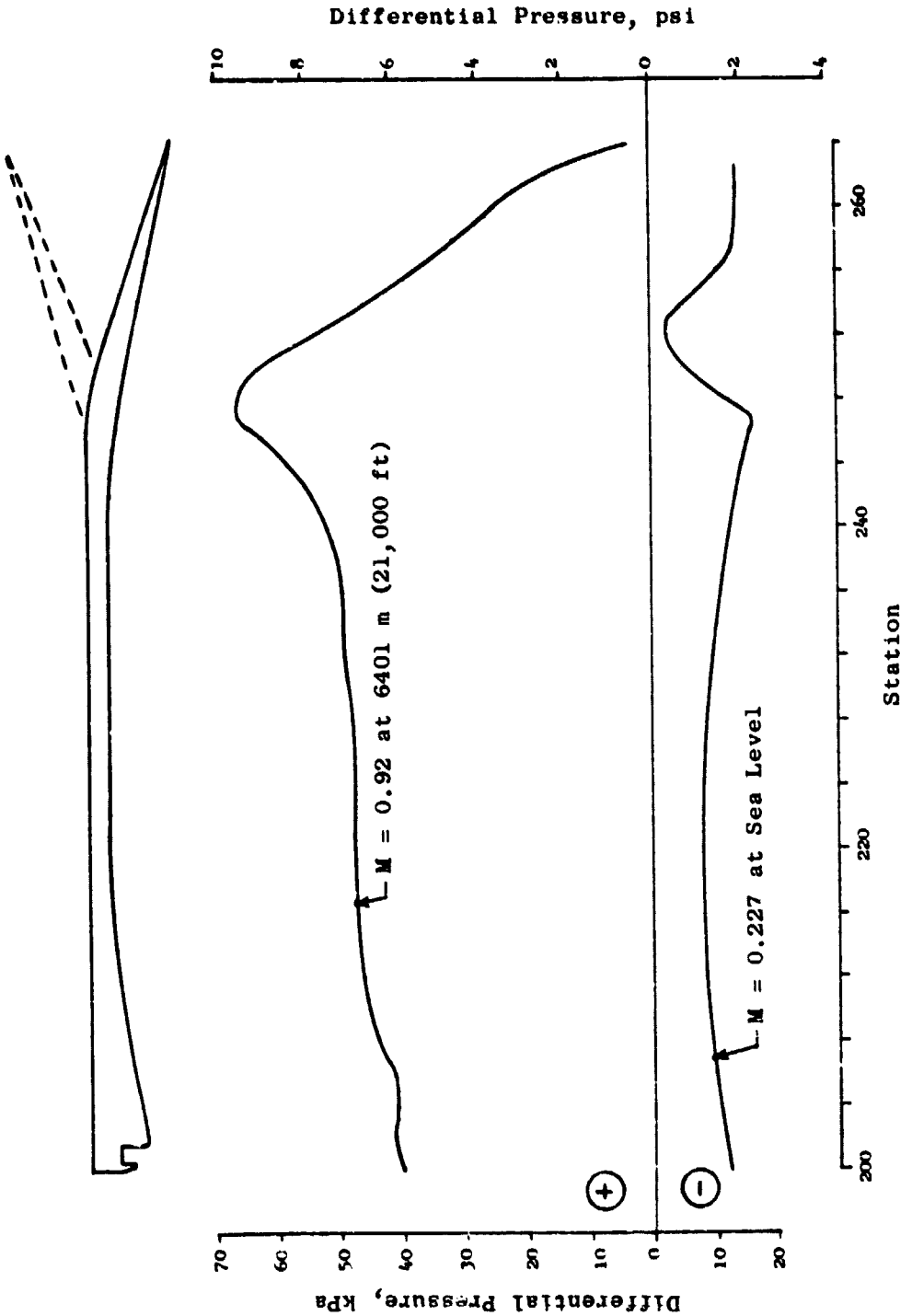

Figure 28. Bypass Duct Differential Pressures.

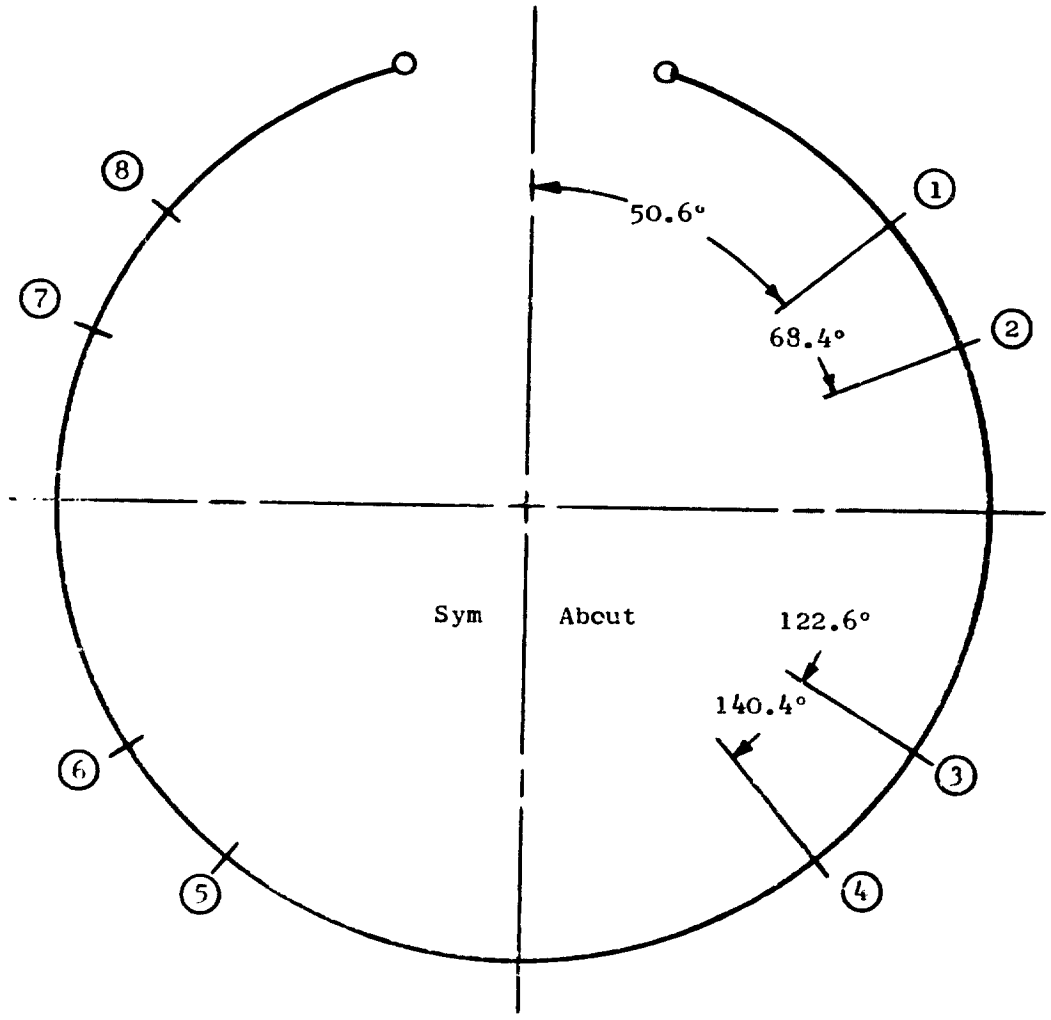

Aft Looking Forward

+ Radial = Forward

+ Axial = Forward

+ Tangential = Clockwise

Position	Load		
	Radial, N (lb)	Axial, N (lb)	Tangential, N (lb)
1	+17,473 (3,928)	+15,324 (3,445)	-645 (145)
2	+5,623 (1,264)	+6,357 (1,439)	-645 (145)
3	+4,568 (1,027)	+2,820 (634)	+1,855 (417)
4	+19,768 (4,444)	+19,959 (4,487)	-1,855 (417)
5	+19,768 (4,444)	+19,959 (4,487)	-1,855 (417)
6	+4,568 (1,027)	+2,820 (634)	-1,855 (417)
7	+5,623 (1,264)	+6,357 (1,439)	+645 (145)
8	+17,473 (3,928)	+15,324 (3,445)	+645 (145)

Figure 29. Bypass Duct Aft Ring Loads, Maximum Forward Thrust Case.

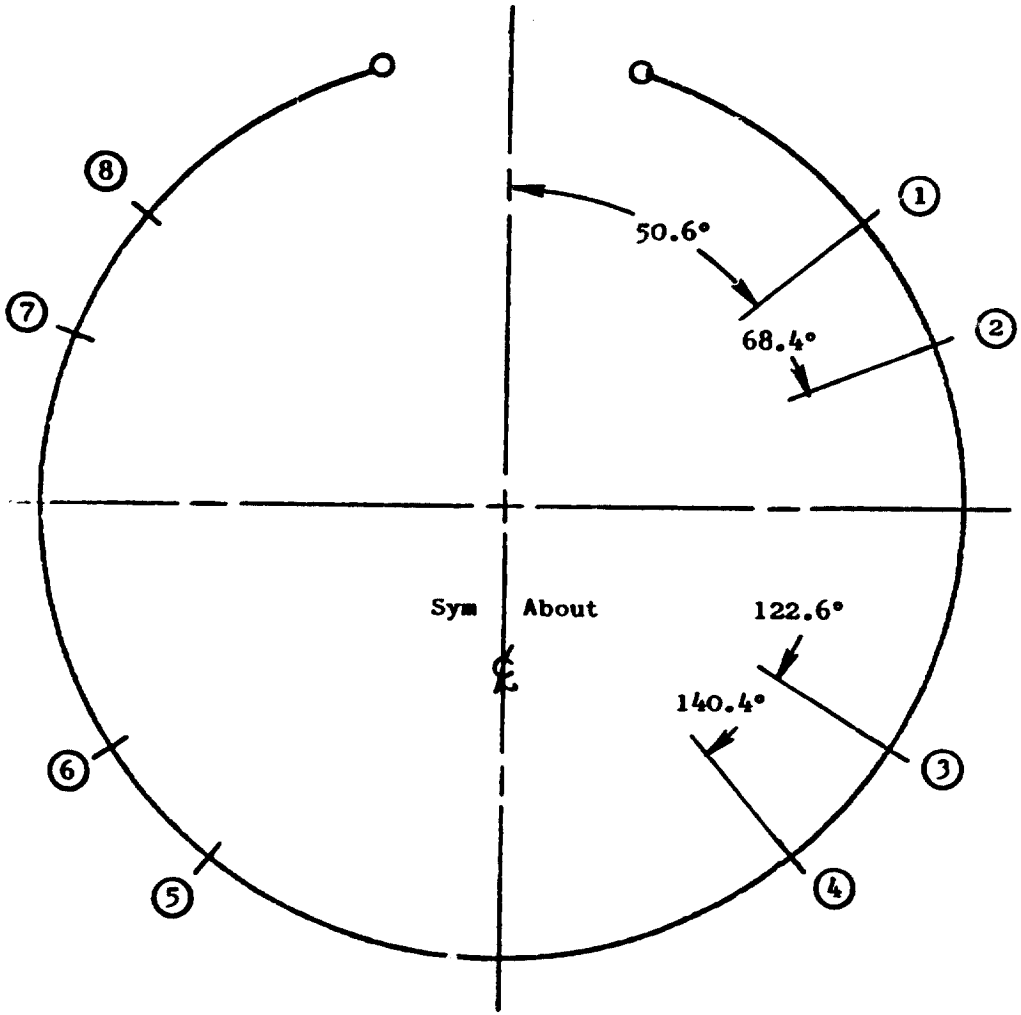

Aft Looking Forward

+ Radial = Outward
+ Axial = Forward
+ Tangential = Clockwise

Position	Load		
	Radial, N (lb)	Axial, N (lb)	Tangential, N (lb)
1	-5,129 (1,153)	-10,070 (2,264)	+387 (87)
2	-1,931 (434)	-3,074 (691)	+387 (87)
3	-1,197 (269)	-1,477 (332)	-592 (133)
4	-6,018 (1,353)	-12,081 (2,716)	-592 (133)
5	-6,018 (1,353)	-12,081 (2,716)	+592 (133)
6	-1,197 (269)	-1,477 (332)	+592 (133)
7	-1,931 (434)	-3,074 (691)	-387 (87)
8	-5,129 (1,153)	-10,070 (2,264)	-387 (87)

Figure 30. Bypass Duct Aft Ring Loads, Maximum Reverse Thrust Case.

Table VI. Bypass Duct Stresses.

Load Condition	Component	Mode	Calculared Stress/Load	Allowable Stress/Load
Forward Thrust	Outer Skin	Tension	39.07 MPa (5,667 psi)	270.96 MPa (39,300 psi)
Forward Thrust	Inner Skin	Tension	24.41 MPa (3,541 psi)	301.99 MPa (43,800 psi)
Forward Thrust	Outer Skin	Buckling	184.5 MPa (26,760 psi)	453.30 MPa (65,740 psi)
Forward Thrust	Honeycomb Core	Shear	0.18 MPa (26 psi)	0.52 MPa (75 psi)
Forward Thrust	Forward Ring	Compression	1.65 MPa (240 psi)	9.10 MPa (1,320 psi)
Forward Thrust	Septum	Tension	89.94 MPa (13,045 psi)	379.21 MPa (55,000 psi)
Forward Thrust	Aft Ring	Bending	232.77 MPa (33,760 psi)	772.21 MPa (112,000 psi)
Forward Thrust	Aft Ring	Shear	35.96 MPa (5,215 psi)	111.70 MPa (16,200 psi)
Reverse Thrust	Aft Ring	Bending	91.77 MPa (13,310 psi)	772.21 MPa (112,000 psi)
Reverse Thrust	Aft Ring	Shear	14.17 MPa (2,055 psi)	111.70 MPa (16,200 psi)
Forward Thrust	Actuator Access Cover	Bending	81.07 MPa (11,768 psi)	276.48 MPa (40,100 psi)
Forward Thrust	Actuator Access Cover Fastener	Shearout	74.33 MPa (10,780 psi)	275.79 MPa (40,000 psi)
Forward Thrust	Piano Hinge Fastener	Bearing	10,782 N (2,424 lb)	52,698 N (11,847 lb)
Forward Thrust	Piano Hinge Fastener	Shearout	10,782 N (2,424 lb)	86,527 N (19,452 lb)
Forward Thrust	Latch Housing Fastener	Shearout	26.25 MPa (3,807 psi)	68.95 MPa (10,000 psi)
Jammed Actuator	Nozzle Hinge Clevis Lug	Shearout/ Bearing	17,495 N (3,933 lb)	32,160 N (7,230 lb)
Jammed Actuator	Nozzle Hinge Clevis Fastener	Bearing	133.55 MPa (19,080 psi)	482.63 MPa (70,000 psi)
Jammed Actuator	Actuator Mount Lug	Shearout/ Bearing	12,010 N (2,700 lb)	31,849 N (7,160 lb)
Jammed Actuator	Actuator Mount Fastener	Bearing	4,275 N (961 lb)	7,940 N (1,785 lb)
Jammed Actuator	Actuator Quick-Disconnect Pin	Shear	22,402 N (5,400 lb)	52,222 N (11,740 lb)

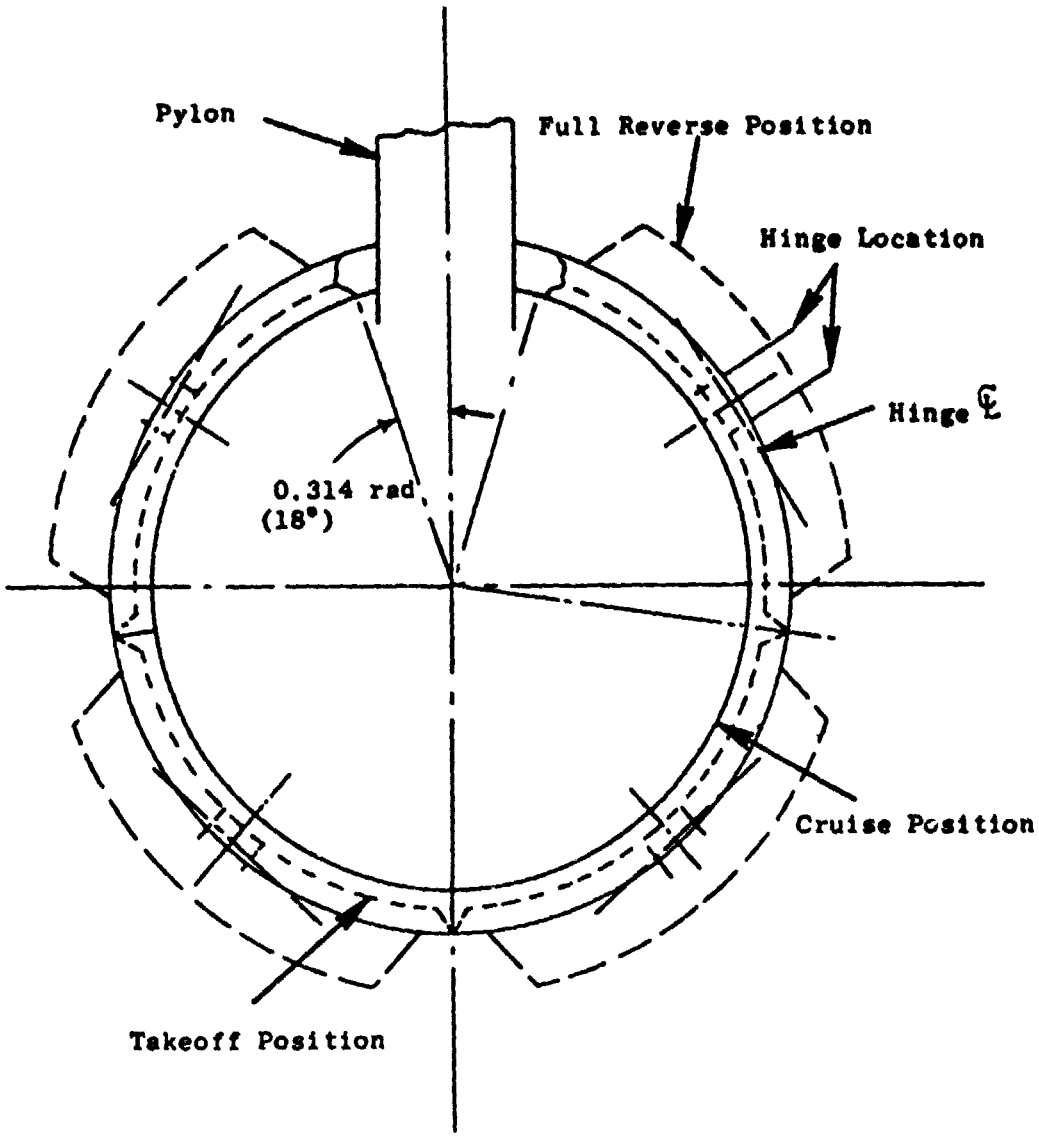

Figure 31. Flare Nozzle Flap Schematic.

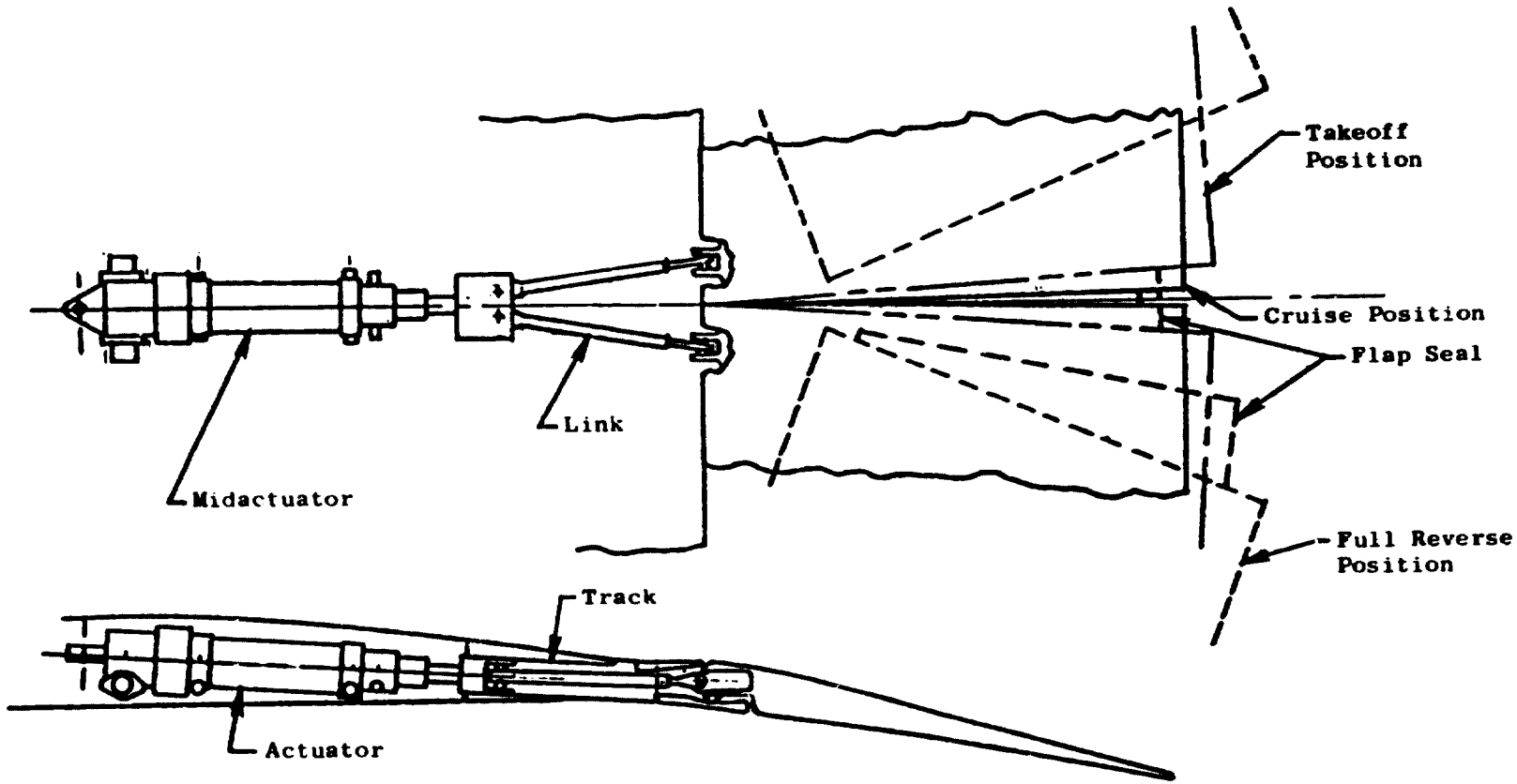

Figure 32. Variable-Flap Nozzle.

closeout. The flaps are connected to the actuation system in the fan duct by links at link clevises which are located 0.438 radian (25.119°) outboard of each hinge. The links have spherical bearing rod ends to preclude any binding during flap operation. The flaps are designed so that they can be rotated from an angle of about 0.227 radian (13°) in toward the engine centerline to an outward angle of approximately 0.489 radian (28°). Figure 33 shows the linkage in the reverse thrust position.

The synchronization of the upper and lower flaps in each bypass duct half is accomplished by the midactuator which is joined to both flaps (see Figure 34). The synchronization between duct doors is accomplished by the actuation system synchronization cables. The upper and lower actuators are connected to the flaps by a single link only.

Located along the axial edges of each flap are intraflap seal assemblies (see Figure 35), which are designed to give full sealing from a minimum nozzle area of 11,903.2 cm^2 (1845 $in.^2$) to a maximum sealed nozzle area of 16,781 cm^2 (2601 $in.^2$). From this maximum sealed nozzle area to the full-reverse flap position the seals will be disengaged allowing a triangular-shaped void between the flaps. Sealing is not required while in the reverse mode.

The intraflap seal assemblies are spring-loaded pivoted bumpers, one of which (in each pair) has a soft face in order to provide good sealing; otherwise, the seal components are identical between seal assemblies. The spring forces are such as to cause the seals to maintain contact with each other as the flaps move outward, except that when the nozzle reaches an area of 16,781 cm^2 (2601 $in.^2$), a slot in each seal slider bottoms out against a fixed pin mounted in the seal housing thereby preventing further seal travel. The seals will then stay in the same position (relative to the flap they are mounted in) for any nozzle area greater than the 16,781 cm^2 (2601 $in.^2$).

A circumferential seal is also provided along the forward inner edge of each flap. This seal contacts a contoured lip extension from the aft ring of the fan outer duct (see Figure 36). The seal will also provide full sealing over the same range as the axial intraflap seals.

The seal at the flap/pylon interface is fixed in the axial closeout of the flap (see Figure 37). This seal will be adjusted at assembly of the outer duct and nozzle to the pylon to have good contact with the sealing face on the pylon. Having this seal fixed necessitated the pylon sealing face being parallel to the line of travel of the upper flap as it rotates.

The construction of the flaps is similar to the rest of the nacelle (see Figure 38 through 40). They are of the full-depth honeycomb-sandwich-type with the outer face sheet fabricated of Kevlar 49/epoxy, the inner face sheet and the forward closeout are graphite/epoxy, and the core is a flexible honeycomb made from 5052 aluminum foil. The outer face sheet is basically a three-ply laminate oriented +45°, 0°, and -45° with three doubler plies incorporated for the first 25.0 cm (9.8 in.) and oriented so as to make a symmetrical layup. The inner face sheet is eight plies oriented 0°, $\pm$45°, $90°_2$, $\pm$45°,

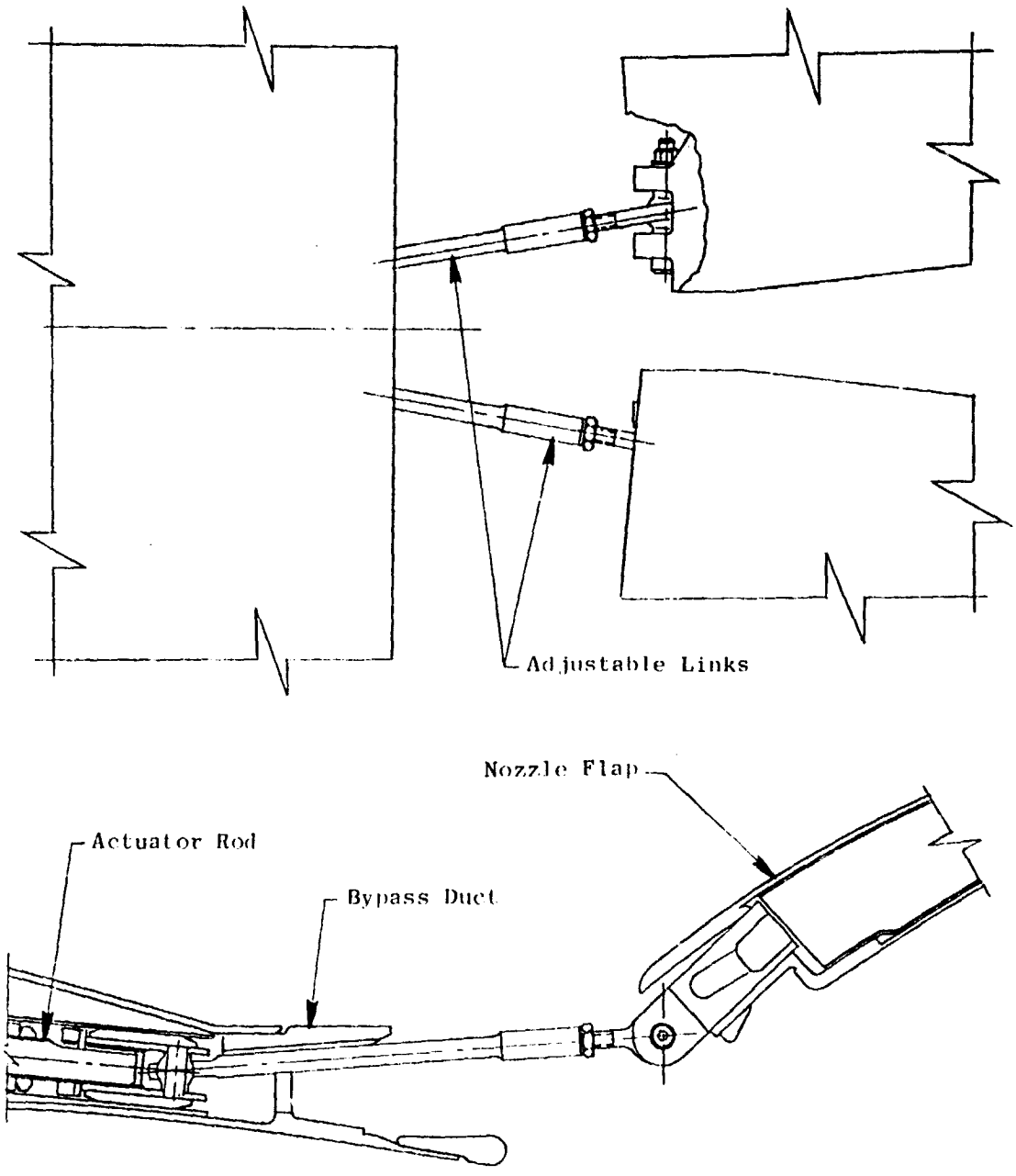

Figure 33. Variable Nozzle Linkage, Reverse Thrust Position.

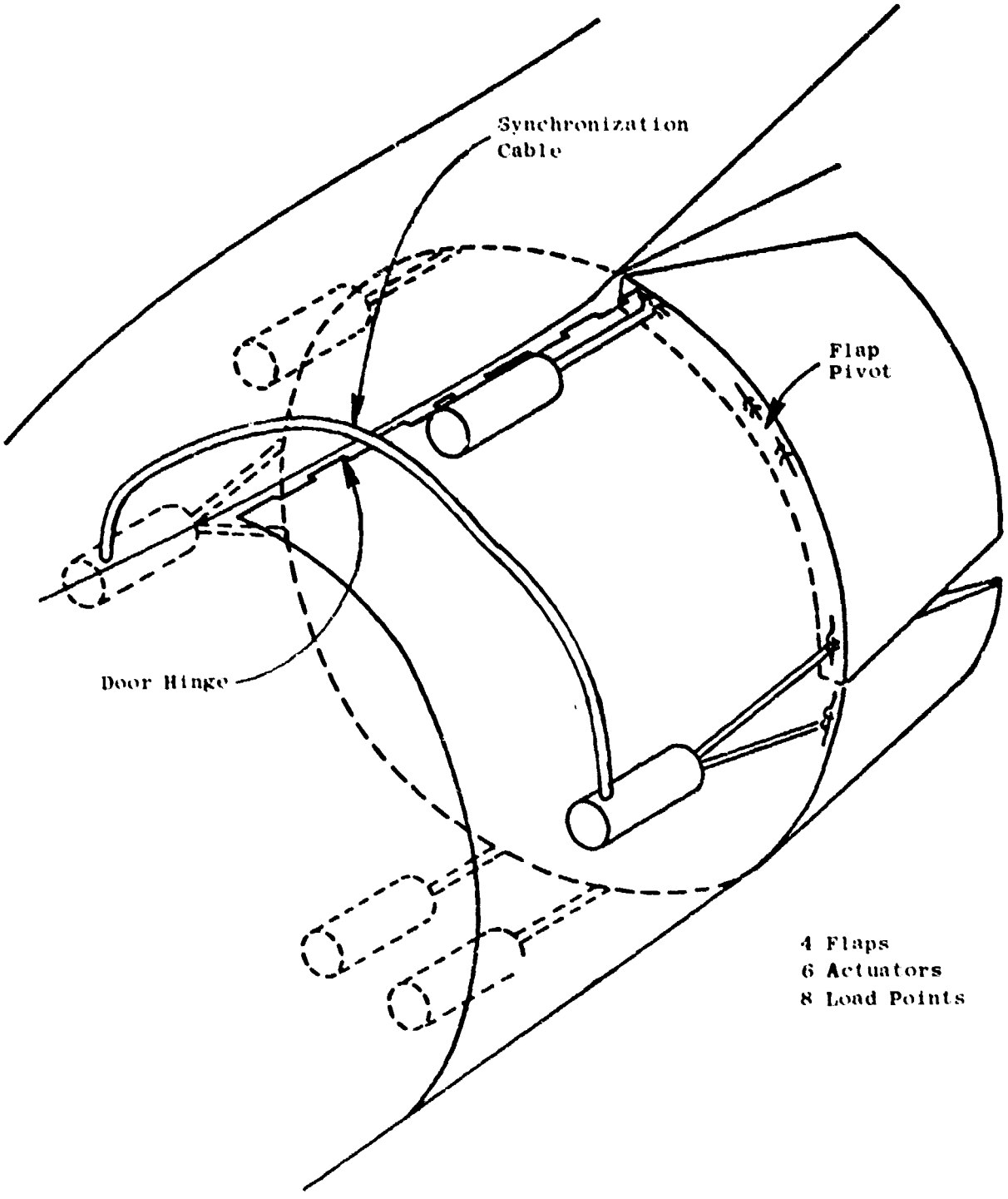

Figure 34. Variable Nozzle Actuation Schematic.

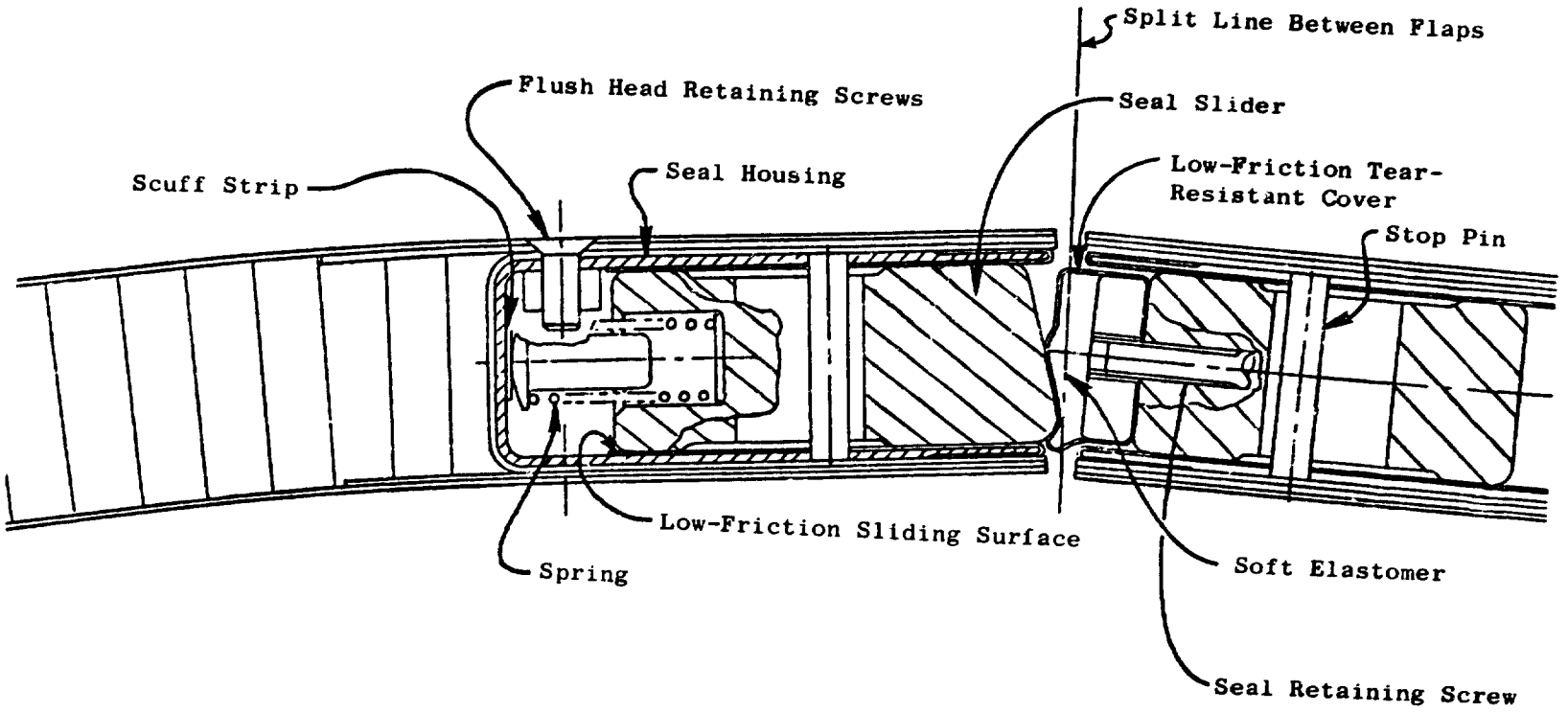

Figure 35. Intraflap Seal Schematic.

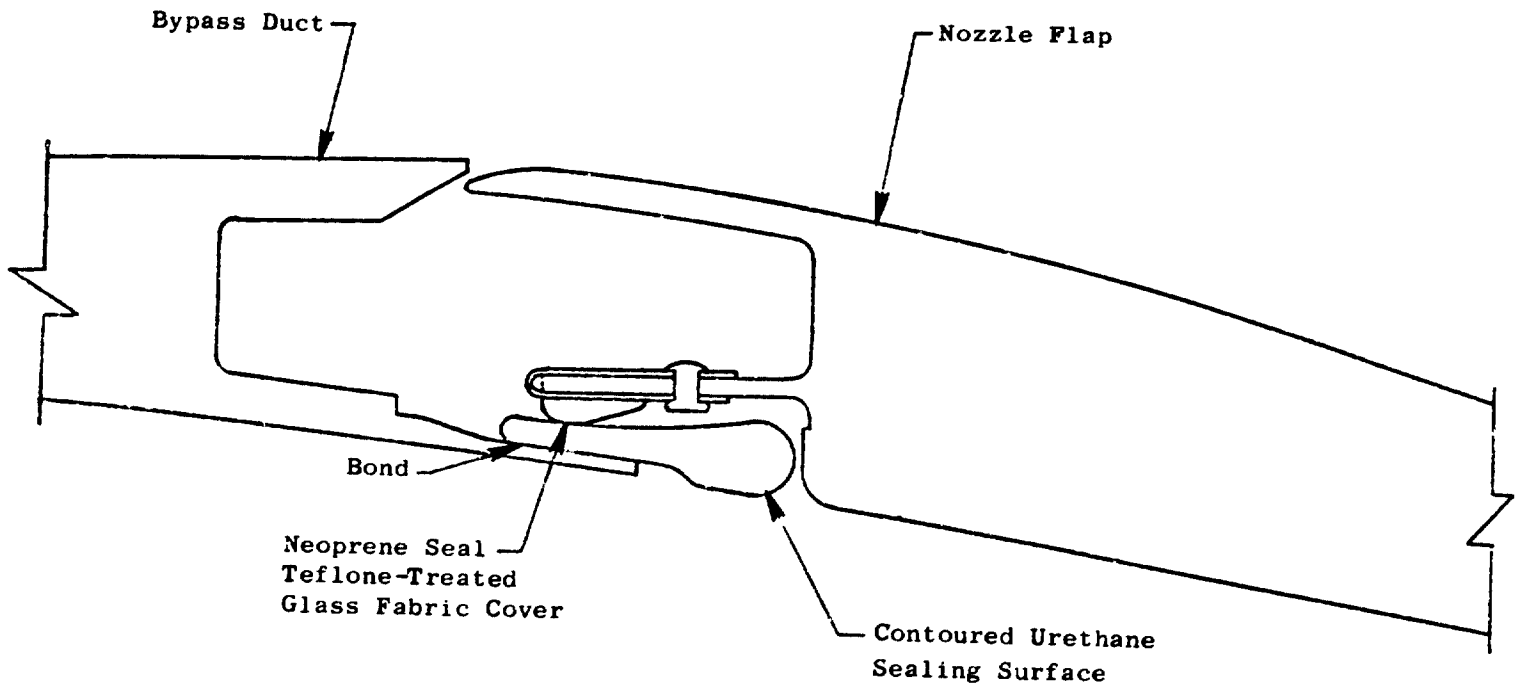

Figure 36. Bypass Duct/Nozzle Flap Circumferential Seal.

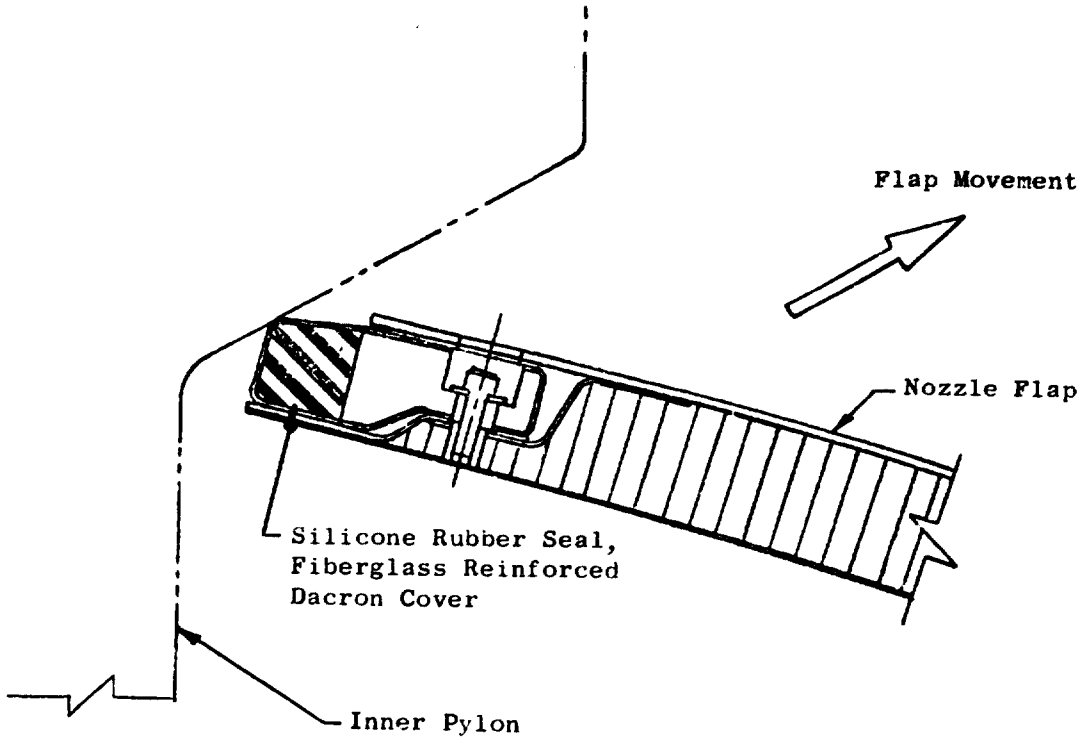

Figure 37. Nozzle Flap/Pylon Interface Seal.

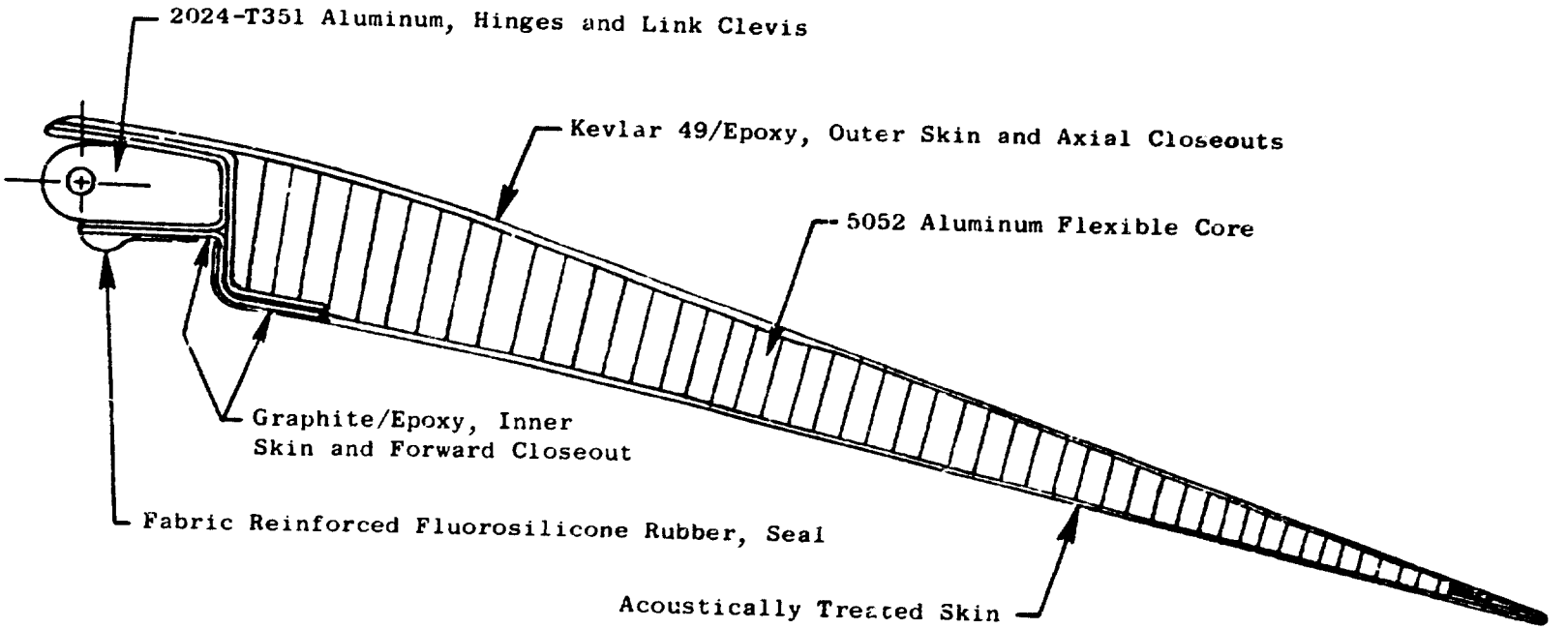

Figure 38. Nozzle Flap Cross Section.

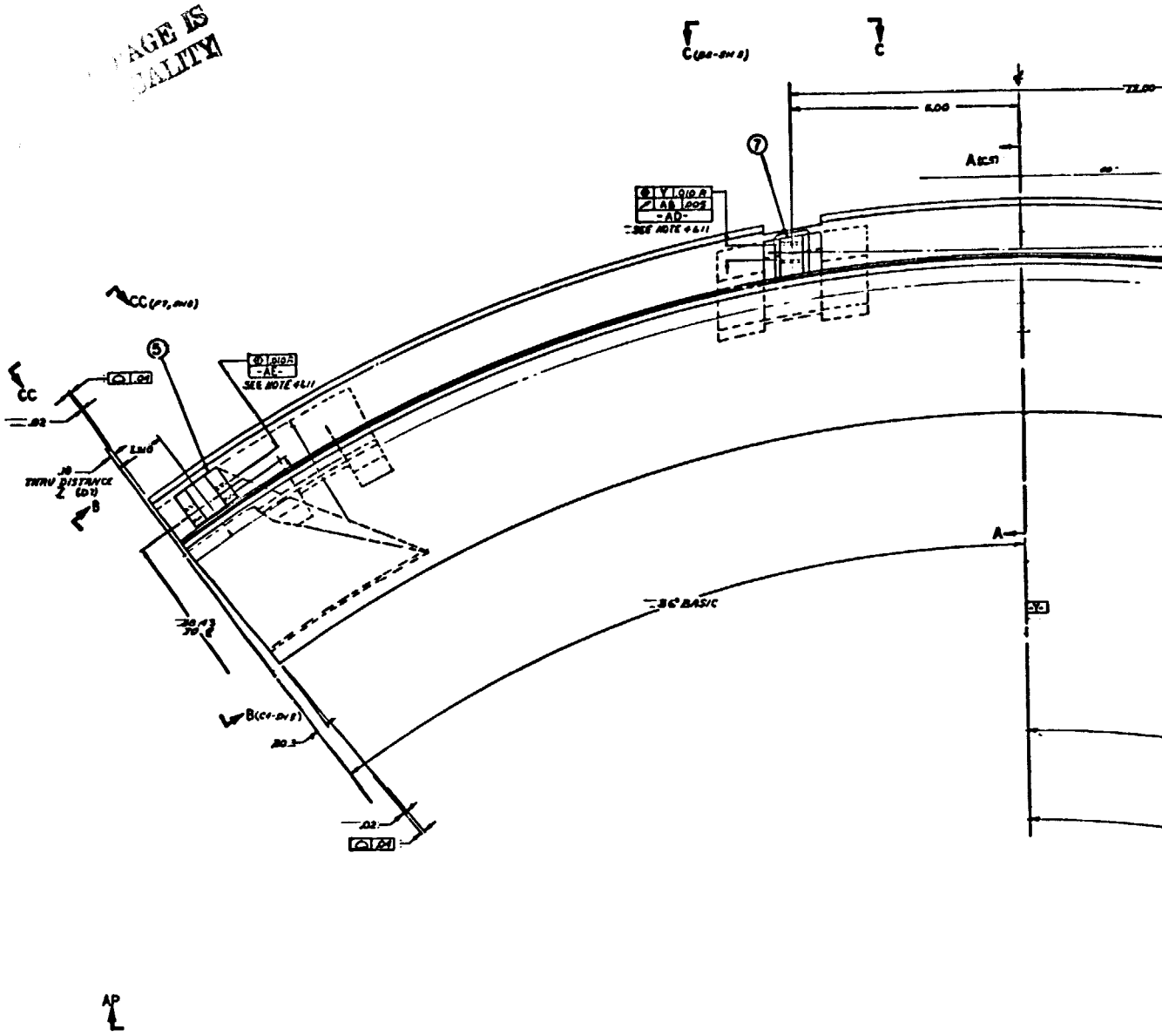

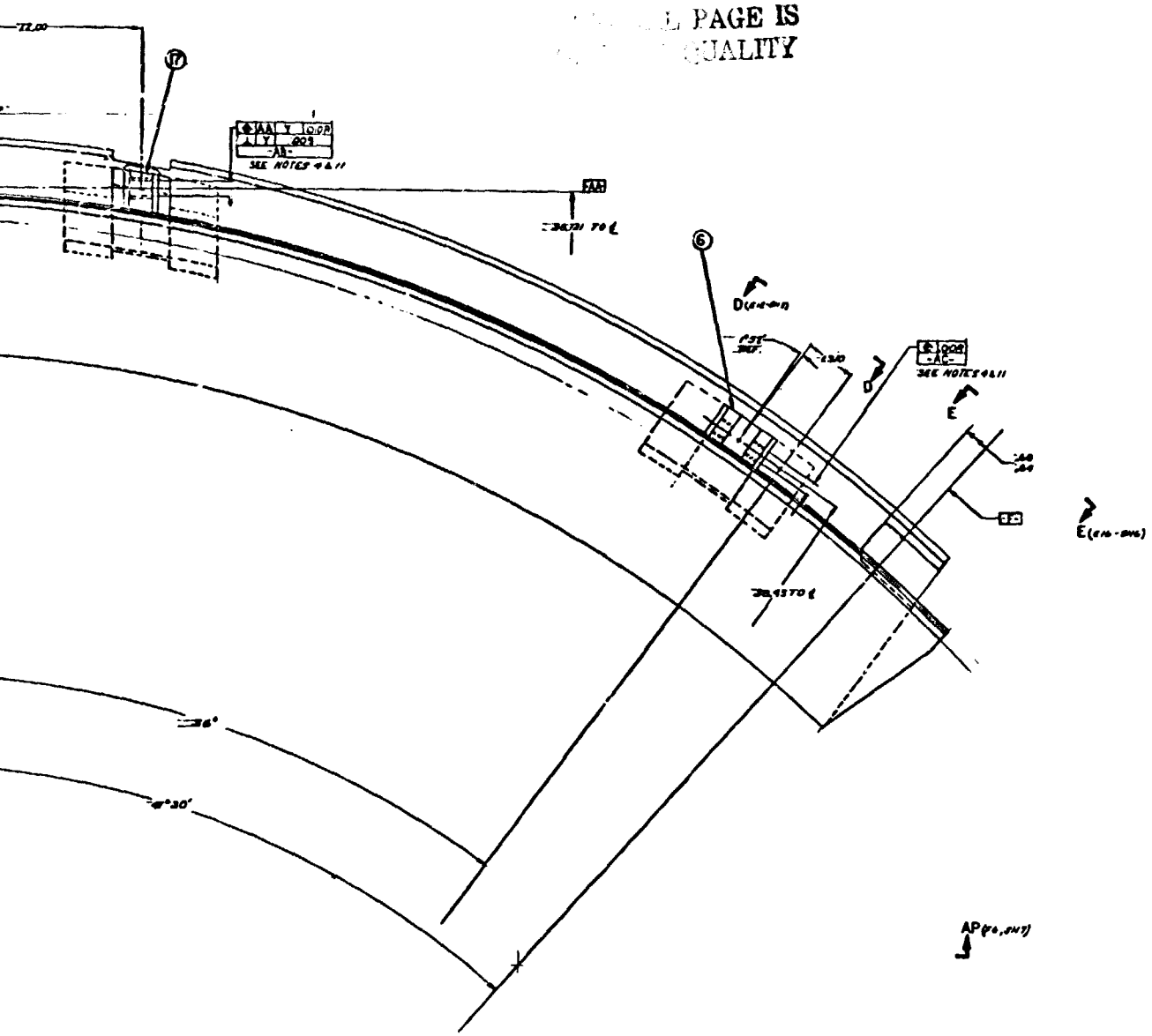

Figure 39. Nozzle Upper Flap, End View.

FOLDOUT FRAME

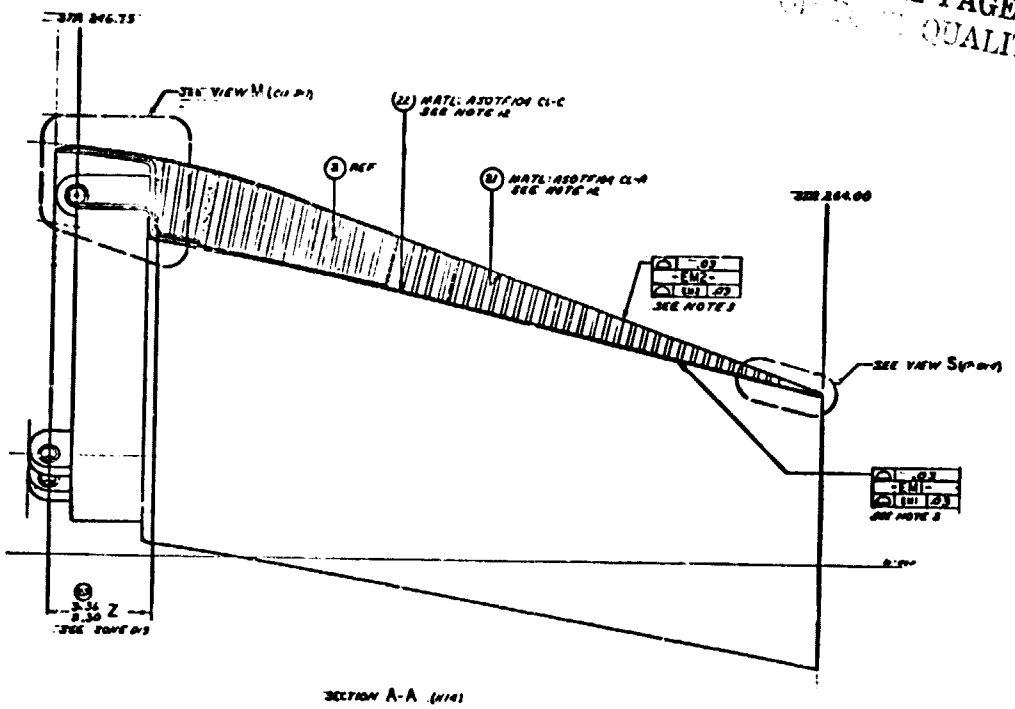

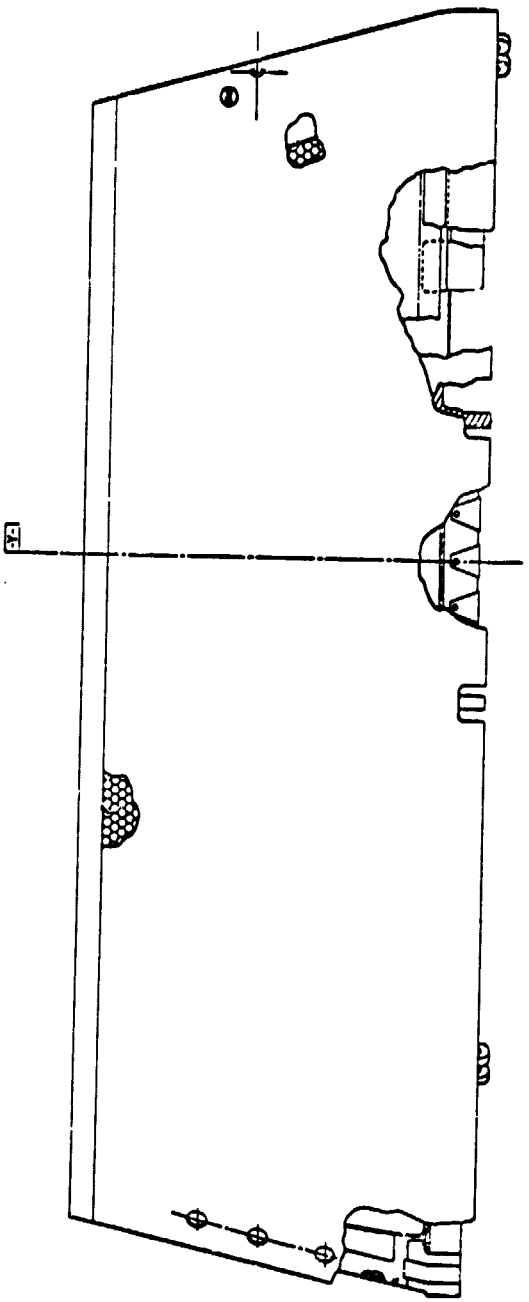

Figure 40. Nozzle Upper Flap, Plan View.

and 0° with four doubler plies for the first 20.6 cm (8.1 in.) of axial length. The inner face sheet is perforated from the forward closeout to within 12.7 cm (5.0 in.) of the trailing edge so as to provide acoustical suppression. Figure 41 shows the perforated inner skin prior to assembly. The forward closeout is composed of three sections, each molded of 12 graphite/epoxy laminae. These sections were bonded together to form a single component prior to assembly into the flap. The trailing edge is built up of Kevlar 49/epoxy plies between the inner and outer face sheets and edge-wrapped with two plies of fiberglass/epoxy to prevent delamination. This was also done to the leading edge. Deep channel-shaped closeouts made of three plies of Kevlar 49/epoxy are provided in the axial edges. These cavities are deep enough to accept the axial seal seal assemblies. The hinges and link clevises are machined from 2024-T351 aluminum; in the interest of providing low-cost items, much of the material was not removed such as would be done in a lighter-weight flight item. These fittings are integral with the honeycomb structure (as can be seen in Figure 42), with the main body submerged in the bondment with the fastener lugs extending through the flap forward closeout. The fittings are bonded in place and provide extensive interfaces with the face sheets and closeouts for transfer of loads at low stresses. Figure 43 shows two flaps in their relative circumferential position.

The flap was analyzed for the design conditions shown in Table VII. The critical forward thrust case was arrived at by comparing flap differential pressures at various points along the maximum flight envelope. This study indicated that the Mach 0.92, 6401-m (21,000-ft) case would give the greatest flap loading. The ±20-g buffet factor is based on experience obtained in the design of components for the C-5A transport and the DC-10 aircraft. For the reverse thrust case, while the normal landing speed is 41.2 m/sec (80 kn), it was decided that the 77.17-m/sec (150-kn), M_O = 0.227, case would sufficiently cover an emergency landing or aborted takeoff condition. In addition, a one-time ultimate load case of a jammed flap actuator imposed on the maximum forward thrust case was analyzed.

The integral load distribution for the flap was determined using a finite-element computer program which represented the flap as a combination of curved beams, straight beams, and curved plates, all capable of having orthotropic material properties. Figure 44 shows a schematic of the computer program model. Table VIII shows critical calculated stresses/loads versus the allowables.

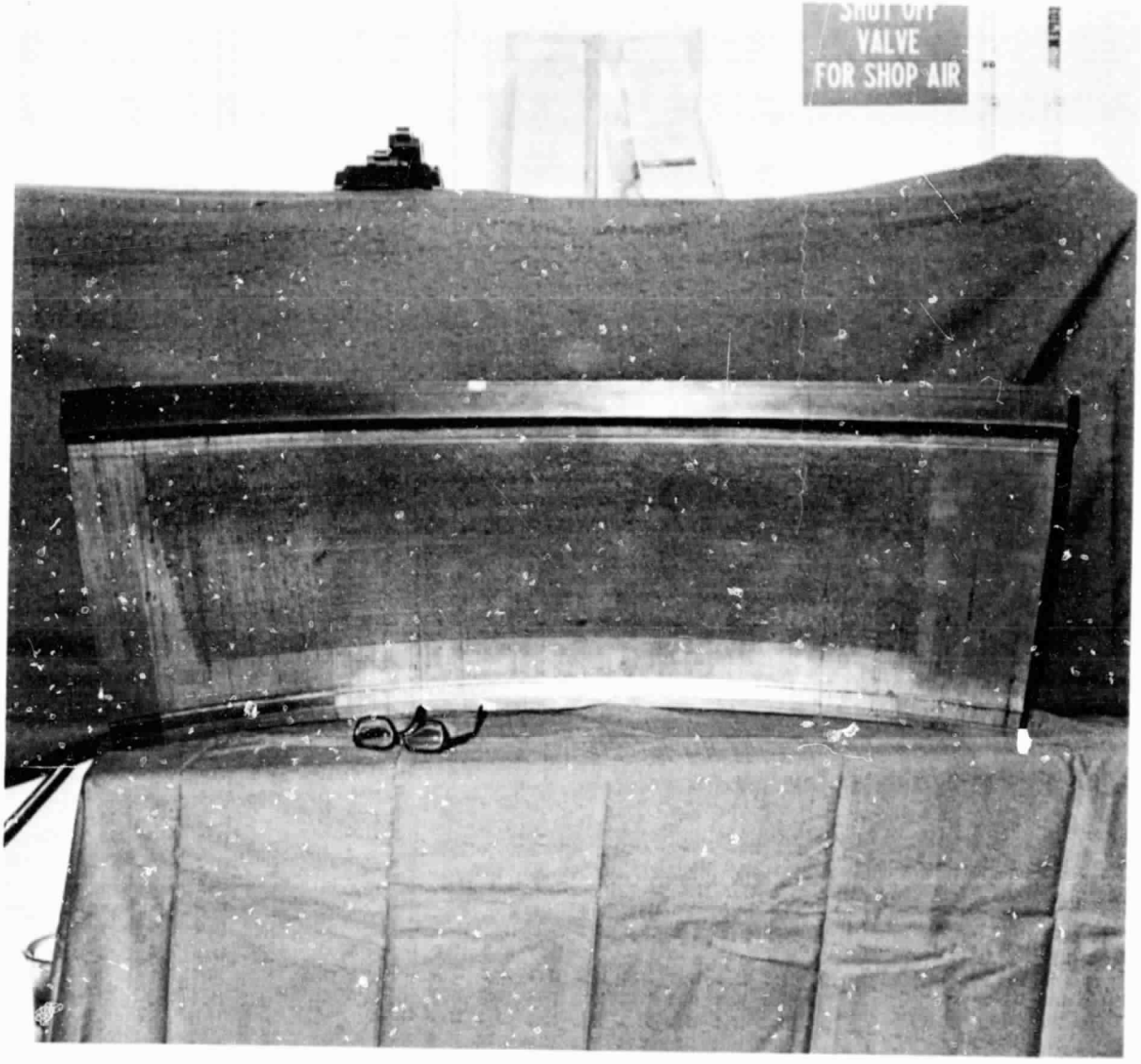

Figure 41. Flap Perforated Inner Skin.

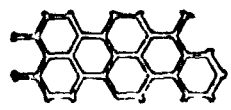

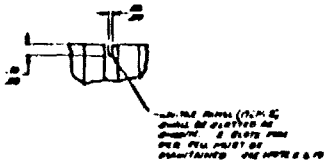

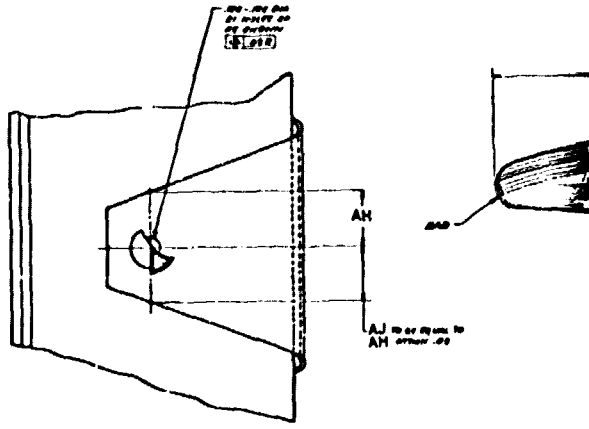

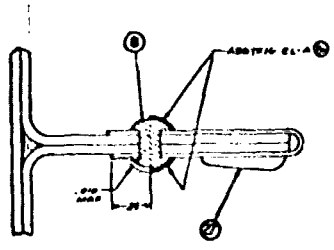

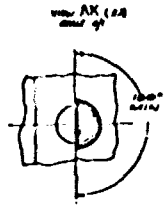

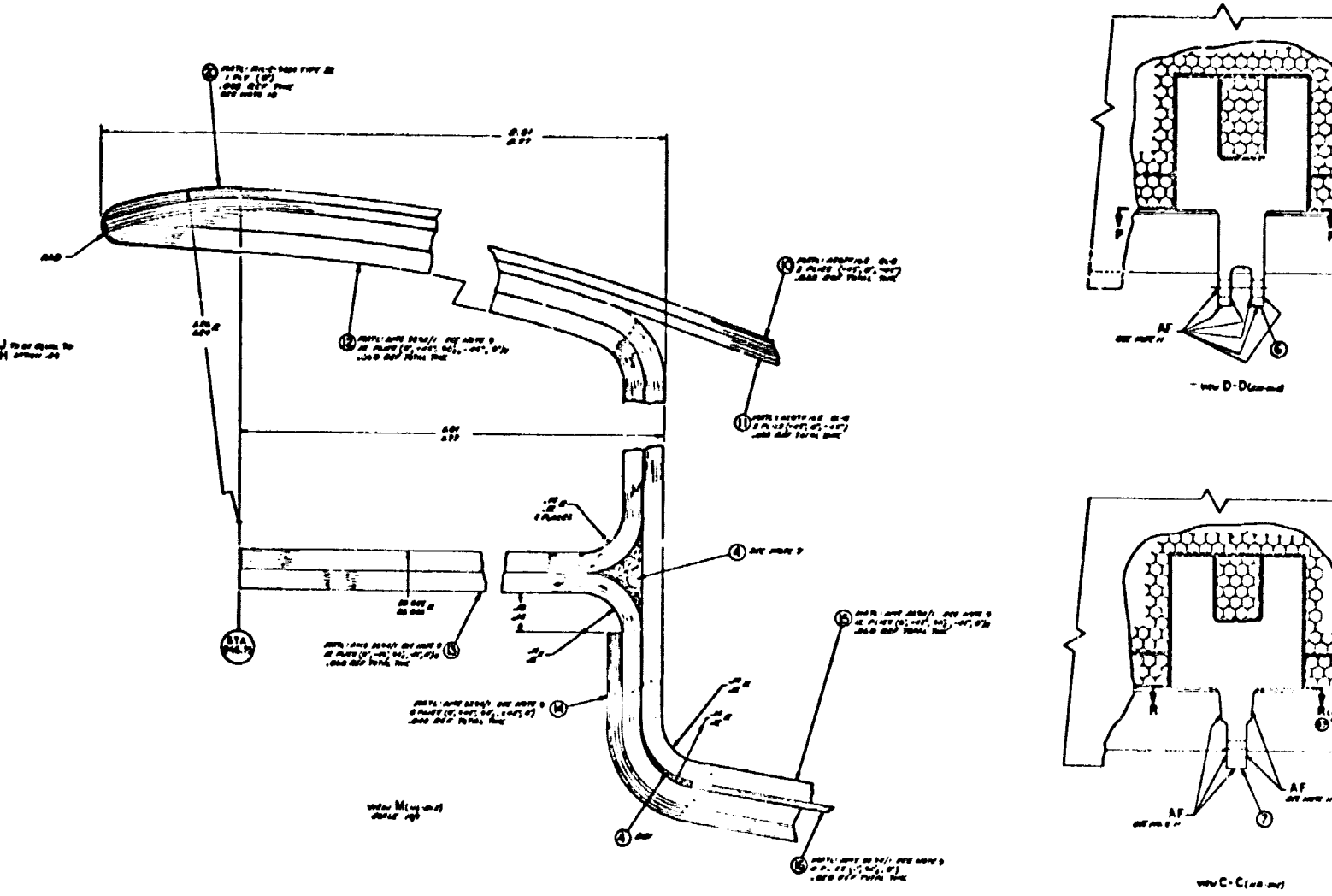

Figure 42. Nozzle Upper Flap, Fittings Installation.

FOLDOUT FRAME 3

ORIGINAL PAGE IS
OF POOR QUALITY

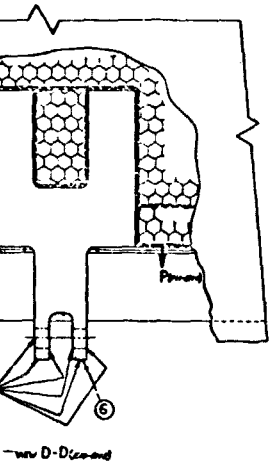

VIEW D-D

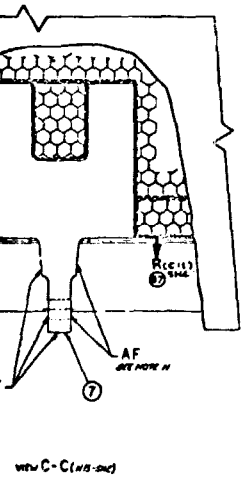

VIEW C-C

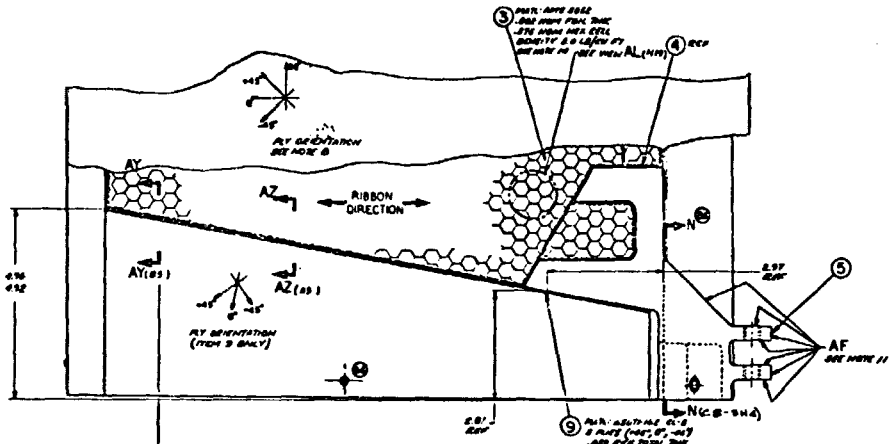

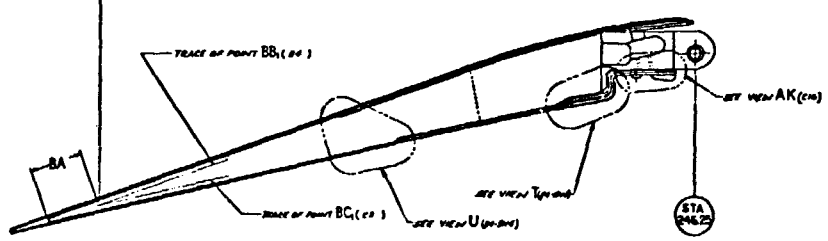

VIEW B-B

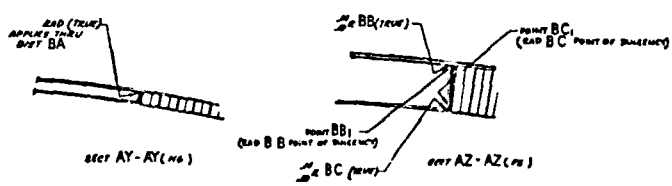

PRECEDING PAGE BLANK NOT FILMED

Figure 43. Upper and Lower Nozzle Flaps.

Table VII. Nozzle Flap Design Conditions.

A. Forward Thrust

- M = 0.92 at 6,401 m (21,000 ft)
- Maneuver Loads
  - 10 g down
  - ±2 g aft
  - 1.5 g side
- Buffet Load
  - ±20 g
- Single jammed actuator

B. Reverse Thrust

- M = 0.227 at SL
- Rejected takeoff or emergency landing

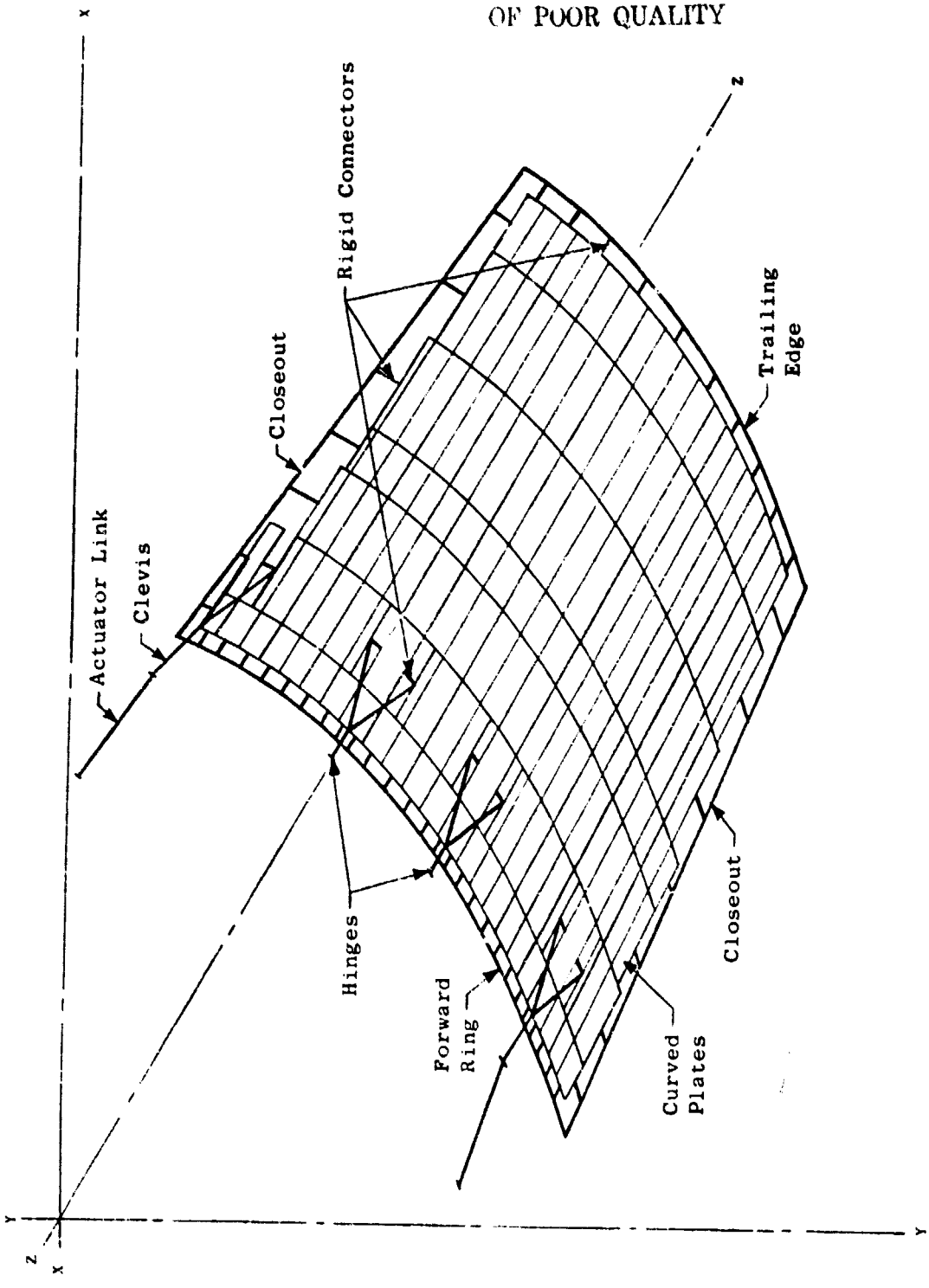

Figure 44. Nozzle Flap Computer Model Schematic.

Table VIII. Nozzle Stresses/Loads.

Component	Mode	Calculated Stress/Load	Allowable Stress/Load	Critical Load Case
Flap Skin	Tension	52.9 MPa (7,670 psi)	211.7 MPa (30,700 psi)	Forward Thrust
Flap Skin	Compression	22.7 MPa (3,290 psi)	109.3 MPa (15,850 psi)	Forward Thrust
Hinge Lug	Shearout/Bearing	34,990 N (7,866 lb)	63,209 N (14,210 lb)	Jammed Actuator
Hinge Pin	Bending	1755 MPa (254,600 psi)	1843 MPa (267,300 psi)	Jammed Actuator
Hinge Lug	Shear	141.7 MPa (20,550 psi)	250.3 MPa (36,300 psi)	Forward Thrust
Hinge Lug	Bending	218.9 MPa (31,750 psi)	256.5 MPa (37,200 psi)	Forward Thrust
Clevis Lug	Shearout/Bearing	21,912 N (4,926 lb)	36,386 N (8,180 lb)	Jammed Actuator
Clevis Lug	Bending	52.7 MPa (7,640 psi)	246.1 MPa (35,700 psi)	Forward Thrust
Clevis Pin	Bending	1,482 MPa (215,000 psi)	1,786 MPa (259,000 psi)	Jammed Actuator
Link	Compression	18,189 N (4,089 lb)	27,579 N (6,200 lb)	Reverse Thrust

3.3.5 Core Cowl

The core cowl doors define the inner boundary of the fan air flowpath from the fan frame to the core nozzle. They also are designed with integral sound-suppression treatment similar to the balance of the nacelle. These doors are hinged to the inner pylon to provide access to the core engine for maintenance purposes. The core cowl configuration is shown in Figure 45.

The core cowl consists of two nearly semicircular, symmetrical, honeycomb sandwich bondments similar in construction to the balance of the nacelle except for the materials. Due to the higher temperature environment in which the core cowl must operate, it is made from materials capable of sustained operation at 561 K (550° F). The face sheets are HMF182HC-66 graphite/PMR15 polyimide laminations, the core is HRH327 fiberglass/polyimide honeycomb, with the whole bonded together with Fiberite Company 9364 BQ polyamide-imide adhesive.

The core cowl doors are supported off the engine inner pylon by hinges spaced along the upper axial closeouts (see Figure 46) and are fastened together along the bottom centerline by four toggle-type flush latches the same as the bypass duct outer doors. At the forward end the doors each contain a steel, radially inward facing, circumferential lug which is bonded in place. These lugs engage a matching groove in the fan frame when the doors are closed and latched. This joint transmits the core cowl axial loads to the engine frame. The aft end of the cowl doors are provided with a steel support ring which is bonded and mechanically fastened to the composite bondment. This ring is supported by, and is allowed to axially slip on, the core exhaust nozle to compensate for differential thermal growth between the engine and the composite core cowl. The ring is also spaced off the core nozzle by a series of individual lugs located around the ring inner surface. This maintained gap serves as an exit for the core cowl cavity cooling air.

When the core cowl doors are closed, the cowl cavity is divided into two separate compartments by virtue of the engine radial fire shield which seals against the inner surface of the cowl doors approximately halfway along the doors. Located on either side of this seal plane is a series of holes through the bondment which allows fan exhaust air to be vented into the compartments as a cooling medium. In addition, on the experimental cowl doors, cooling air manifolds (one per compartment) are mounted around the inside of the doors in the same region as the fan air cooling holes. These manifolds direct secondary, externally supplied, cooling airflow fore and aft from the engine radial fire shield along the cowl inner periphery. A stainless-steel-covered thermal blanket is mounted on standoffs from that portion of the cowl doors that cover the cavity aft compartment, the secondary cooling air being directed between this blanket and the cowl and then exited through the door aft slip joint. Figure 47 shows the inner surface of a core cowl door with the manifolds and thermal blanket in place.

The outer (flowpath) cowl face sheet is perforated and the honeycomb core depth is stepped to meet the acoustic requirements. Figure 48 shows the perforated surface in a completed door. The installed relationship of a set of cowl doors is shown in Figure 49.

FOLDOUT FRAME

ORIGINAL PAGE IS
OF POOR QUALITY

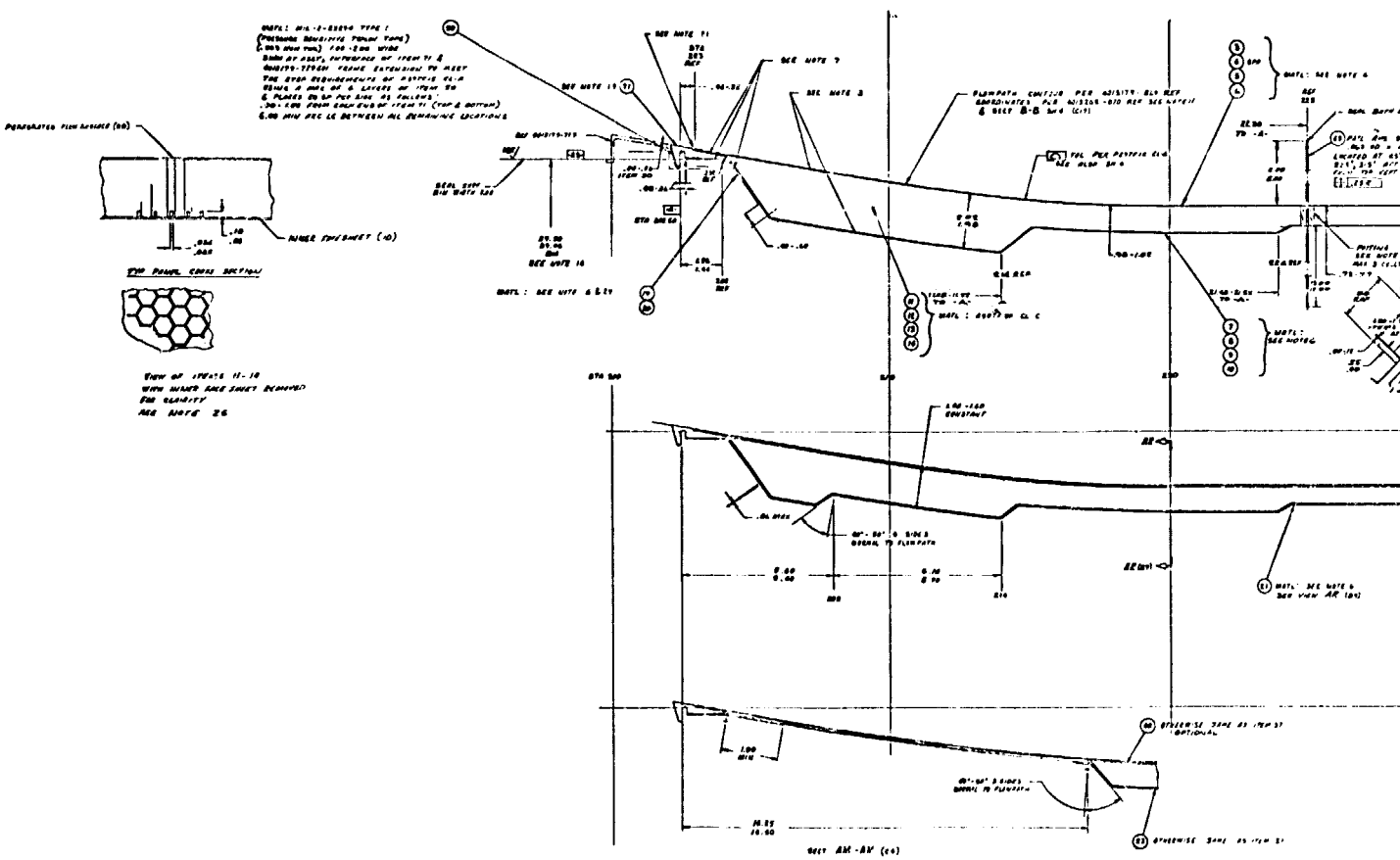

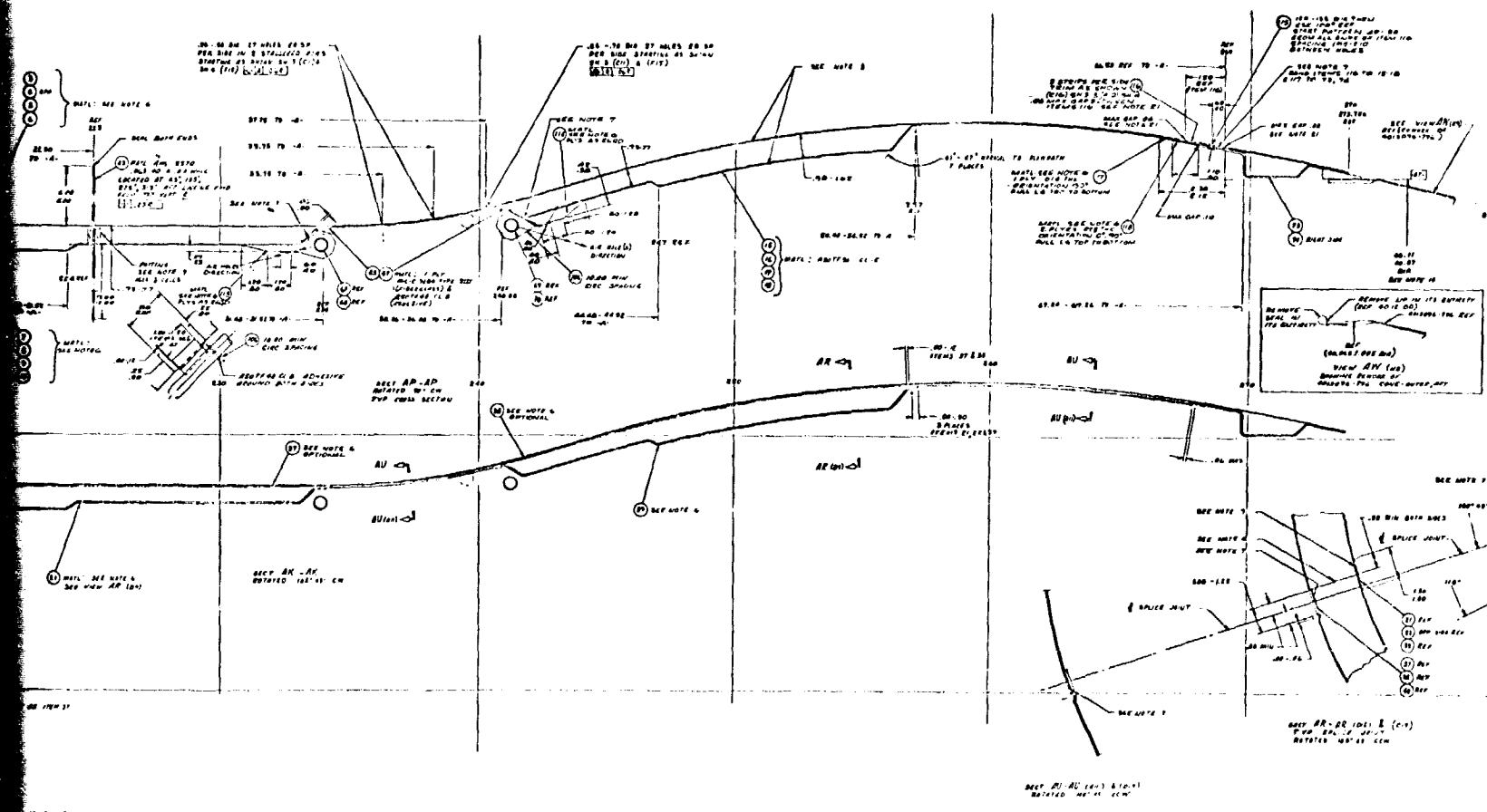

Figure 45. Core Cowl Configuration.

FOLDOUT FRAME 3

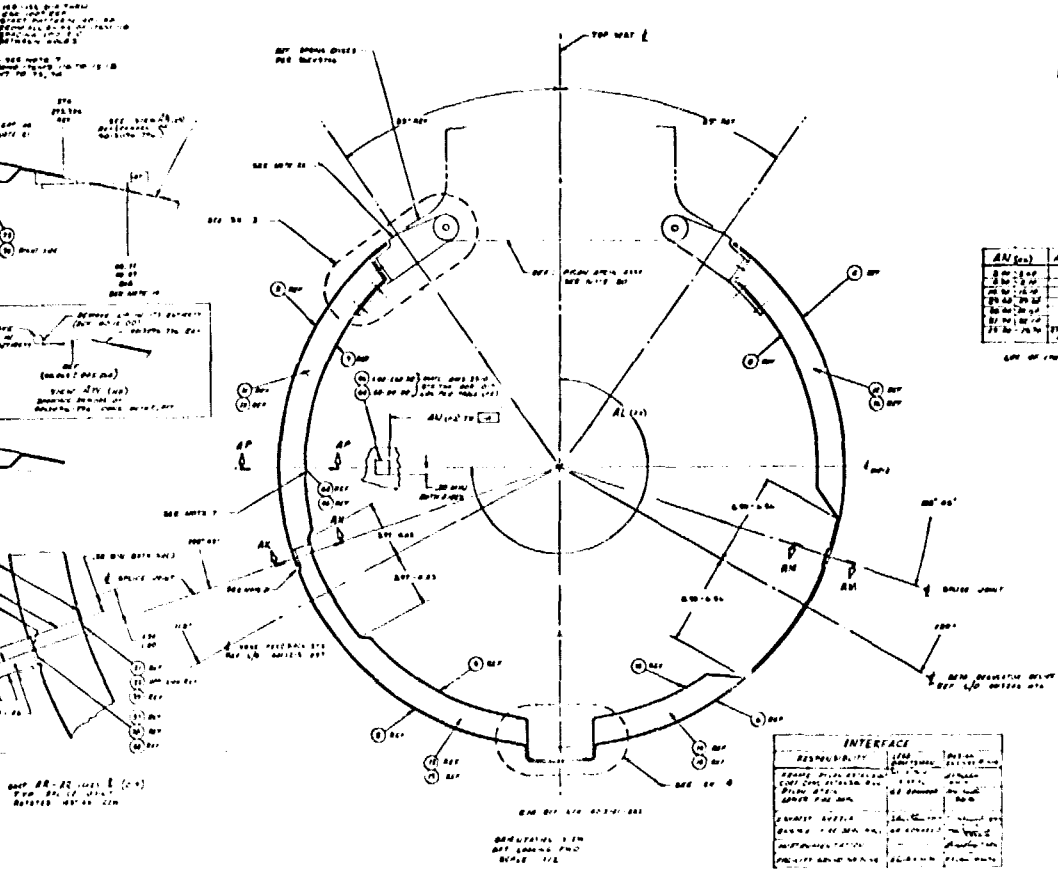

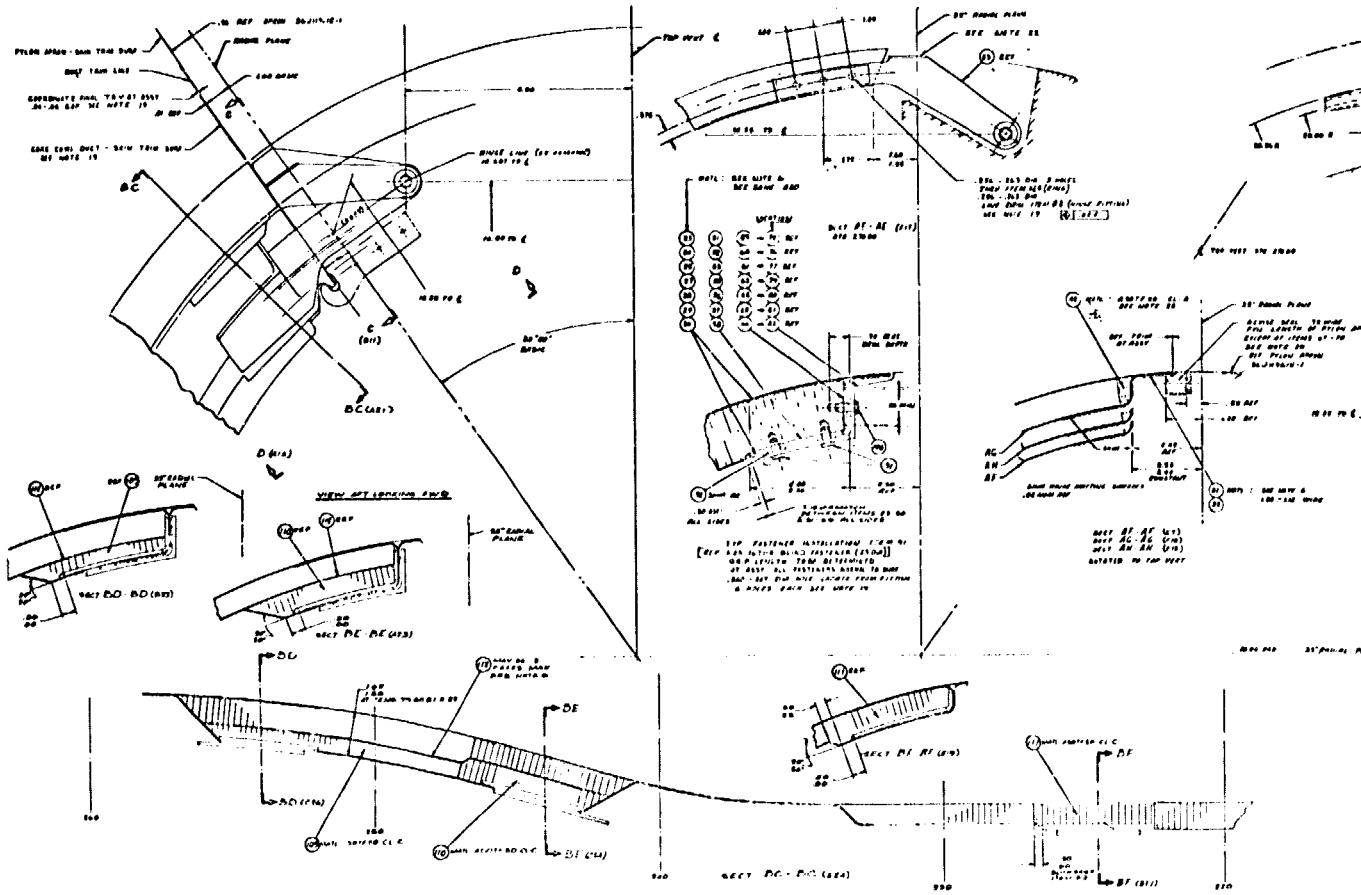

FC[illegible]T FRAME 2

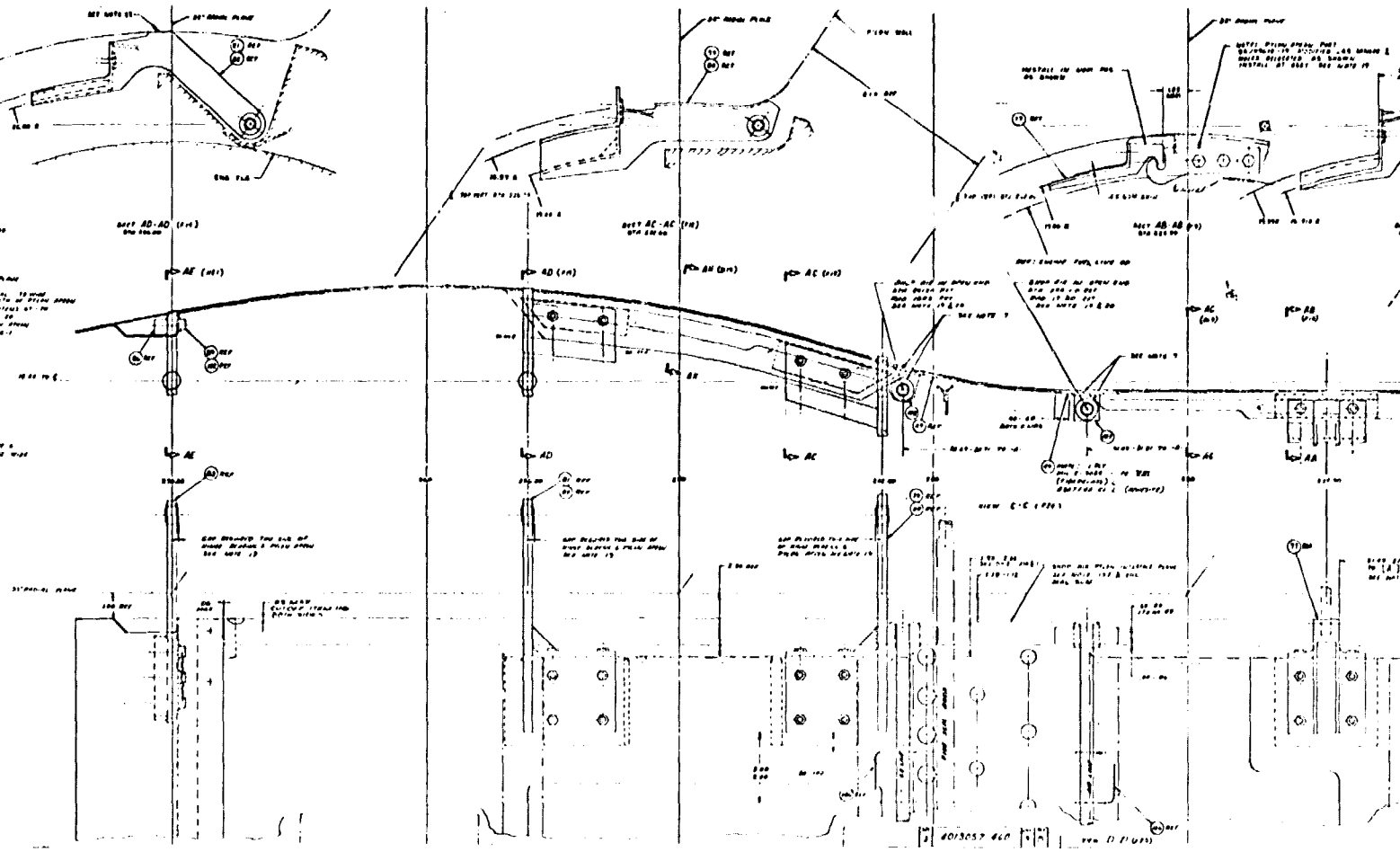

Figure 46. Core Cowl Hinge Arrangement.

FRAME 3

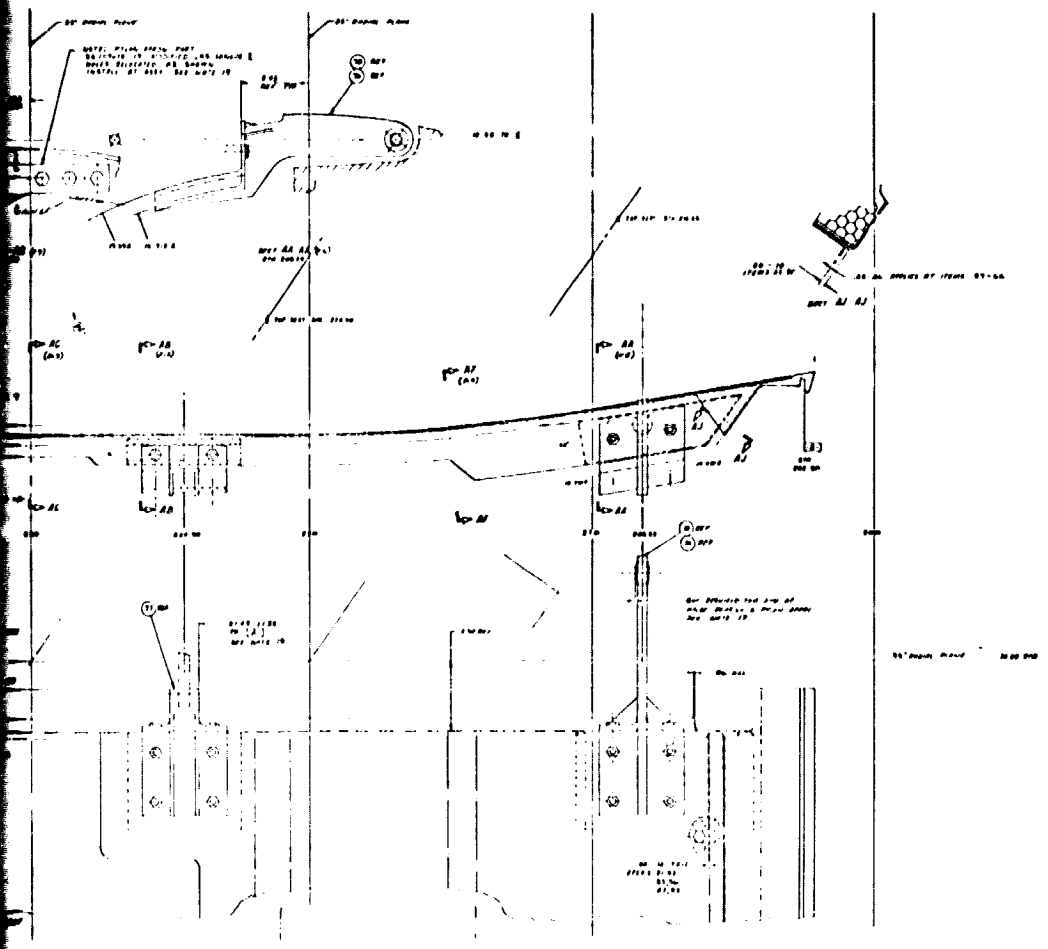

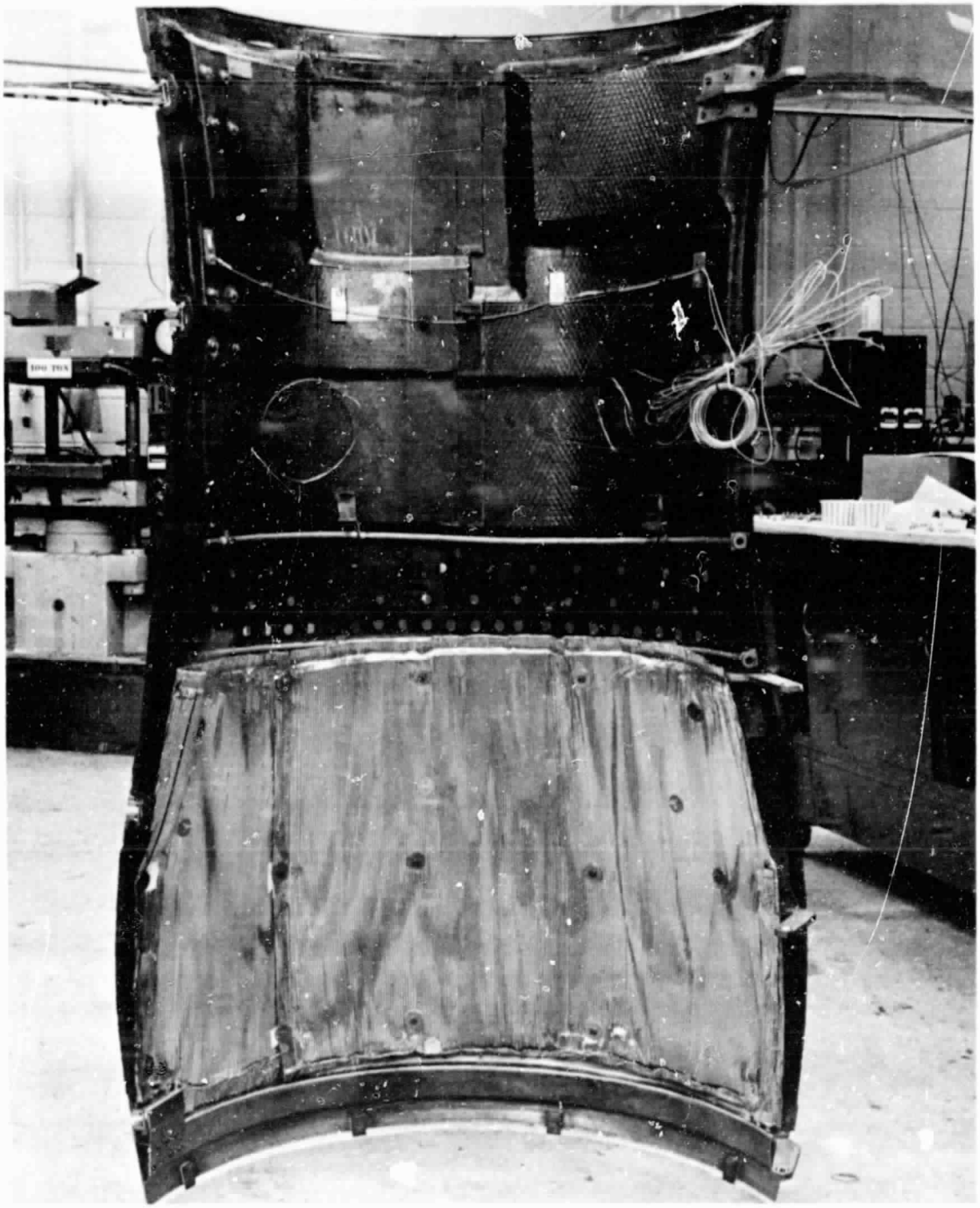

Figure 47. Core Cowl Door Inner Surface.

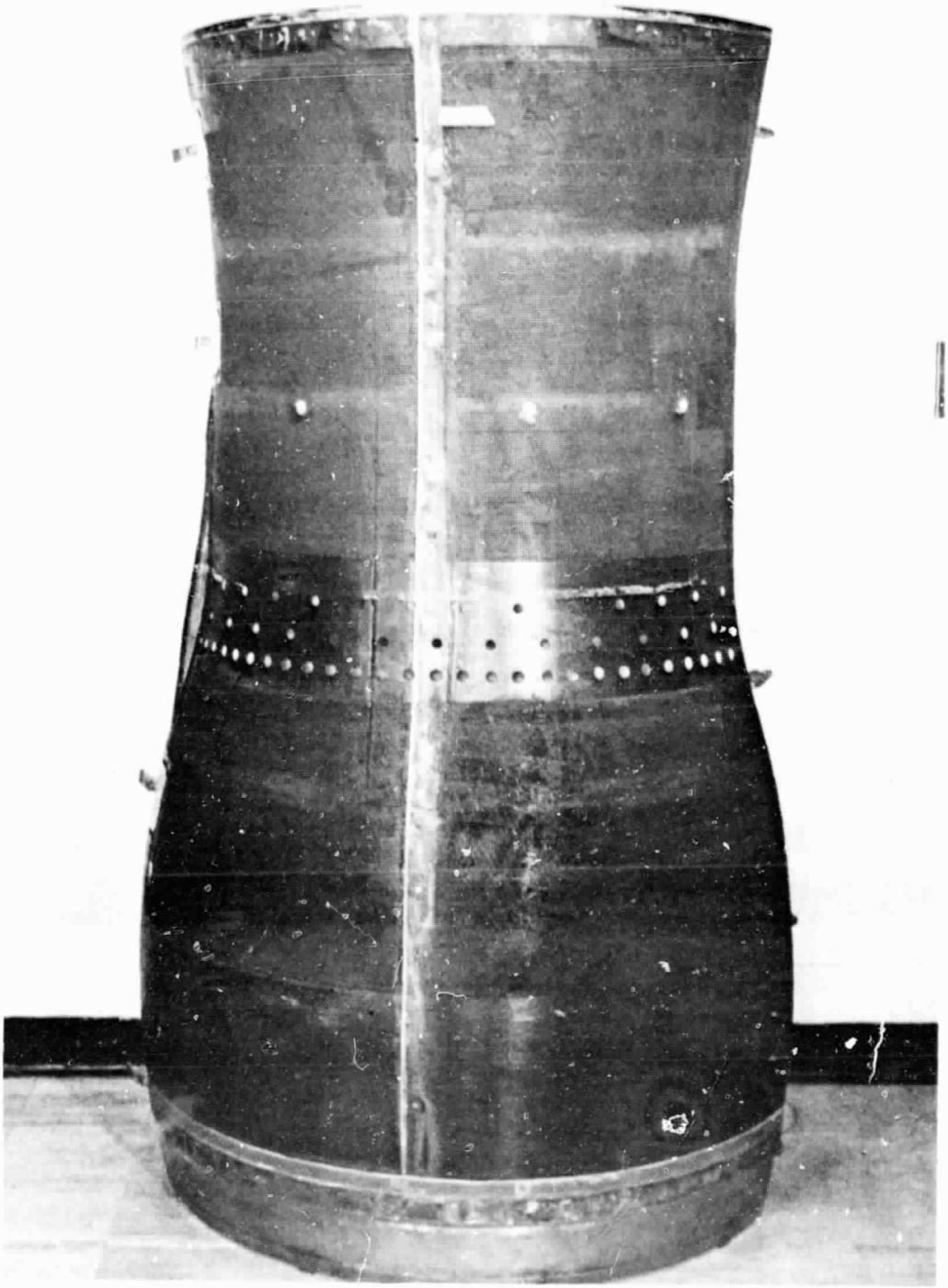

Figure 48. Core Cowl Door Outer Surface.

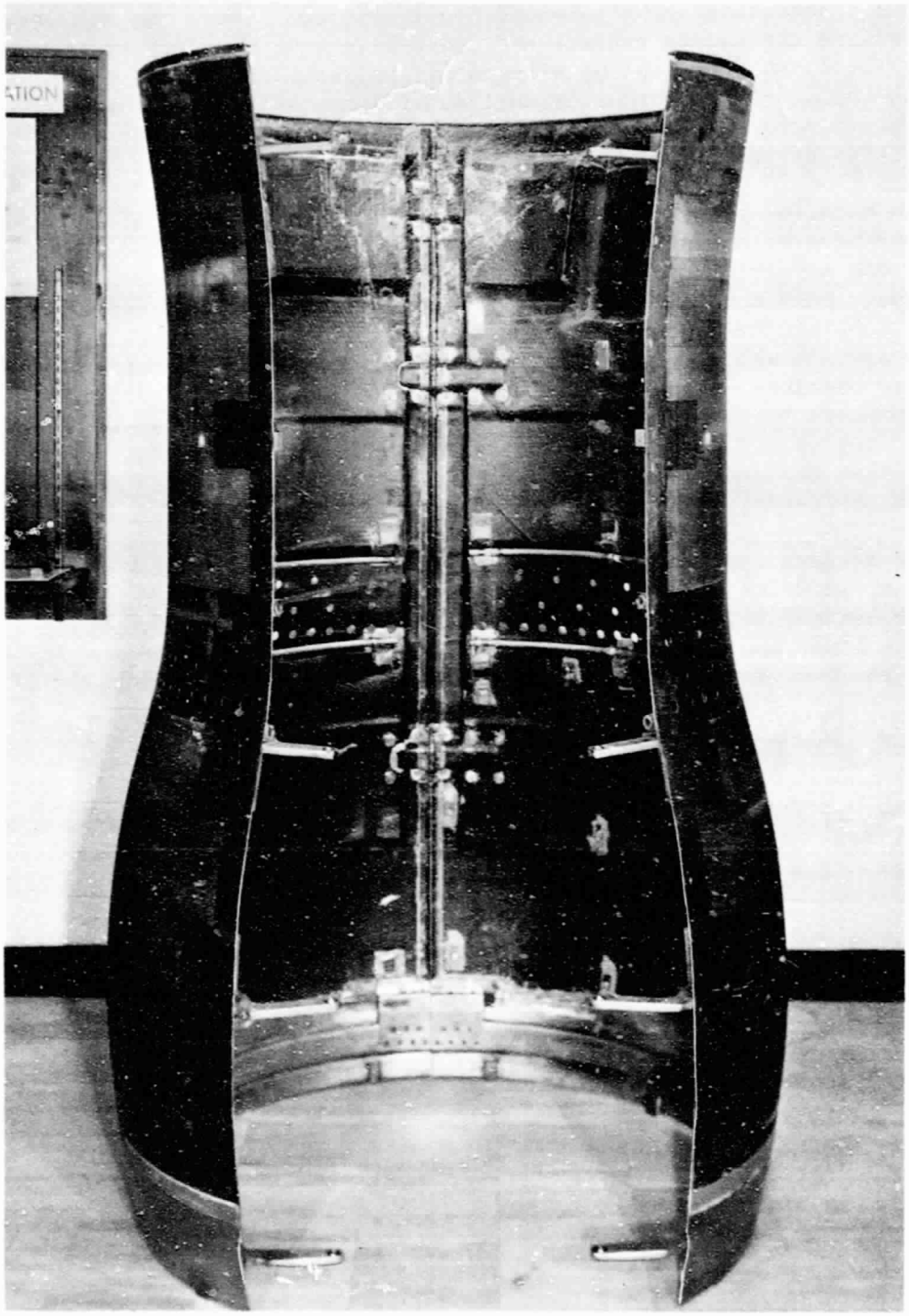

Figure 49. Core Cowl Doors.

C-2

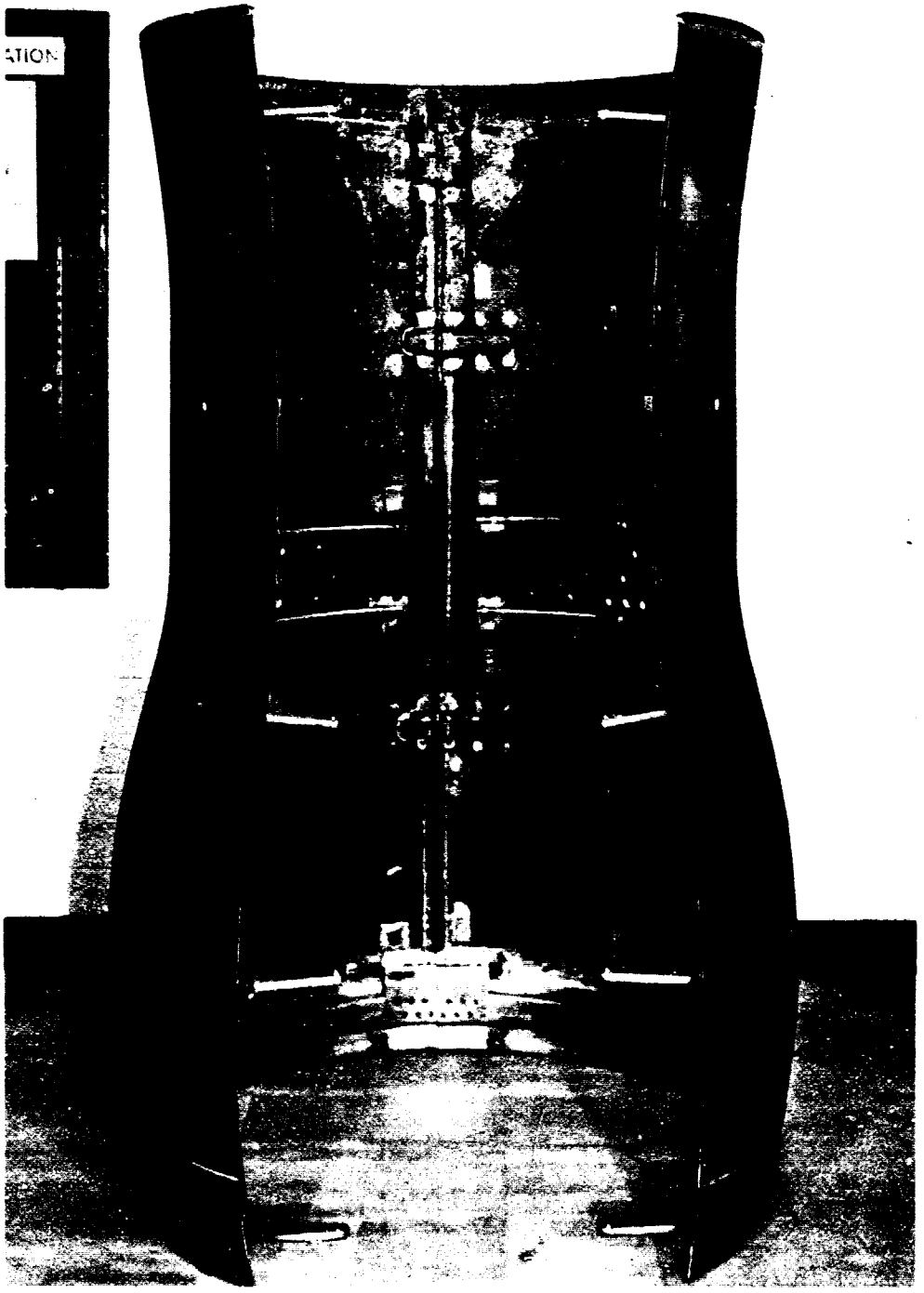

Figure 49. Core Cowl Doors.

C-2

Temperature considerations were of primary importance in determining the core cowl construction materials and configuration. The inner surfaces of the doors are exposed to radiant and convective heat from the engine casings and are insulated from cooling effects of the fan airstream by the honeycomb sandwich walls. A heat transfer analysis (Figure 50) showed that cooling air and a shield were needed to keep the maximum cowl skin temperature within the capabilities of the composite materials.

The material properties used in the design and analysis of the composite core cowl were established by an element test program conducted on both perforated and nonperforated specimens at room temperature and at elevated temperatures. Only short-term data were accumulated. Table IX summarizes the element test program. The test results are shown in Table X. The data shown are the average values obtained from the testing. Values for the perforated skin were obtained on specimens with a diamond pattern configuration. A square pattern perforation was used in the actual design which would only cut half as many graphite fibers as the diamond pattern; therefore, it was assumed that the design allowables are twice as great as those obtained from the element testing of the perforated specimens.

The maximum cowl loadings occur at (1) forward thrust at Mach 0.92, 6,401-m (21,000-ft) maximum cruise power setting and (2) at Mach 0.227, sea level at maximum reverse thrust power setting (takeoff power). Table XI shows the hinge and latch loads at these conditions. A summary of the analysis of the cowl inner and outer face sheets is shown in Table XII.

3.3.6 Subcomponent Tests

To verify the structural integrity of the critical joint areas, a subcomponent test program was conducted and the results compared against the requirements. The test summary is shown in Table XIII.

(1) Maximum Estimated Engine Casing Temperature

(2) Fire Wall Location

(3) Estimated Unshielded Cowl ID Maximum Temperature with 1 Change/Minute of Air

(4) Estimated Unshielded Cowl ID Maximum Temperature with 380 Changes/Minute of Air

(5) Estimated Cowl ID Maximum Temperature with Radiation Shield and 292 Changes/Minute of Air

(6) Estimated Cowl ID Maximum Temperature with Radiation Shield, Thermal Blanket, and 180 Changes/Minute of Air

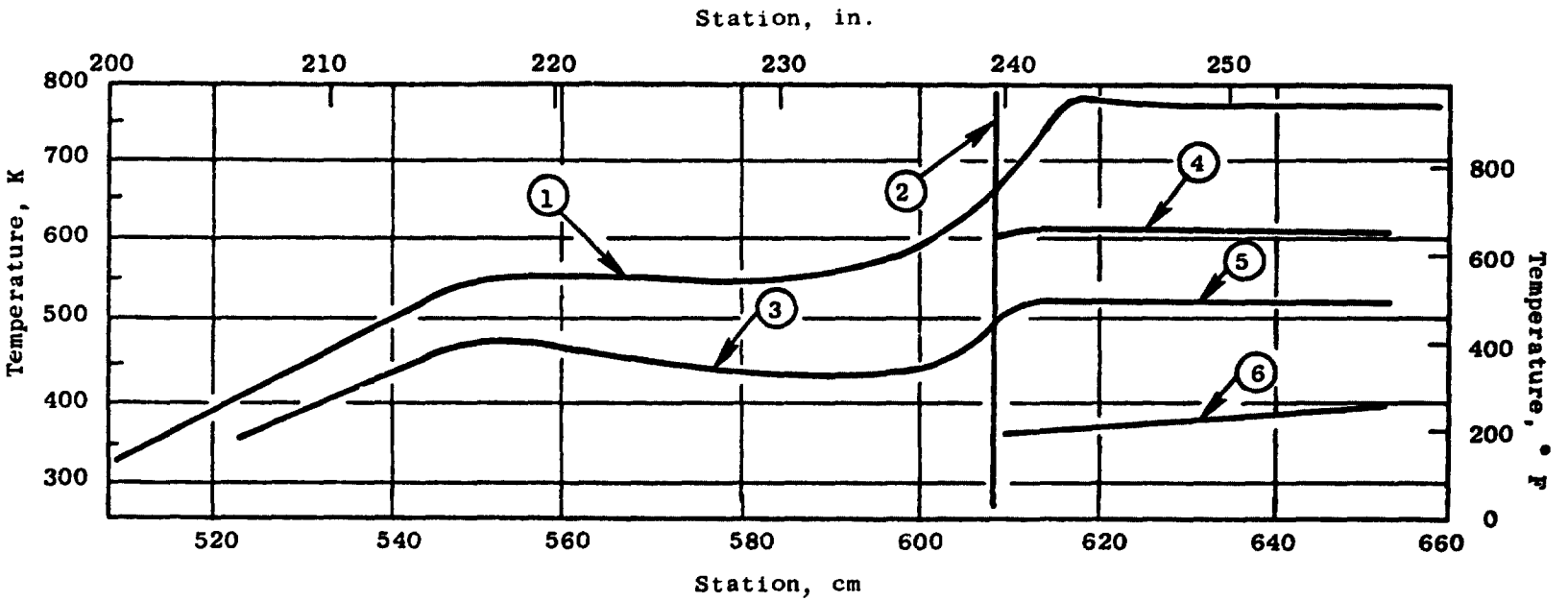

Figure 50. Inner Core Cowl Estimated Temperatures.

Table IX. Core Cowl Element Test Program.

Test	219.3 K (-65° F)	294.3 K (70° F)	394.3 K (250° F)	449.8 K (350° F	533.2 K (500° F)	560.9 K (550° F)
IITRI Tensile (NP)		X		X		X
IITRI Tensile (P)		X		X	X	
Compressive (NP)		X		X	X	
Interlaminar Shear (NP)		X		X		X
Rail Shear (NP		X		X		X
Coefficient of Expansion	X		X		X	

Table X. Core Cowl Element Test Results.

Test	219.3 K (-65° F)	299.3 K (70° F)	394.3 K (250° F)	449.8 K (350° F)	533.2 K (500° F)	560.9 K (550° F)
IITRI Tensile (NP)	---	460.9 MPa (66,850 psi)	---	376.2 MPa (54,570 psi)	---	523.2 MPa (75,900 psi)
IITRI Tensile (P)	---	95.9 MPa (13,910 psi)	---	94.2 MPa (13,660 psi)	96.3 MPa (13,970 psi)	---
Compressive (NP)	---	501.7 MPa (72,770 psi)	---	377.2 MPa (54,710 psi)	300.7 MPa (43,610 psi)	---
Interlaminar Shear (NP)	---	28.3 MPa (4,110 psi)	---	25.2 MPa (3,650 psi)	---	26.3 MPa (3,820 psi)
Rail Shear (NP)	---	11.8 MPa (1,710 psi)	---	9.9 MPa (1,440 psi)	---	9.0 MPa (1,310 psi)
Coefficient of Expansion	2.448×10^{-6} cm/cm/K (1.36×10^{-6} in./in./° F)	---	2.07×10^{-6} cm/cm/K (1.15×10^{-6} in./in./° F)	---	1.449×10^{-6} cm/cm/K (0.805×10^{-6} in./in./° F)	---

(NP) - Nonperforated

(P) - Perforated

Table XI. Core Cowl Hinge and Latch Loads.

Component	Torsion Load (Reverse Thrust)	Compression Load (Forward Thrust)
Hinge No. 1	1,681 N (378 lb)	7,509 N (1,688 lb)
Hinge No. 2	1,681 N (379 lb)	8,741 N (1,965 lb)
Hinge No. 3	2,491 N (560 lb)	8,287 N (1,863 lb)
Hinge No. 4	1,837 N (413 lb)	6,361 N (1,430 lb)
Hinge No. 5	778 N (175 lb)	547 N (123 lb)
Latch No. 1	1,592 N (358 lb)	7,126 N (1,602 lb)
Latch No. 2	2,117 N (476 lb)	10,520 N (2,365 lb)
Latch No. 3	3,265 N (734 lb)	11,988 N (2,695 lb)
Latch No. 4	1,503 N (338 lb)	1,815 N (408 lb)

Table XII. Core Cowl Stresses.

Load Condition	Component	Mode	Calculated Stress MPa (psi)	Allowable Stress MPa (psi)
Forward Thrust	Outer Face Sheet	Tension	84.8 (12,300)	192.4 (27,900)
Reverse Thrust	Outer Face Sheet	Compression	22.9 (3,324)	124.8 (18,100)
Reverse Thrust	Inner Face Sheet	Tension	31.4 (4,550)	461.9 (67,000)
Forward Thrust	Inner Face Sheet	Compression	114.2 (16,560)	299.9 (43,500)
Forward Thrust	Forward Flange Bond	Shear	0.6 (85)	13.8 (2,000)
Forward Thrust	Aft Skin	Tension	173.5 (25,160)	524.0 (76,000)
Forward Thrust	Aft Support	Compression	194.4 (28,200)	266.8 (38,700)

Table XIII. Nacelle Subcomponent Test Results.

Specimen Configuration	Condition (1)	Test Mode	Design Load (2)	Average Test Failure Load
A. Inlet				
Inlet Wall				
Flat Panel, Precured	a	Bending	42.1 MPa (6,100 psi)	215.1 MPa (31,900 psi)
Flat Panel, Cocured	a	Bending	42.1 MPa (6,100 psi)	179.2 MPa (25,990 psi)
Curved Panel, Precured	a	Bending	42.1 MPa (6,100 psi)	171.9 MPa (24,930 psi)
Curved Panel, Cocured	a	Bending	42.1 MPa (6,100 psi)	115.2 MPa (16,705 psi)
Axial Splice Joint	b	Tension	54.2 MPa (7,860 psi)	213.6 MPa (30,980 psi)
B. Bypass Duct Doors				
Curved Wall Panel	c	Bending	29.0 MPa (4,206 psi)	210.6 MPa (30,545 psi)
Piano Hinge	c	Tension	32,347 N (7,272 lb)	34,474 N (7,750 lb)
Cowl Latch	c	Tension	25,995 N (5,844 lb)	25,666 N (5,770 lb)(3)
Actuator Mount	c	Tension	52,364 N (11,772 lb)	49,598 N (11,150 lb)(3)
Splitter Attachment	d	Bending	133 N (30 lb)	5,703 N (1,282 lb)
Fan Nozzle Hinge, Cowl Side	e	Tension	34,990 N (7,866 lb)	52,267 N (11,750 lb)
C. Variable Fan Nozzle				
Fan Nozzle Hinge, Flap Side	e	Tension	34,990 N (7,866 lb)	70,816 N (15,920 lb)
Actuator Link Clevis	e	Tension	21,912 N (4,926 lb)	59,437 N (13,362 lb)
D. Core Cowl Doors				
Curved Wall Panel	c	Bending	68.8 MPA (9,972 psi)	157.9 MPa (22,900 psi)
Cowl Hinge	f	Tension	3,737 N (840 lb)	68,502 N (15,400 lb)
Cowl Latch	f	Tension	4,897 N (1,101 lb)	25,577 N (5,750 lb)

(1) a - 3-g Stall at M = 0.4 at Sea Level
b - Maximum Cruise at M = 0.6 at Sea Level
c - Maximum Cruise at M = 0.92 at 6,401 m (21,000 ft)
d - Takeoff
e - Jammed Actuator
f - Reverse Thrust

(2) Three times operating load for composites; 1.5 times for metal parts.

(3) Design was strengthened based on this test, but the test was not rerun.

4.0 WEIGHT

The UTW composite nacelle weight status at the completion of the fabrication of the individual components is shown in Table XIV. Differences between the experimental nacelle and projected flight nacelle weights are the result of design differnces made to reduce program cost and to meet the noise goals of a shorter takeoff for the experimental propulsion system. In addition, included in the experimental nacelle weights are accommodations for supporting system test instrumentation. These differences are itemized in detail in Table XV.

Table XIV. Nacelle Weight.

	Experimental Composite		Equivalent Flight	
	kg	lb	kg	lb
Inlet	242	533	150	330
Fan Duct	125	275	91	201
Flare Nozzle	41	90	30	67
Core Cowl	69	153	41	91
Total Composite Nacelle	477	1,051	312	689

As shown, while the individual composite nacelle component equivalent flight weights have varied from the design objectives, the total nacelle equivalent flight weight of 312 kg (689 lb) is within 4% of the nacelle total objective weight of 301 kg (663 lb). This increase in projected flight nacelle weight will only reduce the installed thrust-to-weight ratio from 4.32 to 4.30 (Reference: NASA CR-134847, Quiet Clean Short-Haul Experimental Engine (QCSEE) Under-the-Wing (UTW) Final Design Report, dated June 1977).

Table XV. Experimental and Flight Nacelle Weight Differences.

Component	Δ Weight kg	Δ Weight lb	Justification
Inlet	-92	-203	The flight inlet will not require the test installation instrumentation and slipring strut supports. Refined manufacturing methods and redesign of outer barrel to skin and stringer design further reduce weight.
Fan Cowl	-34	- 74	The flight duct has no acoustic splitter [required only for a 609.6-m (2000-ft) runway] and is 19.1 cm (7.5 in.) shorter. Hydraulic tube tunnel area redesigned for weight reduction.
Flare Nozzle	-11	-23	Experimental nacelle uses simplified machined metal fittings for program cost reduction.
Core Cowl	-28	-62	Savings due to 19.1-cm (7.5-in.) shorter length, removal of axial splice joints and core potting, and redesign of metal components for weight reduction.

APPENDIX A

QCSEE UTW ENGINE OUTER COWL STATIC LOAD TEST

1.0 SUMMARY

This appendix to the QCSEE UTW nacelle design report presents the results of the outer cowl static load test. This test had as its objectives the verification of the capability of the cowl to sustain the design flight loads imposed by the fan nozzle and the maintenance of cowl integrity during on-engine testing. This test was not part of the original QCSEE test plan but was added at a later date.

The outer cowl is constructed primarily of composite materials with the sandwich core being flexible aluminum honeycomb. The outer skin and closeouts are fabricated from Kevlar 49 fabric in an epoxy matrix and the perforated inner skin and aft ring are graphite/epoxy.

The applied loads were those calculated to be the extreme conditions for both forward and reverse thrust cases; they included maneuver and buffet loads in the forward thrust case and buffet loads in the reverse thrust case. Full-load application was achieved in the reverse thrust mode (including buffet loads), but the test was halted during the forward thrust mode at approximately 75% of the maximum calculated load conditions when some delamination was noticed in the bonded joint between the aft ring and the outer skin. Examination of the untested cowl door revealed similar unbonded areas in the same joint leading to the conclusion that the initial unbond was present prior to the start of the test and was not a result of the testing. These areas were repaired and structurally upgraded by the addition of fiberglass wraparounds and mechanical fasteners. As the actual applied loads exceeded those calculated for the static on-engine test conditions, it was decided not to set up and run the forward thrust case to 100% of maximum condition subsequent to the repair.

The results of the static testing showed that the cowl was capable of sustaining the on-engine testing and reverse thrust flight loads.

1.1 TEST PLAN

1.1.1 Test Objective

The purpose of this test was to verify that the QCSEE UTW outer cowl was capable of sustaining the maximum calculated flight loadings from the fan nozzle flaps in both the forward and reverse thrust modes. These loads were those calculated from pressure data obtained from five-inch model testing with maneuver and buffet loads superimposed for the extreme flight envelope conditions. These conditions were deemed to be a forward flight condition at maximum cruise power setting at a Mach number of 0.92 at 6400-m (21,000-ft) altitude with a 10-g load, a 2-g aft load, and a 1.5-g side load. Also includ-

ed were a 20-g buffet loading on the fan nozzle flaps plus a reverse thrust condition (at maximum reverse thrust power setting) at Mach Number 0.227 at sea level with a 20-g buffet loading on the flaps. The objective was not to run the test to failure, but to determine the response of the cowl within the limits of 100% of the extreme load conditions without causing damage to the cowl, as it was required for the composite nacelle on-engine testing.

1.1.2 Test Configuration

The left-hand (aft looking forward) outer cowl door was used for the test as the instrumented flap for on-engine testing (lower left-hand) would be mounted to this door and, therefore, some duplication of strain gaging and better correlation of test data could be achieved between the two tests.

The outer cowl doors are basically a full-depth sandwich construction with composite skins and closeouts and flexible aluminum honeycomb core. The outer skin is of woven Kevlar 49 in an epoxy matrix and the perforated inner skin and aft ring are graphite in an epoxy matrix. Bonded to the forward closeout is a series of aluminum lugs facing radially inward which engage the fan frame at assembly. Four fan nozzle flap hinge clevises were mounted in the aft ring by a series of flush head, radially oriented screws and nuts. The door was mounted - forward side down - on the floor with a semicircular plate engaging the door forward lugs and preventing axial movement. The cowl door axial piano hinge and the bottom latches were fastened to upright posts bolted to the floor. Four hydraulic actuators were connected to the fan nozzle flap hinge clevises such that the loads were applied the same vectorially as calculated for each individual flap hinge for each flight condition. The test setup is shown in Figures 51 through 53. Figure 54 shows the required applied loads and the angular direction with respect to the horizontal centerline for each hinge clevis.

1.1.3 Test Instrumentation

Each actuator was attached to a load cell for actuation force determination and eight strain gages (four on each sandwich skin) were mounted on the outer cowl door in the vicinity of the lower hinge clevis mounting screws (Figures 54 and 55 show the strain gage arrangement). This hinge location was chosen as it has the greatest applied loads in both flight conditions.

1.1.4 Test Facility

The outer cowl static load test was conducted in the Static Testing Laboratory of the General Electric Company, Evendale, Ohio.

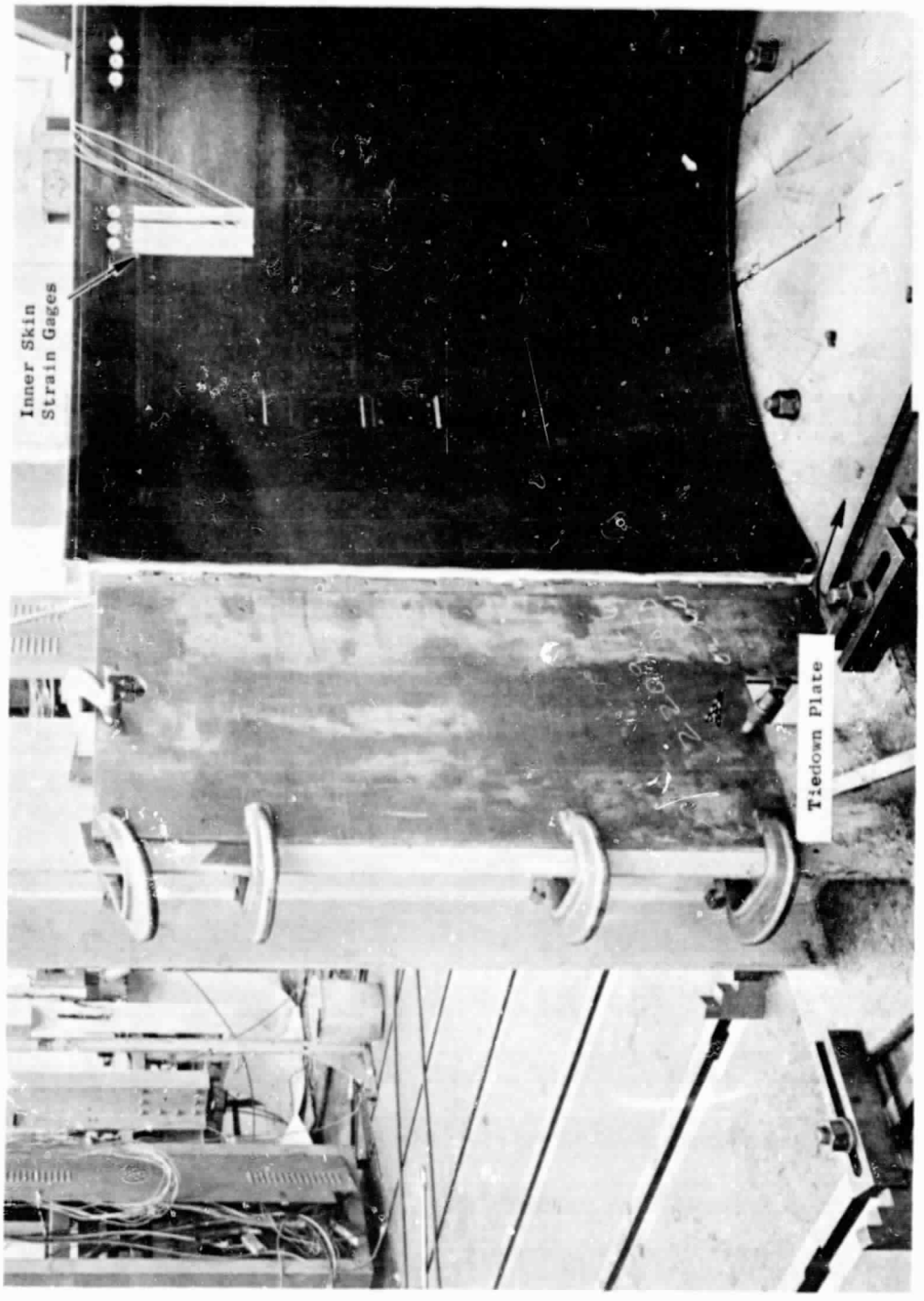

Figure 51. Outer Cowl Door Static Test Setup.

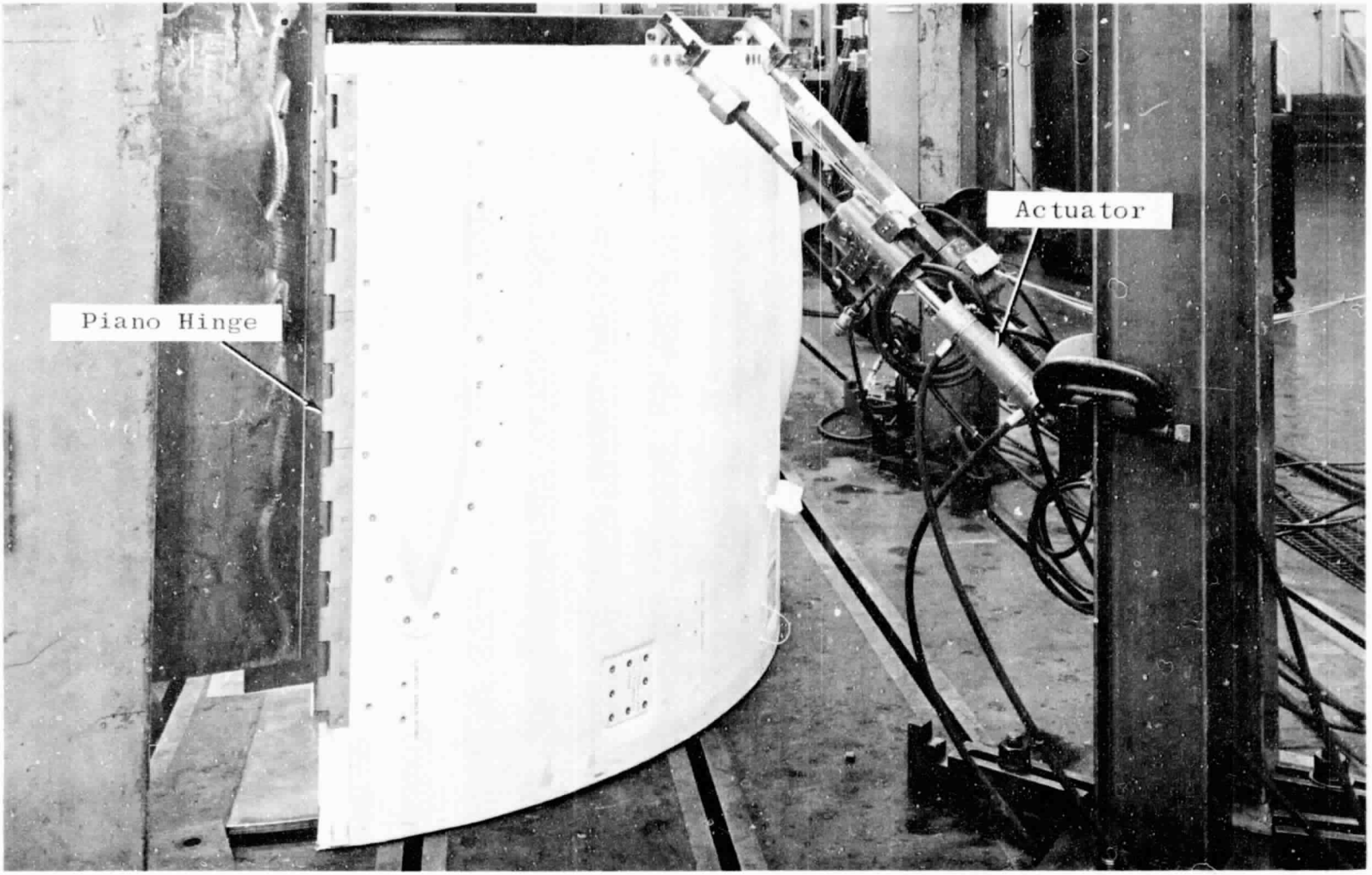

Figure 52. Outer Cowl Door Static Load Test, Piano Hinge Side.

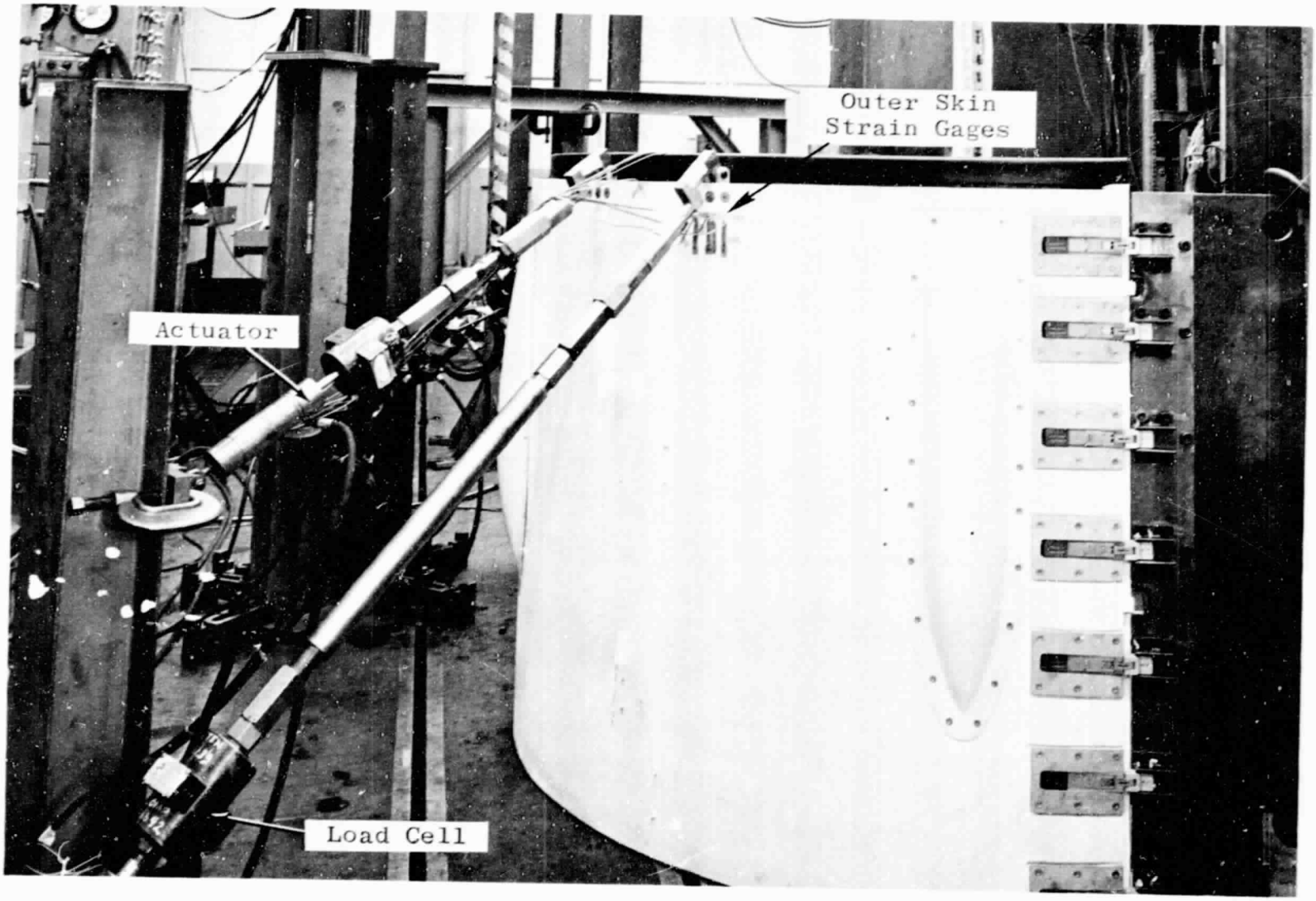

Figure 53. Outer Cowl Door Static Load Test, Latch Side.

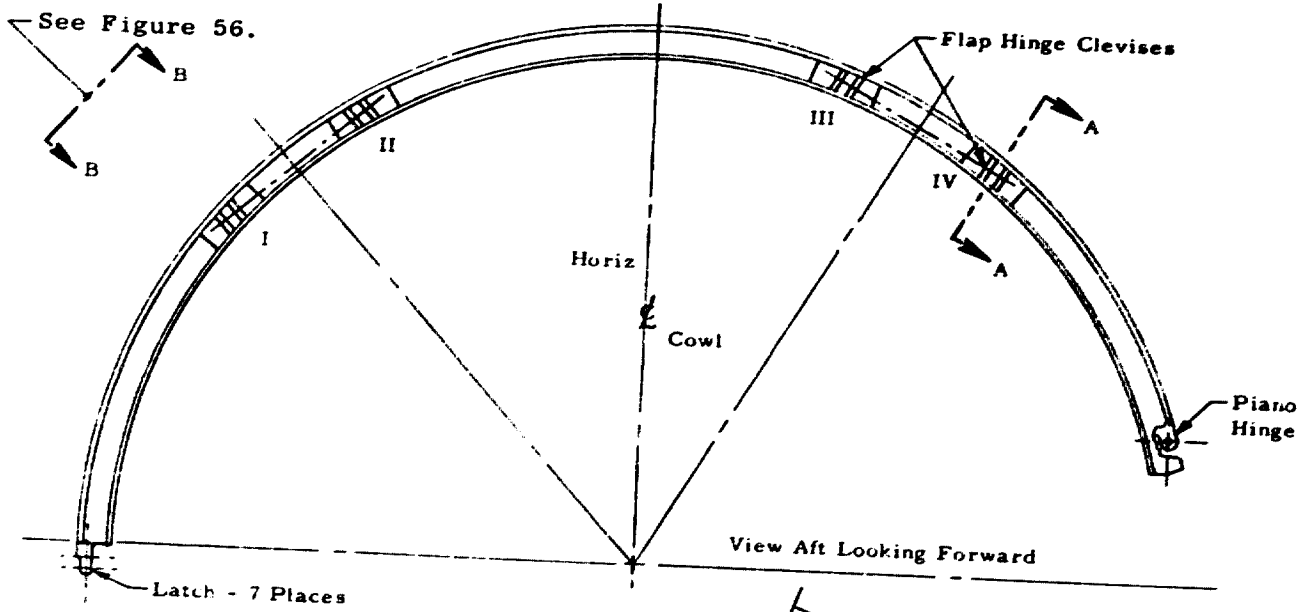

Position	FORWARD THRUST		REVERSE THRUST	
	Load	∝	Load	∝
I	+28,091 N (+6,315 lb)	44.7°	-13,496 N (-3,034 lb)	26.5°
II	+5,369 N (+1,207 lb)	58.3°	-1,899 N (-427 lb)	30°
III	+8,518 N (+1,915 lb)	41.3°	-3,630 N (-816 lb)	32.1°
IV	+23,242 N (+5,225 lb)	48.7°	-11,303 N (-2,541 lb)	27°

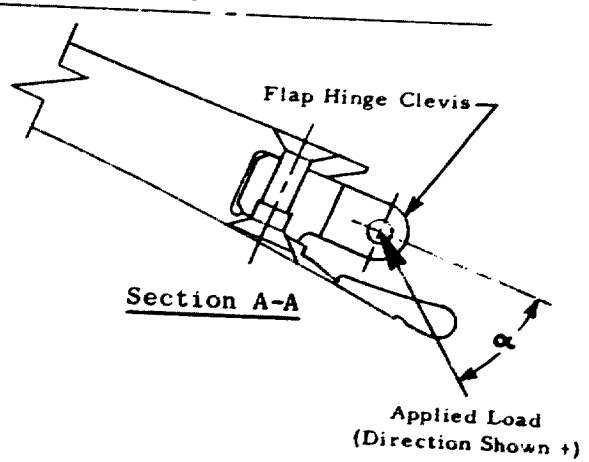

Figure 54. Flap Hinge Loads.

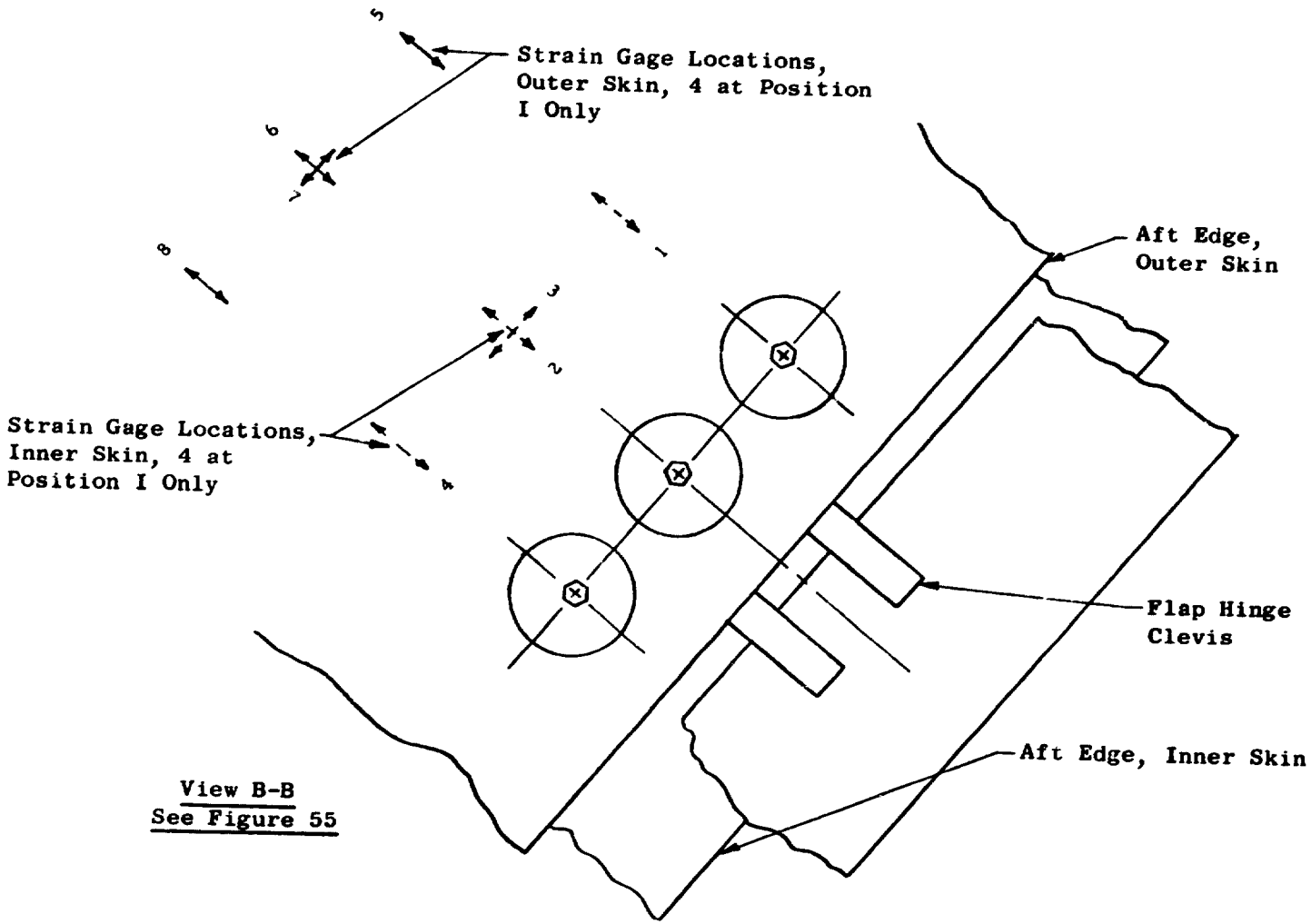

Figure 55. Outer Cowl Strain Gage Locations.

1.1.5 Test Results

Forward Thrust - The forward thrust case was the first case tested. Thirty percent of the required loadings as specified in Figure 54 were first applied at each hinge clevis location and a set of strain gage readings was taken. The load was then increased in 10% increments at each actuator with strain gage readings taken when all loadings were at the same percentage plateaus. At approximately 75% of the maximum load, delamination was noticed in several areas between the outer skin and the aft ring - the test was terminated (see Figures 56, 57). Examination of the untested right-hand cowl door revealed similar unbonded areas between the outer skin and the aft ring. This lead to the conclusion that the delaminations in the door being tested were present prior to the start of the test, and were not caused by the test loadings, but were aggravated by it. It was decided not to continue the forward thrust case testing, but to change the setup to the reverse thrust condition and run that test. The basis for this decision was the fact that the maximum reverse thrust loadings were less than those already applied to the cowl during the forward thrust case. The maximum loads applied to hinge clevises I, II, III and IV (see Figure 54) during forward thrust testing were: 20,858 N (4,689 lb); 3,269 N (735 lb); 6,432 N (1,446 lb); and 18,540 N (4,168 lb), respectively. Figures 58 through 61 show plots of the strain versus the load for each strain gage during forward thrust testing. Table XVI shows the maximum skin stresses achieved.

Reverse Thrust - The reverse thrust case test was conducted in the same manner as the forward thrust case test except that 10% of the required loading was applied as the first plateau and then advanced in 10% increments. The maximum required loadings and angular relationship to the horizontal centerline are shown in Figure 54. The reverse thrust loads act in the opposite direction from the forward thrust loads. No increase in distressed areas was noted and the application of the maximum reverse thrust loads was achieved on all load points. Figures 62 through 65 show the plots of the strain versus the applied load for each strain gage and Table XVI shows the maximum skin stresses.

Repair - At the conclusion of the test, the cowl doors were returned to the vendor for repair of the unbonded areas for a rework of the aft ring/outer skin joint to increase its structural integrity. See Figure 57 for a definition of the rework.

1.1.6 Conclusion

The cowl demonstrated its ability to withstand the calculated maximum reverse-thrust flap-hinge loadings, even with several unbonded areas, without increasing distress. It also demonstrated that it could sustain the maximum calculated static-engine forward-thrust test loadings without damage. Incorporation of the aft ring/skin rework into the design will allow the cowl to withstand the most severe flight loadings.

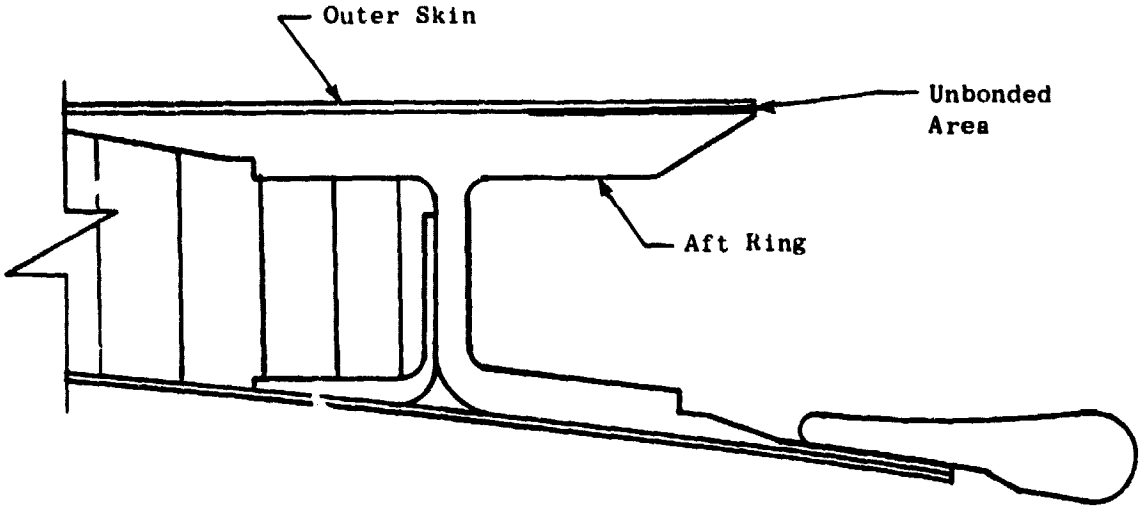

Figure 56. Aft Ring/Outer Skin Delamination.

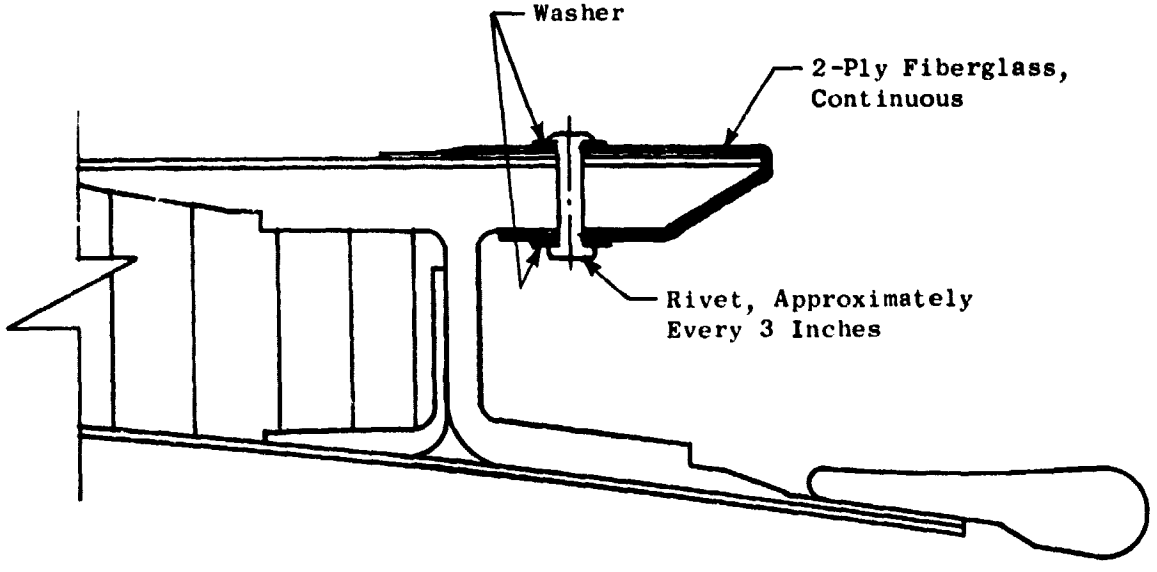

Figure 57. Aft Ring/Outer Skin Redesign.

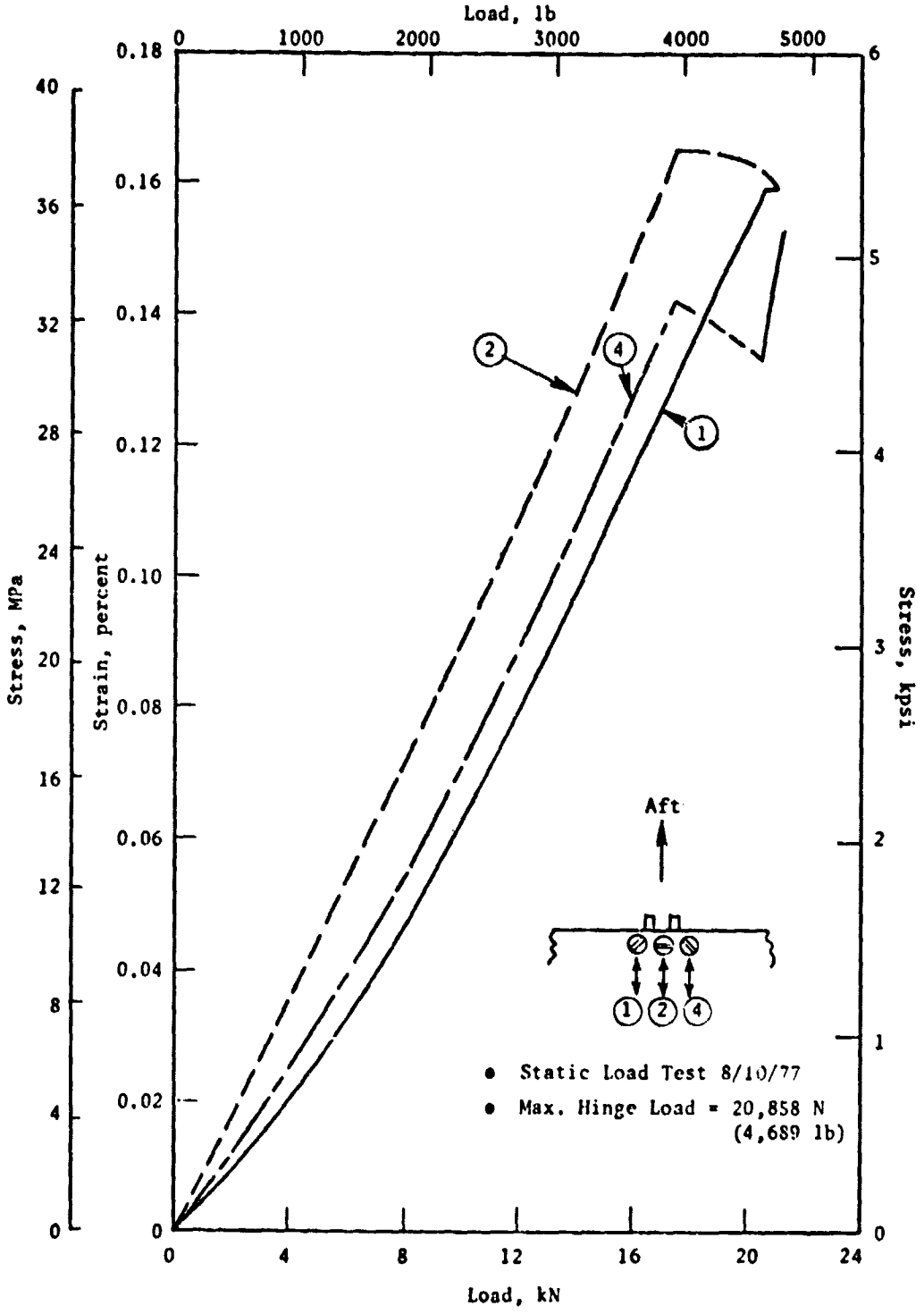

Figure 58. Inner Skin Strain Gages, Axial Forward Thrust Case.

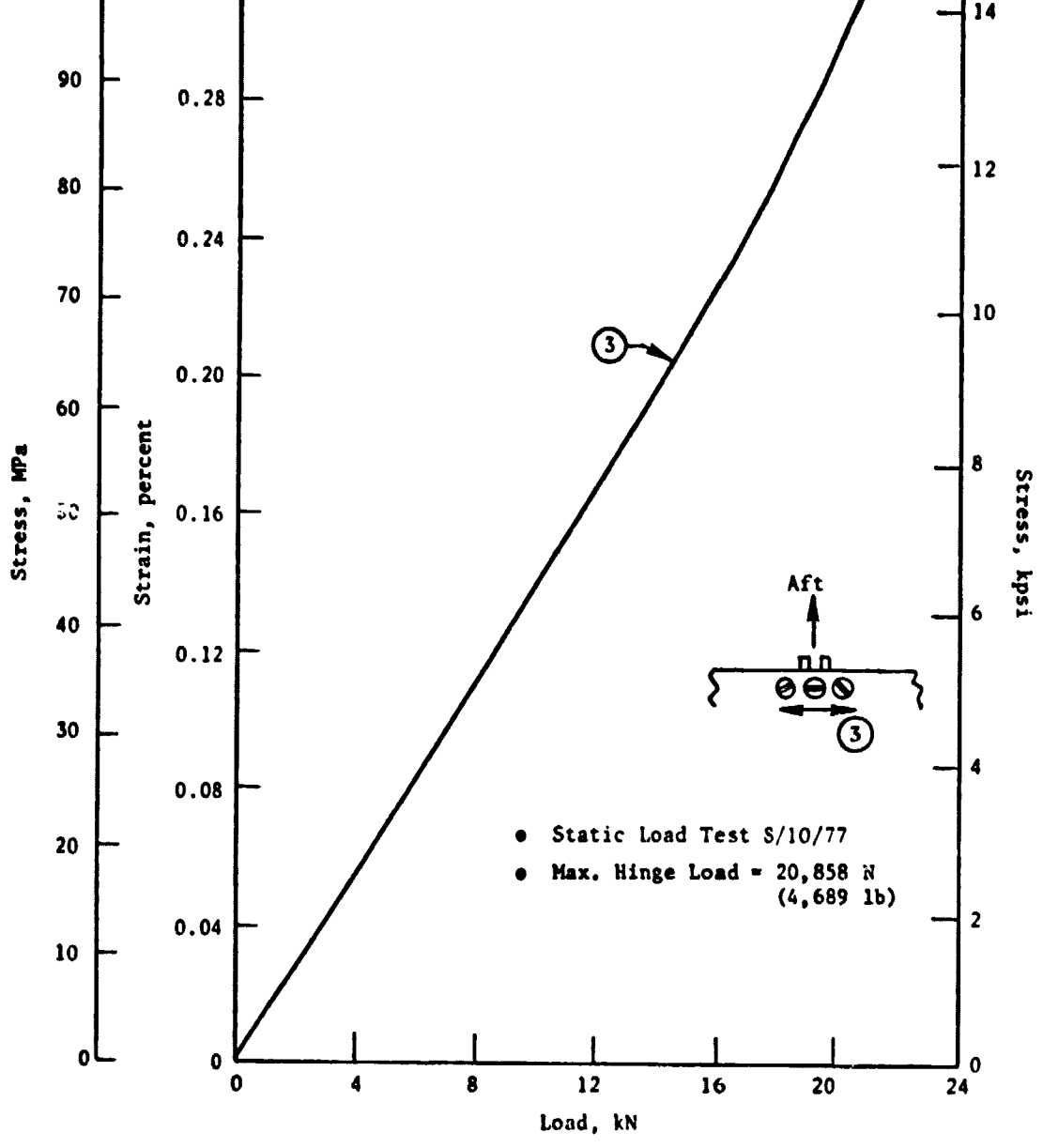

Figure 59. Inner Skin Strain Gage, Circumferential Forward Thrust Case.

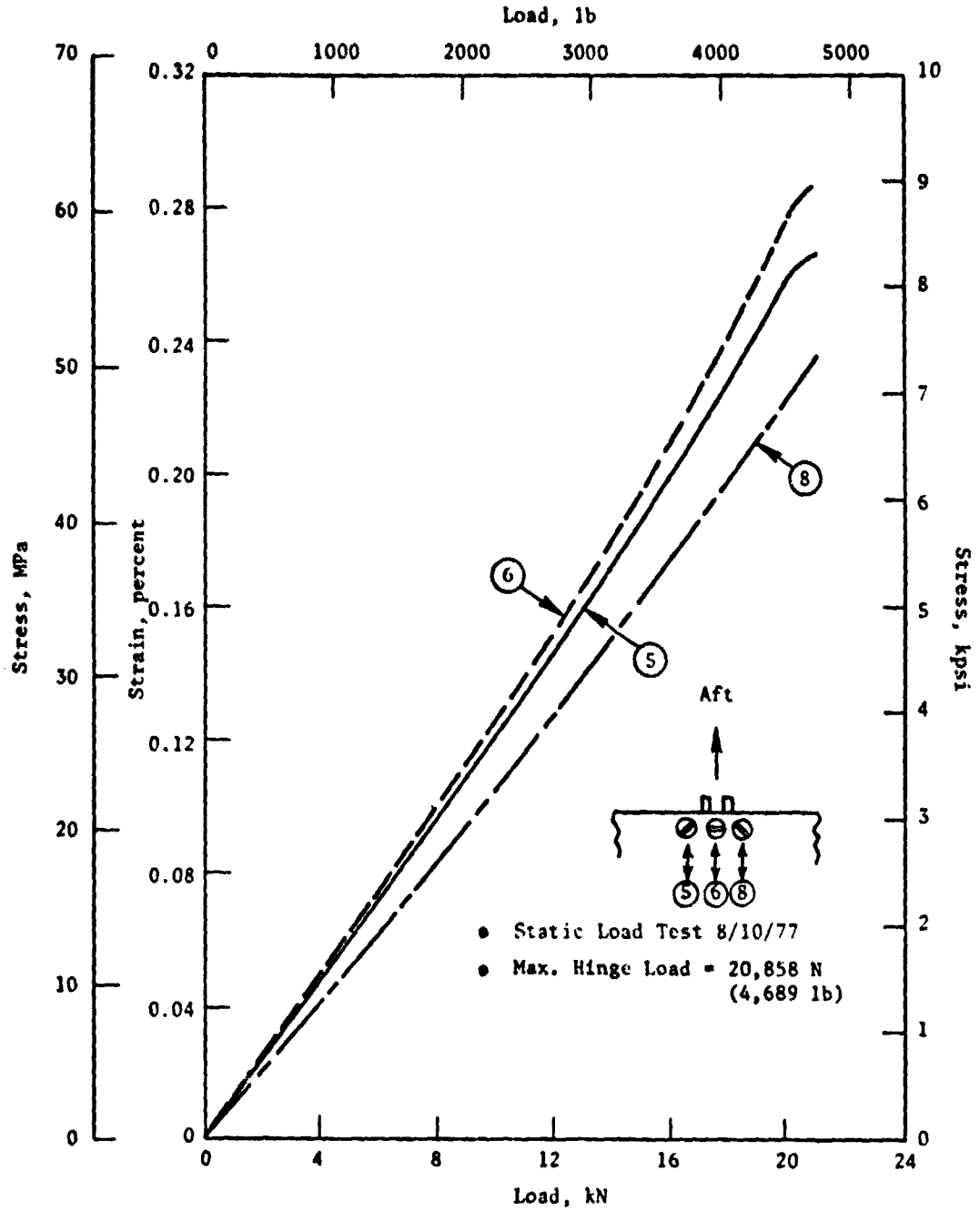

Figure 60. Outer Skin Strain Gages, Axial Forward Thrust Case.

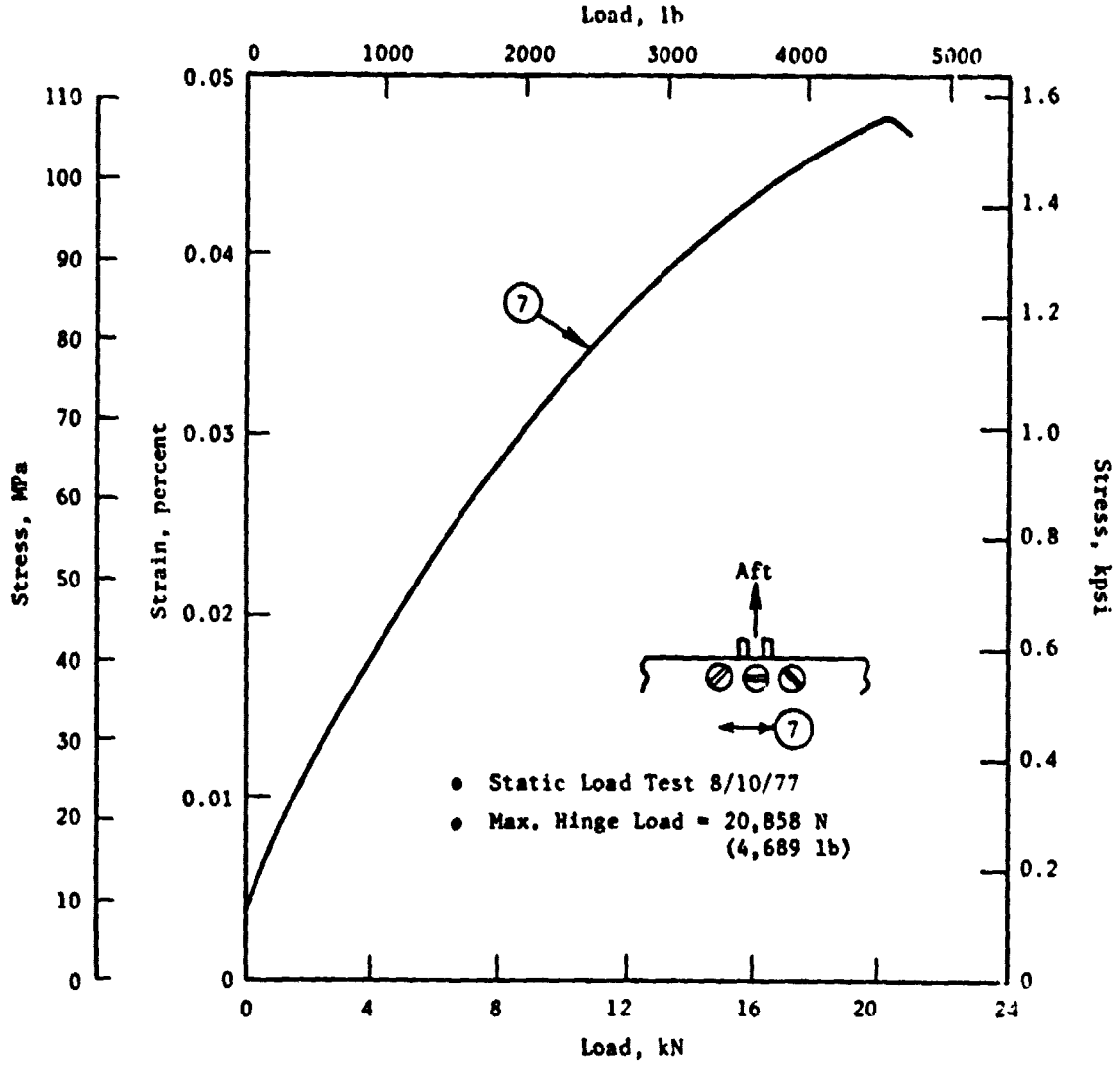

Figure 61. Outer Skin Strain Gage, Circumferential Forward Thrust Case.

Table XVI. Outer Cowl Skin Stresses.

Component and Stress Mode	Stress Direction	Measured Stress	Allowable Stress
A. Forward Thrust			
• Outer Skin Maximum Tension	Circumferential	9.72 MPa (1,410 psi)	314.40 MPa (45,600 psi)
• Outer Skin Maximum Compression	Axial	61.52 MPa (8,923 psi)	137.90 MPa (20,000 psi)
• Inner Skin Maximum Tension	Axial	36.73 MPa (5,327 psi)	219.94 MPa (31,900 psi)
• Inner Skin Maximum Compression	Circumferential	100.61 MPa (14,592 psi)	301.99 MPa (43,800 psi)
B. Reverse Thrust			
• Outer Skin Maximum Tension	Axial	29.96 MPa (4,346 psi)	314.40 MPa (45,600 psi)
• Outer Skin Maximum Compression	Circumferential	6.24 MPa (905 psi)	137.90 MPa (20,000 psi)
• Inner Skin Maximum Tension	Circumferential	46.06 MPa (6,680 psi)	301.99 MPa (43,800 psi)
• Inner Skin Maximum Compression	Axial	20.44 MPa (2,965 psi)	219.94 MPa (31,900 psi)

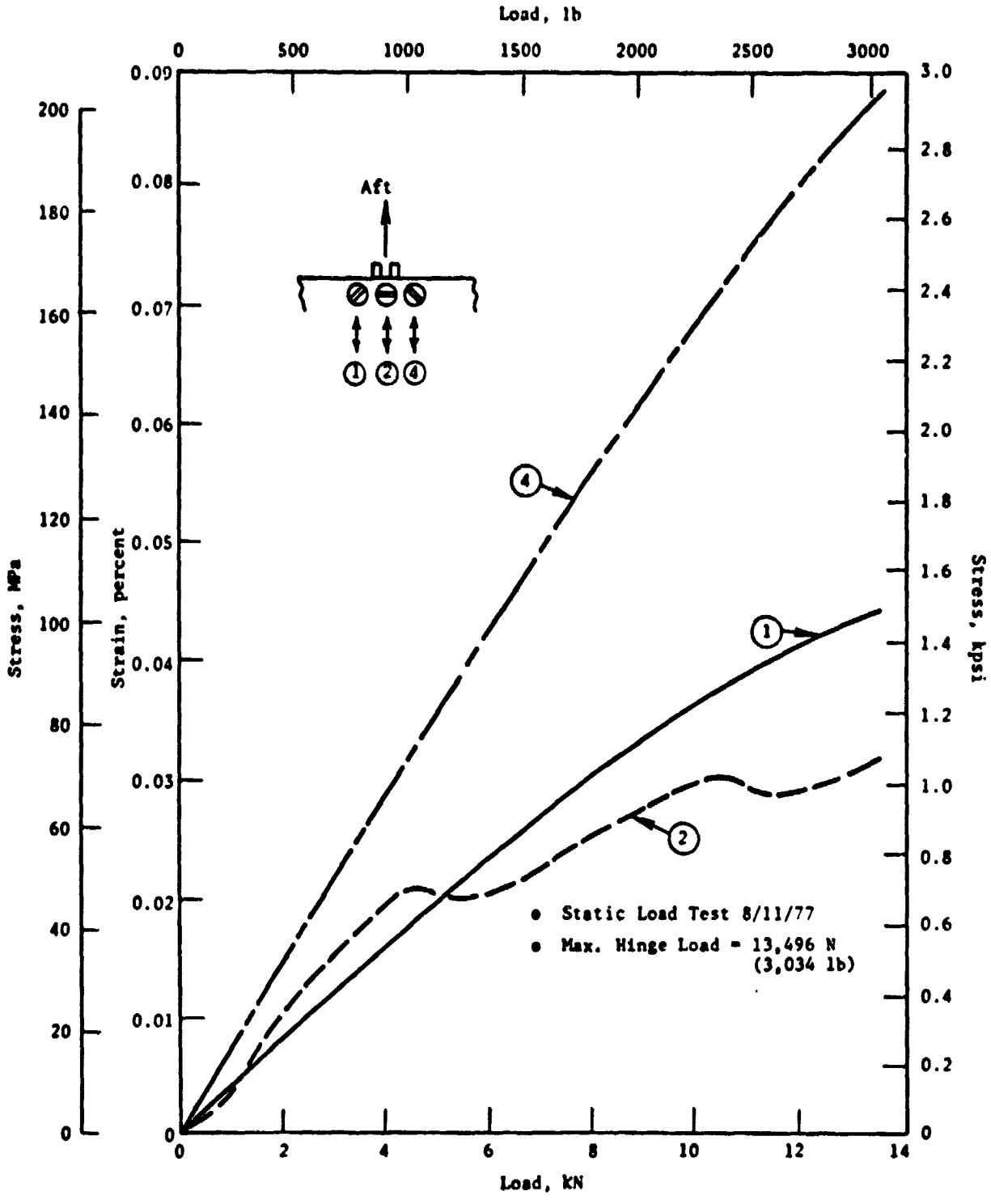

Figure 62. Inner Skin Strain Gages, Axial Reverse Thrust Case.

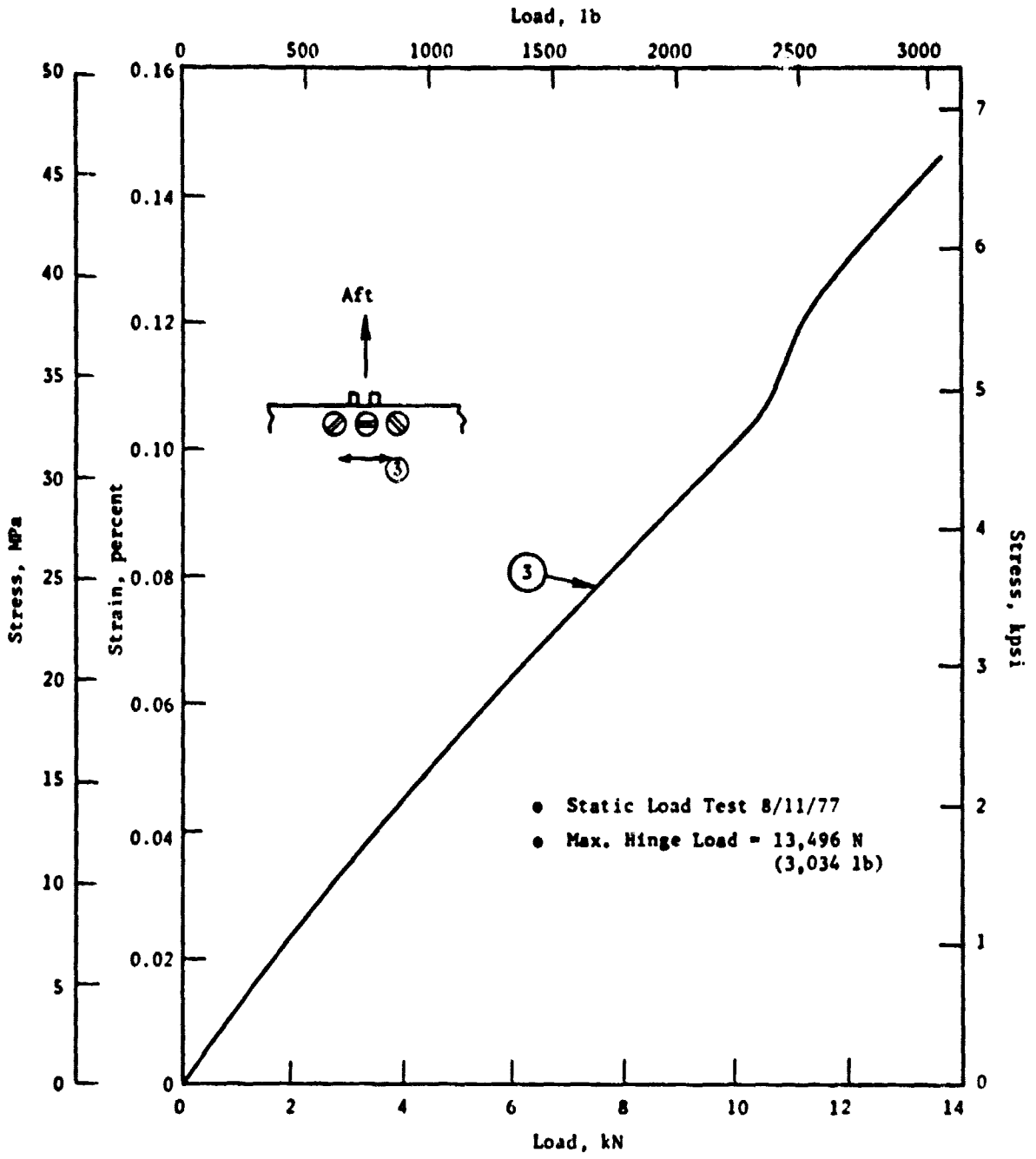

Figure 63. Inner Skin Strain Gage, Circumferential Reverse Thrust Case.

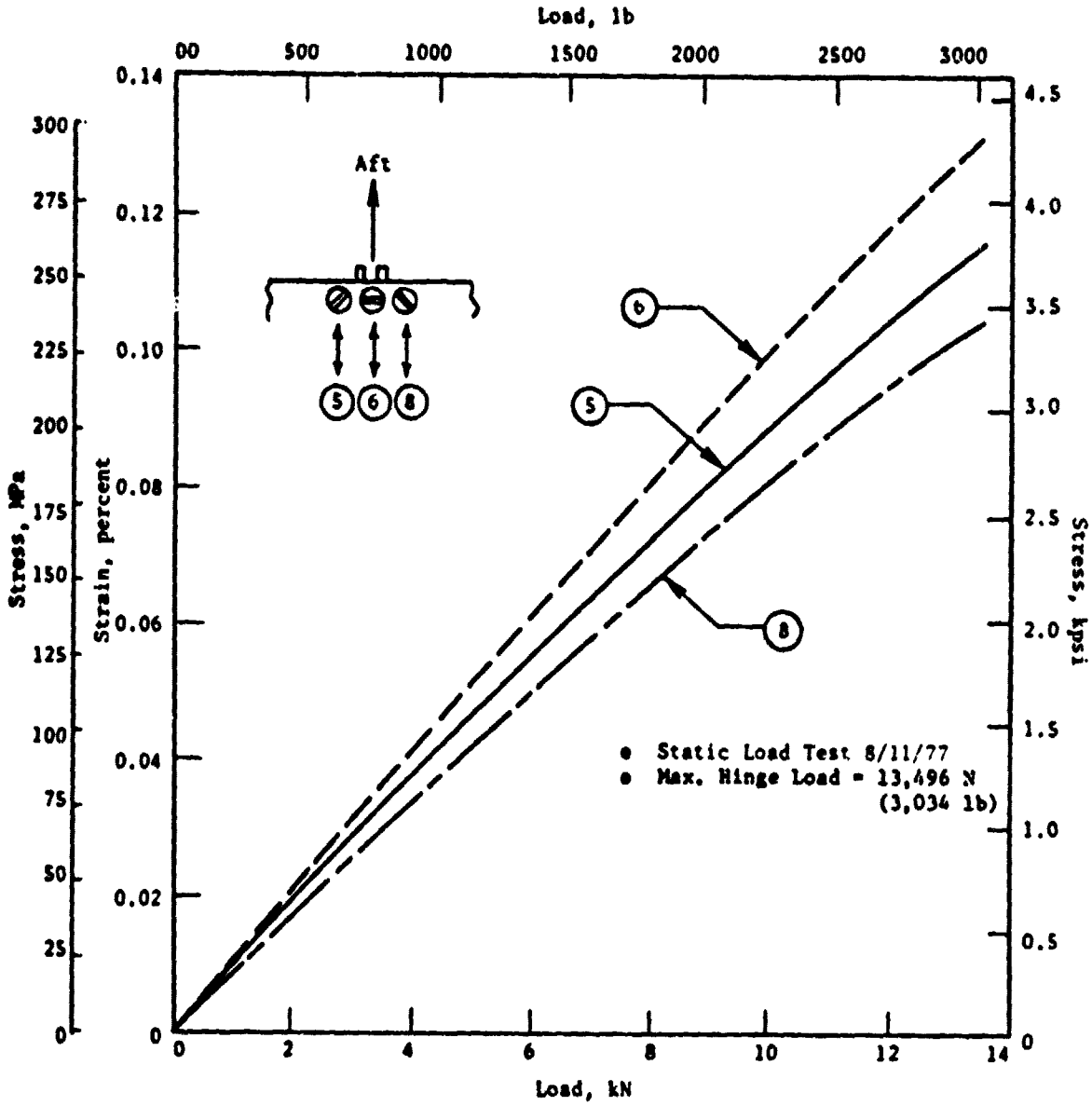

Figure 64. Outer Skin Strain Gages, Axial Reverse Thrust Case.

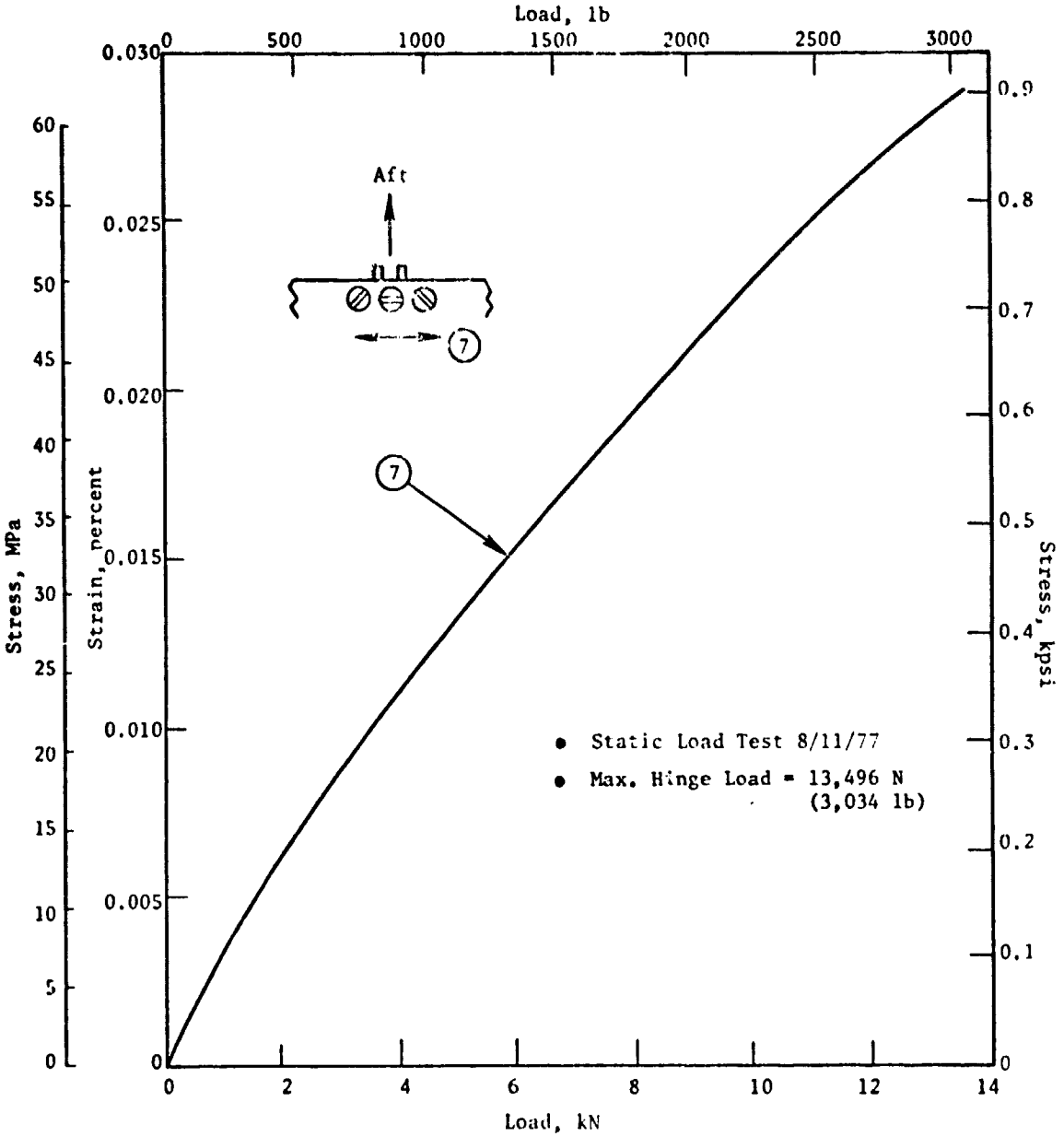

Figure 65. Outer Skin Strain Gage, Circumferential Reverse Thrust Case.